UNIVERSIDAD NACIONAL AUTÓNOMA DE MÉXICO

PROGRAMA DE MAESTRÍA Y DOCTORADO EN INGENIERÍA
ELÉCTRICA – INSTRUMENTACIÓN

FABRICATION OF OPTICAL FIBER PHOTONIC LANTERNS AND MICRORESONATORS

TESIS

QUE PARA OPTAR POR EL GRADO DE:
DOCTOR EN INGENIERÍA

PRESENTA:

AMADO MANUEL VELÁZQUEZ BENÍTEZ

TUTOR PRINCIPAL

DR. JUAN ARNALDO HERNÁNDEZ CORDERO
INSTITUTO DE INVESTIGACIONES EN MATERIALES (IIM)

COMITÉ TUTOR

DR. MATHIEU CHRISTIAN ANNE HAUTEFEUILLE
FACULTAD DE CIENCIAS

DR. NASER QURESHI
CENTRO DE CIENCIAS APLICADAS Y DESARROLLO TECNOLÓGICO (CCADET)

MÉXICO, CD. MÉXICO, ENERO 2017

JURADO ASIGNADO:

Presidente:	Dr. Augusto García Valenzuela
Secretario:	Dr. Mathieu Christian Anne Hautefeuille
Vocal:	Dr. Juan Arnaldo Hernández Cordero
1er Suplente:	Dr. Ramón Gutiérrez Castrejón
2do Suplente:	Dr. Nicolas K. Fontaine

Lugar o lugares donde se realizó la tesis:

Instituto de Investigaciones en Materiales (IIM), UNAM; México

CREOL - The College of Optics and Photonics, University of Central Florida (UCF); USA

Bell Laboratories / Nokia, Crawford Hill; USA

TUTOR DE TESIS:

Dr. Juan Arnaldo Hernández Cordero

FIRMA

(Segunda hoja)

CONTENT

FIGURES AND TABLES

AGRADECIMIENTOS / ACKNOWLEDGMENTS

En primer lugar quiero agradecer a mis padres y hermano por todo su apoyo incondicional día a día, sin ellos no hubiese podido terminar este trabajo. Infinitas gracias por todas las enseñanzas, consejos de vida y por darme fuerzas y ánimo en todo momento y ocasión. Lo que he logrado es gracias a ustedes.

Agradezco enormemente a mi tutor Juan Hernández Cordero por haberme guiado en todos mis estudios y preparación a lo largo del posgrado. Gracias por compartir sus conocimientos, ofrecerme excelentes oportunidades para desarrollarme, por las largas pláticas en diversos temas, su confianza y en especial su amistad.

Gracias a los miembros del jurado, los Drs. Augusto García Valenzuela, Ramón Gutiérrez Castrejón, Mathieu Hautefeuille y Nicolas Fontaine, por su tiempo, observaciones y sugerencias. Adicionalmente agradezco a los miembros de mi comité tutor, Drs. Mathieu y Naser, quienes a lo largo de mis estudios de doctorado me proporcionaron siempre consejos para la realización de mi trabajo de investigación, y sobre todo por esas preguntas inocentes que son siempre las más difíciles de contestar pero de las que más aprende uno.

I would like to thank Dr. Rodrigo Amezcua-Correa from CREOL for the great opportunity to work with him. It was an extraordinary and enlightening experience for me, in which I acquired an immense amount of knowledge, experience, and impacted my professional career in a remarkable way. I also would like to thank to Dr. Guifang Li and his research group for the very important collaboration. I would like to include Enrique Antonio-Lopez and Juan C. Alvarado-Zacarías, for their invaluable help and partnership to conduct my research during my stay in CREOL.

I want to thank to Drs. Nicolas Fontaine, Roland Ryf, and Haoshuo Chen from Bell Labs/Nokia for allowing me to perform research under their supervision. Especially, I want to thank to Nick for all the help during my time in Bell Labs, for his trust, fun at the lab, and friendship. Also, I would like to thank to all the people that I met in Bell Labs, particularly to Guilhem De V., Gregory R., Damiano B., Joseph K., and Pat for their kindness, good moments, and help in so many aspects.

In addition, I would like to thank to Dr. Sergio León-Saval and Dr. Chigo Okonkwo for their valuable advices during the conferences and collaborations.

Gracias a todos los compañeros del laboratorio de Fotónica y Dispositivos de Fibra óptica del IIM-UNAM (Violeta, Yadira, Mildred, Beatriz, Reinher, Natanael, Giovani y Rodrigo). Gracias a ustedes aprendí mucho dentro y fuera del laboratorio, además de que siempre me ayudaron en todo lo

posible. También quiero mencionar a todos aquellos que de alguna forma indirecta me apoyaron para poder dar término a esta etapa de mi vida; gracias a todos mis amigos y personas especiales.

Por último, quiero agradecer a las instituciones que hicieron posible la realización de mi trabajo de investigación. Gracias al Instituto de Investigaciones en Materiales de la UNAM por las instalaciones y el equipo proporcionado durante estos años. Gracias al Dr. Francisco Sánchez Arévalo por permitirme hacer uso de su laboratorio y equipo. Le agradezco al Dr. Omar Novelo por la asistencia en las sesiones de microscopía electrónica, vitales para obtener resultados de mi tesis. Gracias a la UNAM por el apoyo brindado mediante la beca de doctorado y los proyectos PAPIIT IN102112, IN108016 y IT101215.

Gracias también al CONACyT por la beca otorgada durante mis estudios de Doctorado, el apoyo de beca mixta para poder realizar mis estancias de investigación en CREOL ubicado en la Universidad Central de Florida, USA, así como por el apoyo mediante el proyecto 154464.

RESUMEN

Los dispositivos de fibra óptica han probado ser una de las tecnologías más eficientes para la transmisión y procesamiento de la luz durante las últimas décadas. Este trabajo se centra en los detalles y parámetros de la fabricación de dos tipos de dispositivos totalmente de fibra óptica: linternas fotónicas y micro resonadores de anillo. Las linternas fotónicas de fibra óptica son de gran interés para la siguiente generación de sistemas de comunicaciones. La selectividad modal en estos dispositivos fue lograda mediante los procesos de fabricación descritos en este trabajo. Dicha característica otorga la capacidad de generar diferentes modos espaciales de manera independiente mediante cada una de las fibras de entrada, donde fue capaz de demostrar dispositivos de hasta nueve diferentes modos linealmente polarizados en las fibras. La diversidad de núcleos de las fibras ópticas y sus posiciones específicas dentro de las linternas fotónicas para lograr de manera exitosa estos resultados fueron halladas experimentalmente. Adicionalmente, un nuevo método de fabricación para estos dispositivos mediante preformas micro estructuradas especiales fue utilizado para demostrar la posibilidad de escalar la fabricación de dispositivos con un gran número de fibras. Los dispositivos fabricados fueron caracterizados analizando los patrones de luz generados en su puerto de salida. Los resultados obtenidos en este trabajo proveen las bases para la fabricación de dichos dispositivos en desarrollo con selectividad modal.

Una nueva técnica para fabricar micro resonadores mediante el uso de elementos cilíndricos recubiertos con múltiples capas de polímero es igualmente presentada, incluyendo fibras ópticas estándar de vidrio y tubos capilares de vidrio. Mediante esta técnica, las características espectrales de los resonadores pueden ser establecidas para satisfacer requerimientos específicos. La posibilidad de emplear materiales funcionalizados fue comprobada utilizando como recubrimientos polímeros fluorescentes y reconfigurables, los cuales mostraron ser útiles para ajustar la respuesta espectral de los resonadores. El procedimiento de fabricación de estos dispositivos y las consideraciones consecuentes son discutidos, incluyendo su uso potencial para el desarrollo de elementos de sensado.

ABSTRACT

Fiber optic devices have proved to be one of the most efficient technologies for light transmission and processing over the last decades. This works covers the relevant details and parameters for the fabrication of two types of all-fiber devices: photonic lanterns and micro-ring resonators. All-fiber photonic lanterns are of interest for the next generation of optical communication systems. Modal selectivity of these devices was achieved following the fabrication procedures described in this work. This feature grants the capability to address independently different spatial modes with each input fiber, and we were able to demonstrate devices exciting up to nine different LP fiber modes. The required diversity of fiber core diameters and their specific positions within the photonic lanterns to successfully achieve these results were found experimentally. Additionally, a novel fabrication approach using special microstructured preforms was used to demonstrate the possibility to scale the fabrication of devices with a larger number of fibers. The fabricated devices were characterization by analyzing the light patterns generated at the output end. Results obtained in this work provide the foundations for the fabrication of these emerging fiber devices with modal selectivity.

A new technique to fabricate micro ring resonators is also presented using polymer multilayer coatings on cylindrical elements, including standard glass fibers and glass capillaries. With this technique, the spectral features of the resonators can be tailored to fulfill specific requirements. The possibility to employ functionalized materials was validated using fluorescent and optical reconfigurable polymers as coatings, which were show to be useful for tuning the spectral response of the resonators. The procedure to fabricate these devices and further fabrication considerations are discussed, including their potential use for developing sensing elements.

CHAPTER I: INTRODUCTION

The use of light has quickly spread into several fields of life with a great number of applications ranging from the understanding of matter, to new ways of entertainment. In science and technology, it has proved to be extremely useful in a wide variety of applications. Major applications ranges technological areas involving data transmission, material processing, imaging, and sensing; other purposes include biological organisms and their interaction with light, as well as exploration of new horizons in astrophotonics and manipulation of miniature objects [1-10]. Therefore, elements capable of perform light processing are required for numerous purposes, such as light shaping, filtering, sensing, etc. Light confinement and transmission are also crucial features for optical interconnection of photonic systems, where optical fibers have demonstrated to be remarkably efficient and versatile.

Among the many characteristics of optical fibers, the most attractive are the intrinsic minimal losses, micrometric size, good compatibility with existing technologies, and low cost. Their physical features (e.g., geometry, size, etc.) can also be further modified by post-processing or by the addition of materials in specific sections, aiming at providing additional functionalities for different applications. Post-processing of optical fibers is in fact one of the most used approaches for fabrication of fiber optic devices such as couplers, allowing linking not only optical fibers but also between photonic structures. A wide variety of devices working on this principle are currently available, e.g. fiber couplers, long period gratings, mode scramblers, etc. These devices can redistribute optical signals either in the frequency or in the spatial domain. Frequency-selective devices allow to separate and to manipulate wavelengths in a very precise manner, a useful feature for redirecting a signal or for filtering. Spatial-selective devices offer the capacity to manipulate the light intensity distribution confined within a specific area of a photonic structure.

Fiber optic technology has grown enormously owing to the versatility and advantages of the use of light on the last years. Many of the applications use single-mode fibers and hybrid free space/fiber optic devices for their simplicity of fabrication, ease of analysis, and the extensive availability of tools and equipment already developed for these purposes. In general, fiber optic systems are developed aiming at avoiding the use of free-space optical devices because this results in less complex assemblies and lower losses due to coupling and interconnection. A desired approach to reach these goals is the inclusion of all-fiber devices able to perform a series of light processing functions. Additionally, switching from single-mode to multimode devices offers the opportunity of increasing the capabilities for information acquisition and processing. Low losses and high compatibility with standard fiber technologies are hence highly desirable features for current fiber devices. The focus of the present work is centered on the fabrication and characterization of optical fiber devices

intended for optical telecommunications and sensing applications: photonic lanterns and micro-ring resonators.

I.1 BACKGROUND

I.1.1 SPACE DIVISION MULTIPLEXING (SDM)

Optical communications is an area of technology that has expanded all over the world during the last decades thanks to the use of optical fibers. The increasing progress in electronics and informatics demands a growth in communications capable of handling the immense amount of data [11]. Increase in deployment of actual single-mode optic fiber (SMF) systems is not a feasible option due to high cost of equipment and devices. Various techniques to increase data transmission in a sole SMF have made use of wavelength division multiplexing (WDM), time division multiplexing (TDM), polarization division multiplexing (PDM), and modulation of phase and quadrature of optical signals [11-13]. However, because of the non-linear Shannon limitation of single-mode fiber systems a different approach is necessary to overcome capacity crunch in optical systems.

Space division multiplexing (SDM) has emerged as an alternative to increase data transmission in a single optical fiber. SDM technique consists in using the different spatial modes as independent transmission channels. This technique involves the use of multimode fibers which have a bigger core diameter and hence the fiber non-linearity decreases [11-13]. The use of SDM in telecommunications has been already demonstrated to work successfully for a few modes [14]. Nevertheless, the need for multiplexers (MUX) and demultiplexers (DEMUX) are required as critical components to link single-mode to multimode devices. Previous implementations for the generation of spatial modes were based on bulk phase masks or integrated devices to directly excite the modes in multimode fibers [15, 16]. A drawback from phase masks are the large insertion losses and scaling to a high number of modes is thus severely limited [17, 18]. Alike phase masks, an approach to excite the linear combination of modes was by spot launching technique by means of bulk optics [19]. Similarly, spot arrays can be generated by 3D laser inscribed waveguides proving to be a compact and passive element compatible with multimode fibers [18, 20]. Resonant fiber and waveguide-based mode MUX such as fused fiber couplers, long period gratings, Y-junctions, and micro-ring resonators have also been proposed [21, 22]. A solution based on optical fibers has emerged to solve this problematic, the *photonic lantern* [23]. These all-fiber devices are able to perform as MUX/DEMUX devices with low-insertion loss and precise modal control based on the fabrication parameters, proving to be an exceptional alternative.

I.1.2 OPTICAL MICRO–RING RESONATORS

Optical sensing techniques are currently very popular because of their potential for highly sensitive detection of micro- and nanometer scale particles; these are also capable of detecting diminutive change in some materials properties [24, 25]. Non-contact sensing and risk-free techniques are also available; hence, offering advantages when compared to mechanical and electrical approaches [26]. Light confinement at micrometric scales is an attractive feature that has impelled the fabrication of integrated optical elements based on mature technological platforms. An example of a highly sensitive device, useful for sensing and for light modulation is the micro-ring resonator. This resonant element confines light at specific wavelengths depending on physical parameters such as refractive index, geometry, and optical absorption. A slight modification in any of the resonator parameters will generate a noticeable change in the spectral response.

Fabrication of optical micro-resonators by photolithography processes is a mature technology in integrated photonics devices [27-30]. Nonetheless, a variety of techniques can be implemented to fabricate these devices depending on the sought application. Tapered optical fibers are commonly used in micro-ring devices in order to couple light into micro-spheres or micro-disks [30, 31]. Another fabrication technique involves the entanglement of subwavelength tapered fibers to obtain a micro-knot. This approach, yields devices with good quality response but involves a high difficulty of fabrication [30, 32, 33]. Other techniques require special fibers like photonic crystal fibers [34], thin capillaries [35], or bottle-like resonators [36].

Micro-ring resonators are of great interest due to their wide range of applications. Biosensing is one of the trendiest applications, since single virus and protein or DNA detection can be accomplished [24, 30, 37]. Properties of liquids and solutions such as the change in concentrations or refractive index can also be detected using these elements [38]. Detection and monitoring of thermal effects on small-scale objects is one of the current challenges that have been recently addressed with micro-resonators [39]. Development of miniature lasers is another hot topic in photonics, and micro-resonators have also shown to be useful for implementing micrometer size tunable lasers [40].

I.2 OBJECTIVES

This work focuses on the fabrication and characterization of two optical fiber devices: photonic lanterns and micro-ring resonators. The key aspects and issues found during the fabrication processes of both devices are covered in the following sections. A photonic lantern is sought to create a fiber-based solution for space division multiplexing systems, specifically in the area of optical fiber communications. In essence, a photonic lantern serves as MUX/DEMUX elements for SDM systems. The pursuit to establish a standardized fabrication process is investigated in this work, looking to create photonic lanterns capable of addressing different numbers of modes. Further assessments of the fabrication process include the conditions to obtain devices with modal selectivity and low losses.

The suitability of these devices for fiber optic communications is assessed upon evaluating their modal features, and coupling to multimode fibers. Finally, an alternative approach for the fabrication of micro-ring resonators is explored, aiming at developing versatile devices. The proposed fabrication method involves the use of low-cost materials and standard methodologies used for fiber optic technology. An interesting feature for a wavelength responsive component is a tunable response. This aspect is studied upon modifying the resonant elements using different materials used as coatings on the resonators.

The organization of the present dissertation is as follows: In Chapter II a brief summary of the fundamentals of light propagation in fiber optics relevant for this work, and the basis of the tapering and coupling processes are presented. The operation and fabrication principles of the photonic lanterns and a summary of the required parameters to obtain modal selectivity, as well as the characterization of the fabricated devices, are described in Chapter III. Chapter IV covers an alternative way to fabricate micro-ring resonators based on a functional polymer multilayers approach and the considerations to be taken into account for these devices. Finally, in Chapter V the conclusions and future work are presented. A list of the publications resulting from the entire research conducted during my PhD studies is included in Appendix B.

CHAPTER II: FIBER OPTICS FUNDAMENTALS-PROPAGATION, TAPERING, AND COUPLING PROCESS

Optical fibers are dielectric waveguides with cylindrical geometries formed by two concentric structures: a core and a cladding [1, 2, 41]. Light is confined and transmitted through this structure travelling mostly within the core, while the cladding serves as an isolation medium around the core. Propagation of light in waveguides can be analyzed by geometrical optics approach based on *Snell's law*, describing the total reflection of light inside dielectric structures [1, 41]. This phenomenon is due different refractive indices of the materials used in the cladding and the core, and ultimately defines the propagation features of the light in the fiber waveguide.

Depending on the physical characteristics of the fiber, a certain number of rays will be totally reflected within the core/cladding interface and these represent the optical paths, or modes, that light can follow inside the waveguide. A single-mode fiber (SMF) results when only one trajectory is allowed; if multiple trajectories are allowed, the waveguide is defined as a multimode fiber (MMF). While the diameter of the cladding can range from micrometers to a few millimeters, the core is usually of a few micrometers. Fabrication of fiber-based devices, such as photonic lanterns and micro-resonators, requires full understanding of light propagation in optical fibers. Hence, a detailed description of light propagation in these waveguides will be discussed in the following section.

II.1 PROPAGATION OF LIGHT IN OPTICAL FIBERS

A formal description of light propagation in waveguides with dimensions close to the wavelength requires wave theory. The propagation characteristics within a waveguide can be obtained using Maxwell's equations. For media with no charge, lossless, linear, and isotropic, the electric (**E**) and magnetic (**B**) fields are described by [1, 2, 41]:

$$\nabla \times \mathbf{E} = -\frac{\partial \mathbf{B}}{\partial t} \qquad \text{<II.1>}$$

$$\nabla \times \mathbf{H} = \frac{\partial \mathbf{D}}{\partial t} \qquad \text{<II.2>}$$

$$\nabla \cdot \mathbf{D} = 0 \qquad \text{<II.3>}$$

$$\nabla \cdot \mathbf{B} = 0 \qquad \text{<II.4>}$$

D and **B** are the electric and magnetic flux densities, respectively. These parameters are defined by the constitutive relations:

$$\mathbf{D} = \varepsilon \mathbf{E} \qquad \text{<II.5>}$$

$$\mathbf{B} = \mu \mathbf{H} \qquad \text{<II.6>}$$

where ε and μ are the permittivity and permeability of the medium, respectively.

Upon applying the curl, and after some manipulations of the above equations (*<II.1>* and *<II.2>*), the wave equation for **E** and **H** can be obtained as:

$$\nabla \times \nabla \times \mathbf{E} = -\frac{\partial}{\partial t} \nabla \times \mathbf{B} = -\mu \frac{\partial}{\partial t} \nabla \times \mathbf{H} = -\mu \frac{\partial}{\partial t} \left(\frac{\partial}{\partial t} \mathbf{D} \right) = -\mu \varepsilon \frac{\partial^2}{\partial t^2} \mathbf{E} \qquad \text{<II.7>}$$

$$\nabla \times \nabla \times \mathbf{H} = -\frac{\partial}{\partial t} \nabla \times \mathbf{D} = -\varepsilon \frac{\partial}{\partial t} \nabla \times \mathbf{E} = -\mu \frac{\partial}{\partial t} \left(\frac{\partial}{\partial t} \mathbf{B} \right) = -\mu \varepsilon \frac{\partial^2}{\partial t^2} \mathbf{H} \qquad \text{<II.8>}$$

Using the vector identity $\nabla \times \nabla \times \mathbf{A} = \nabla \left(\nabla \cdot \mathbf{A} \right) - \nabla^2 \mathbf{A}$ on *<II.7>* and *<II.8>*, it yields in:

$$\nabla^2 \mathbf{E} - \mu \varepsilon \frac{\partial^2}{\partial t^2} \mathbf{E} = 0 \qquad \text{<II.9>}$$

$$\nabla^2 \mathbf{H} - \mu \varepsilon \frac{\partial^2}{\partial t^2} \mathbf{H} = 0 \qquad \text{<II.10>}$$

Typically, the **E**-field equation is solved in terms of a harmonic function in the time domain with the form $g\left[t \pm \left(z/v \right) \right] = \cos\left[\omega \left(t \pm z/v \right) \right]$, where ω is the angular frequency $\left(\omega = 2\pi f \right)$, f is the frequency, and v the phase velocity. Further simplifications can be made upon considering field propagation along the *z*-axis and using the complex form $e^{j\omega t}$. The propagation constant, β, is defined as the phase shift rate of the wave when traveling a given distance in *z*. Alternatively, this can also be defined as $\beta \equiv \omega / v$. Using the phasor representation, and defining $k \equiv \omega \sqrt{\mu \varepsilon}$, the wave equations for the electric and magnetic fields yields the Helmholtz equations [1, 41]:

$$\nabla^2 \mathbf{E} + k^2 \mathbf{E} = 0 \qquad \text{<II.11>}$$

$$\nabla^2 \mathbf{H} + k^2 \mathbf{H} = 0 \qquad \text{<II.12>}$$

For light propagation in one direction (*z*-direction) through the waveguide and assuming a planar wave in the *xy*-plane, the propagation constant is given by:

$$\beta = k = nk_0 = \omega\sqrt{\mu\varepsilon} \qquad \text{<II.13>}$$

where k_0 is the propagation constant in free space. Propagation in the z-direction can be represented by a factor $e^{-j\beta z}$ and this result in the following expressions for the electric and magnetic fields:

$$\mathbf{E} = \mathbf{E}(x, y, z) = \mathbf{E}_0(x, y)e^{-j\beta z} \qquad \text{<II.14>}$$

$$\mathbf{H} = \mathbf{H}(x, y, z) = \mathbf{H}_0(x, y)e^{-j\beta z} \qquad \text{<II.15>}$$

The resulting Helmholtz equations are then given by:

$$\nabla^2\mathbf{E}_0 + \left(k^2 - \beta^2\right)\mathbf{E}_0 = 0 \qquad \text{<II.16>}$$

$$\nabla^2\mathbf{H}_0 + \left(k^2 - \beta^2\right)\mathbf{H}_0 = 0 \qquad \text{<II.17>}$$

Then, the refractive index can be described as the impedance of the medium as:

$$n \equiv \frac{\mathbf{E}_0}{\mathbf{H}_0} = \frac{\omega\mu}{k} = \sqrt{\frac{\mu}{\varepsilon}} \qquad \text{<II.18>}$$

Light confinement and propagation in optical fibers is described in terms of the guiding structure. As the fibers possess cylindrical geometry, it is convenient to use cylindrical coordinates: radius r, azimuthal angle θ, and z. Figure II-1 shows a schematic representation of an optical fiber, with a core of radius a surrounded by the cladding, and with a step-index variation.

$$n(r)\begin{cases} n_{co} & 0 \le r \le a, \quad \text{core} \\ n_{cl} & r > a, \quad \text{cladding} \end{cases} \qquad \text{<II.19>}$$

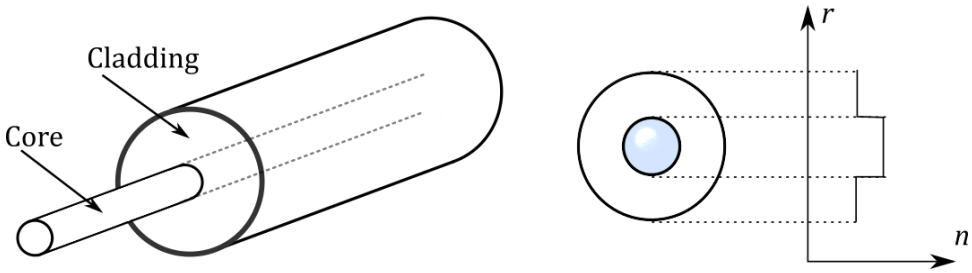

Fig. II - 1. Step-index optical fiber scheme and its refractive index profile.

To fulfill the total internal reflection criteria, the relationship $n_{co} > n_{cl}$ has to be satisfied. Hence, light confinement within the optical fiber is defined in terms of the materials and their refractive indices. For a step-index fiber, such as the one depicted in Figure II-1, the difference in refractive indices is customarily defined as [1, 2, 41, 42]:

$$\Delta = \frac{n_{co}^2 - n_{cl}^2}{2n_{co}^2} \approx \frac{n_{co} - n_{cl}}{n_{co}} = \frac{\delta n}{n_{co}} \qquad \text{<II.20>}$$

Typically, in optical fibers only a small number of trajectories or modes are desired to be transmitted. Such a goal is achieved with small core diameters and by generating a very low-refractive index difference among the core and cladding materials $\left(n_{co}/n_{cl} \cong 1\right)$ [2]. Under these circumstances only one or few modes are allowed to be transmitted, suppressing the rest of the modes. This condition is defined as the *weakly guiding* approximation.

Another important parameter is the maximum acceptance angle of incidence $\left(\theta_{Max}\right)$ for which the light rays can be confined in the waveguide. This angle is defined in terms of the numerical aperture, *NA*, defined as:

$$NA(r) = \sqrt{n_{co}^2(r) - n_{cl}^2} \qquad \text{<II.21>}$$

For simplicity, in what follows only step-index fibers operating in the weakly guiding approximation will be considered to analyze the electric field propagation in optical fibers.

Given the cylindrical geometry of the fibers, transverse fields with an arbitrary state of polarization can be considered for the propagation analysis. The axial components of the electromagnetic wave, $\mathbf{E}_0$ and $\mathbf{H}_0$, can be obtained considering a general function $\psi = \psi(r,\phi)$, and the Helmholtz equation [2, 41, 42]:

$$\nabla^2\psi + \left(k^2 - \beta^2\right)\psi = 0 \qquad \text{<II.22>}$$

The transverse field variations are defined only in terms of r and ϕ; then, using the Laplacian in cylindrical coordinates the above equation is explicitly:

$$\frac{\partial^2\psi}{\partial r^2} + \frac{1}{r}\frac{\partial\psi}{\partial r} + \frac{1}{r^2}\frac{\partial^2\psi}{\partial\phi^2} + \left[k^2(r) - \beta^2\right]\psi = 0 \qquad \text{<II.23>}$$

Each of the solutions for Eq. <*II.23*> represents a mode traveling along the z-direction. These can be obtained using separation of variables. First, azimuthal symmetry allows for 2π–periodic solutions in ϕ; hence, the full solution will read:

$$\psi(r,\phi,z) = \boldsymbol{R}(r)\boldsymbol{\Phi}(\phi)e^{-j\beta z} = \boldsymbol{R}(r)e^{-jp\phi}e^{-j\beta z} \qquad \text{<II.24>}$$

where p is an integer ($p = 0, 1, 2, \ldots$). Substitution of this function in Eq. <*II.23*> yields the corresponding equation for the radial coordinate, $\boldsymbol{R}(r)$:

$$\frac{\partial^2 R}{\partial r^2} + \frac{1}{r}\frac{\partial R}{\partial r} + \left[k^2(r) - \beta^2 - \frac{p^2}{r^2}\right]R = 0 \qquad \text{<II.25>}$$

Since the energy distribution inside the fiber is determined by the physical properties of the structure, the solutions of the wave equation allow for multiple propagating modes. The field distribution on the optical fiber is then established by the core-cladding existing boundary, and two regimes can be defined owing to these sections:

$$\begin{aligned} n_{cl}^2 < \frac{\beta^2}{k_0^2} < n_{co}^2, \quad & \text{guided mode } (r \le a) \\ 0 < \frac{\beta^2}{k_0^2} < n_{cl}^2, \quad & \text{radiated mode } (r > a) \end{aligned} \qquad \text{<II.26>}$$

It is convenient to separate both regions using the following definitions:

$$U = a\sqrt{k_0^2 n_{co}^2 - \beta^2} \qquad \text{<II.27>}$$

$$W = a\sqrt{\beta^2 - k_0^2 n_{cl}^2} \qquad \text{<II.28>}$$

Using these, Eq. *<II.25>* can be separated in two independent equations, one for the core and one for the cladding:

$$\begin{aligned} \frac{\partial^2 R}{\partial r^2} + \frac{1}{r}\frac{\partial R}{\partial r} + \left[\frac{U}{a^2} - \frac{p^2}{r^2}\right] R = 0, \quad & r \le a \\ \frac{\partial^2 R}{\partial r^2} + \frac{1}{r}\frac{\partial R}{\partial r} + \left[\frac{W}{a^2} + \frac{p^2}{r^2}\right] R = 0, \quad & r > a \end{aligned} \qquad \text{<II.29>}$$

The solutions for these equations are in the form of Bessel functions J_p (first kind Bessel function) and K_p (modified Bessel function), where *p* is the order of the corresponding function. Considering the components of the propagated wave, the solutions for **E** and **H** are then obtained in the *z*-direction as [1, 2, 41]:

$$E_z = \begin{cases} A_1 J_p\left(Ur/a\right)\sin\left(p\phi\right)e^{-j\beta z}, & r \le a \\ A_2 K_p\left(Wr/a\right)\sin\left(p\phi\right)e^{-j\beta z}, & r > a \end{cases} \qquad \text{<II.30>}$$

$$H_z = \begin{cases} B_1 J_p\left(Ur/a\right)\cos\left(p\phi\right)e^{-j\beta z}, & r \le a \\ B_2 K_p\left(Wr/a\right)\cos\left(p\phi\right)e^{-j\beta z}, & r > a \end{cases} \qquad \text{<II.31>}$$

where $A_{1,2}$ and $B_{1,2}$ are constants. The radial distribution of the electromagnetic field defined by J_p show an oscillatory behavior inside the core region. Resulting number of oscillations for each mode

will depend on the order *p*, decreasing in amplitude in the radial direction. Similarly, the K_p functions define an exponential decay in the field distribution, and a larger value for *p* indicates a more rapid decay. This decaying field in the cladding region is known as the evanescent field in optical fibers.

II.1.1 MODES IN OPTICAL FIBERS

The solutions of the wave equation determine the multiple modes of the electric and magnetic fields able to propagate inside the core. These solutions define the propagation constants and hence, the modal refractive indices, which are also affected by the core. Since the physical properties of the structure determine the number of modes, fibers with a large core diameter or large refractive index difference are generally capable of supporting numerous modes. The weakly guiding approximation provides a useful means to simplify the analysis of light propagation with scalar calculations in optical fibers [2, 41-43].

In general, fibers can support different EM wave polarizations: transverse electrical (TE), transverse magnetic (TM), or hybrid modes, as in the case of skewed rays (EH and HE). For each of these polarizations, a corresponding solution can be found. However, using the weakly guiding approximation, several TE, TM, EH, and HE modes will have the same propagation constants, i.e., they become degenerate modes. Hence, aggrupation of modes with the same β can be denoted as linearly polarized modes, or LP modes. The solutions are then given in terms of the LP_{lm} modes, in which *l* and *m* represent the azimuthal and radial indices of the modes, respectively. These new sets of indices are related to the index *p* (with multiple solutions of m_{th} order) as [2, 41]:

$$l = \begin{cases} 1 & \text{TE}_{lm}, \text{TM}_{lm}, \quad (m = 0) \\ p+1 & \text{EH}_{lm}, \quad (m \geq 1) \\ p-1 & \text{HE}_{lm}, \quad (m \geq 1) \end{cases} \qquad \text{<II.32>}$$

LP_{lm} modes arise from the assumption of a wave maintaining its polarization during propagation; superposition of degenerate modes is also considered. The values for the subscript *l* indicate the half of the minima or maxima in the intensity pattern, whereas the values of *m* represent the number of maxima along the radial direction. It is worth mentioning that for all of the LP modes, with exception of the LP_{0m}, there will be a set of two degenerate modes, *a* and *b*. The only difference between these degenerate modes is a rotation, yielding a swapping between the minima and maxima in the intensity patterns. Examples of intensity profiles for the twelve lower order LP modes in step-index fibers are shown in Figure II-2. This classification of modes is used in practice to describe the field-intensity profile of the modes. However, during propagation, energy exchange can occur among modes with similar propagation constant, such as the degenerate modes [2, 41, 44]. Table II-1 lists the degenerate modes of the LP modes shown in Figure II-2.

Table II - 1. List of LP fiber modes and their corresponding degenerate modes [41].

LP mode	Degenerate modes
LP_{01}	HE_{11}
LP_{11}	TE_{01}, TM_{01}, HE_{21}
LP_{21}	EH_{11}, HE_{31}
LP_{02}	HE_{12}
LP_{31}	EH_{21}, HE_{41}
LP_{12}	TE_{02}, TM_{02}, HE_{22}
LP_{41}	EH_{31}, HE_{51}
LP_{22}	EH_{12}, HE_{32}
LP_{03}	HE_{13}
LP_{51}	EH_{41}, HE_{61}
LP_{32}	EH_{22}, HE_{42}
LP_{13}	TE_{03}, TM_{03}, HE_{23}

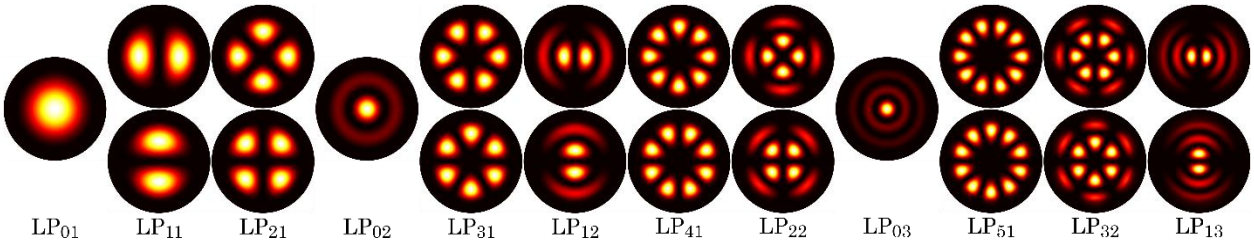

Fig. II - 2. Field-intensity distributions of the first twelve lower order LP modes.

An important parameter, useful to estimate the number of modes and the corresponding propagation constants is the normalized frequency, also called the *V*-number, calculated as [1, 2, 41, 42]:

$$V = \sqrt{U^2 + W^2} = k_0 a \sqrt{n_{co}^2 - n_{cl}^2} = \frac{2\pi a}{\lambda_0} NA \qquad \text{<II.33>}$$

Finally, a complete description of the propagating modes in fibers requires the propagation constant β_{lm} for each LP mode. These can be obtained in terms of the normalized propagation constant, *b*, given by:

$$b = 1 - \frac{U^2}{V^2} = \frac{W^2}{V^2} = \frac{\beta^2 - n_{cl}^2 k_0^2}{n_{co}^2 k_0^2 - n_{cl}^2 k_0^2} \qquad \text{<II.34>}$$

The range of values that *b* can take is $0 < b < 1$, where the normalized cutoff frequency is obtained for $b = 0$. Hence, the propagation constant for each mode can be determined by [41, 42]:

$$\beta_{lm} = n_{cl} k_0 \sqrt{1 + 2b\Delta} \approx n_{cl} k_0 \left(1 + b\Delta\right) = n_{cl} k_0 \left[1 + \Delta\left(1 - \frac{U_{lm}^2}{V^2}\right)\right] \qquad \text{<II.35>}$$

A plot of the normalized propagation constant as a function of the normalized frequency is shown in Figure II-3.

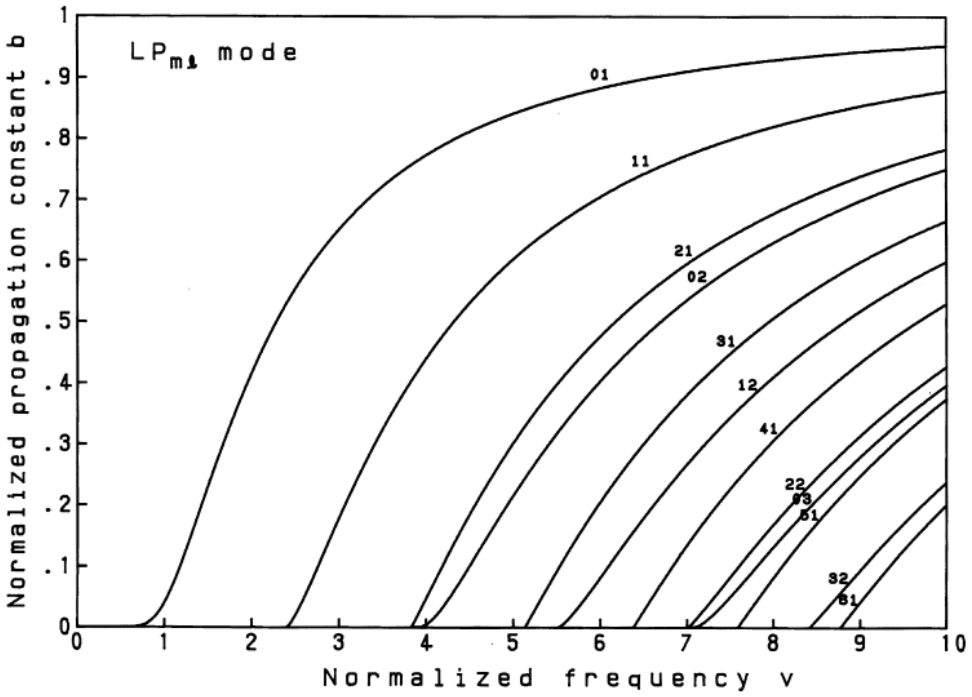

Fig. II - 3. Propagation of the LP modes (marked in the corresponding plot) dependent of normalized propagation constant (b) as function of the normalized frequency (V) in step-index fibers. Taken from [2].

It is clear from Figure II-3 that for a fixed value of *V,* only a given number of modes can propagate in a step-index fiber. Single-mode operation for a fiber guiding only the LP_{01} is achieved when $V \leq 2.405$. Larger values of *V* will result in a fiber capable of supporting propagation of multiple modes (i.e., a multimode fiber). Increasing *V* will therefore increase the number of modes transmitted in a fiber (see Eq. <*II.33*>). In practice, this is achieved using a larger core diameter, or upon increasing the difference in refractive indices of the fiber. In MMFs with a large value of *V,* the number of modes (*N*) can be estimated as [23, 42]:

$$N \approx \frac{V^2}{4} \qquad \text{<II.36>}$$

Habitual core sizes for SMFs used in the telecommunications area range between 4 to 10 μm, whereas for MMFs the core sizes range from 50 to 62.5 μm. For both types of fibers, the outer diameter (cladding size) is typically 125 μm [45-47]. In the last few years, few-mode fibers (FMFs) have attracted a lot of attention due to their capability to operate in the multimode regime, but only propagating a few lower order modes [48, 49]. This type of fiber has been used mostly for optical telecommunications, and in particular in the area of space division multiplexing, employing each mode as an independent channel for data transmission [11, 14, 50]. To date, FMFs are intended to transmit 3, 6, and 9 LP modes with minimum crosstalk [49-53].

II.1.2 GRADED-INDEX FIBERS

In graded-index fibers (GIFs), the value of the refractive index increases gradually from the cladding-core boundary to the center of the core to reach its maximum value. Such a refractive index profile is commonly used to compensate the difference of group velocities of the different modes propagating in MMFs. As a consequence of the gradual variation in refractive index, rays propagating in the core will propagate along curved trajectories as opposed to straight ones, as observed in step-index fibers. Light propagation in GIFs is described using the same equations exposed in the previous section. However, some important variations in the mathematical description arise from considering the radial variation in refractive index. Nonetheless, the propagation constants may also be obtained for each mode using approximated solutions for the appropriate equations [2, 42, 44].

A description of the core refractive index distribution in GIFs is typically given by the function:

$$n^2(r) = n_{co}^2\left[1-2\Delta\left(\frac{r}{a}\right)^q\right] \qquad \text{<II.37>}$$

The steepness of the refractive index profile is determined by the grade profile parameter q. If $q=1$, the change in refractive index will be a linear function of r, whereas if $q\to\infty$, the function represents a step-index profile. The refractive index distribution in the core of the fibers is shown in Figure II-4, illustrating the resulting index profiles for different values of q [1, 2, 42]. GIFs usually support several or many modes; an estimate of the number of modes can be made upon proper modifications of Eq. *<II.36>* taking into account the grade profile parameter:

$$N \approx \frac{q}{2(2+q)}V^2 \qquad \text{<II.38>}$$

For graded-index fibers another criterion is preferred to group the propagated LP modes. Upon considering the refractive index profile, solutions of the propagation constants in GIFs can be obtained by [2, 44]:

$$\beta = kn_{co}\left[1-2\Delta\left(\frac{V}{N}\right)^{q/q+2}\right]^{1/2} \qquad \text{(I.39)}$$

where the principal mode groups are defined by integer solutions of the mode group number (M), defined as [44, 45]:

$$M = 2m+l-1 \qquad \text{(I.40)}$$

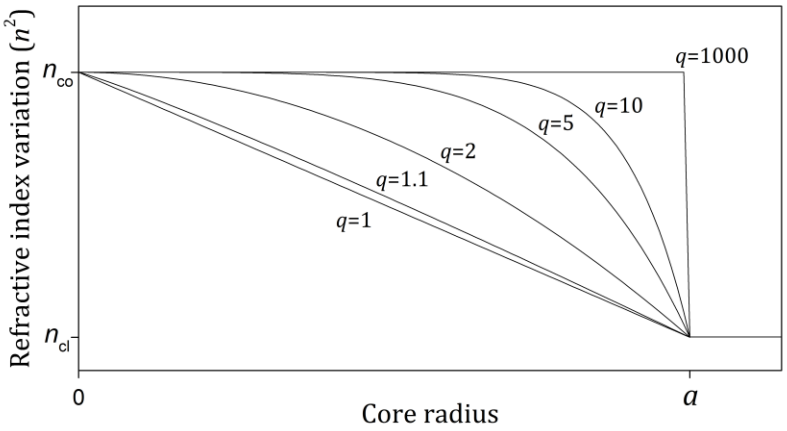

Fig. II - 4. Refractive index distribution of graded index fibers with different grade profile parameter (q).

The use of GIFs represents an advantage when multimode signals are required to be transmitted [45, 46]. Due to its refractive index profile, the propagation of the fundamental mode in this type of fiber is favored over the other supported modes. As a reason of this, GIFs help to improve the losses when fibers are subjected to tapering or fusing processes, as will be discussed in following sections.

Table II - 2. List of LP fiber modes corresponding to the different mode groups classification (M).

Mode Group (*M*)	1	2	3	4	5	6
LP mode	LP_{01}	LP_{11}	LP_{21}, LP_{02}	LP_{31}, LP_{12}	LP_{41}, LP_{22}, LP_{03}	LP_{51}, LP_{32}, LP_{13}

II.2 FABRICATION OF TAPERED OPTICAL FIBERS

Passive optical fiber devices are key elements for a wide variety of applications and construction of optical systems. Many of these devices are constructed employing tapered sections of optical fibers [54, 55]. The main purpose of tapered optical fibers is to gradually reduce the fiber core in order to expose the optical wave to the surrounding media. Fabrication of fused fiber couplers [56, 57], enhancement of nonlinear effects [58], spectral filtering [59], sensing [60, 61], and mode coupling [62], are some of the most reported applications of tapered optical fibers. Tapering down optical fibers involves a reduction of the whole waveguide, cladding and core. The structure resulting from this process comprises three sections: the fiber without tapering, the transition sections, and the waist of the taper. The latter is the section with the smallest constant diameter, with sizes ranging from a few micrometers to submicron diameters. Change from the non-tapered fiber to the waist, and vice versa, takes place in the transition sections [54]. A schematic representation of a tapered optical fiber is shown in Figure II-5.

Light confinement in tapered fibers is diminished at the core upon its reduction. As the radius of the core decreases the effective refractive index of the core decrease as well, causing some coupling of light towards the cladding. When the tapering process continues until reaching a core size smaller than the wavelength, the light will no longer be confined and total coupling of light into the cladding

will occur. In this case, the wave guiding conditions are determined mainly by the cladding material and the surrounding media, since the core is no longer able to confine the light. A consequence of this condition is the exposure of the evanescent wave to the external media, providing the possibility of interaction of the optical wave with other structures or other materials surrounding the tapered section.

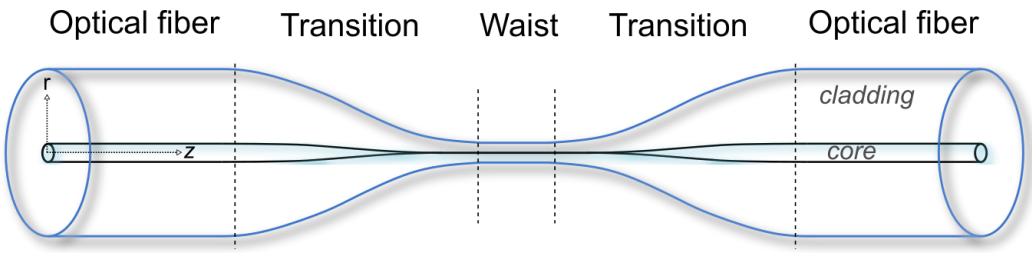

Fig. II - 5. Schematic representation of a tapered optical fiber.

Optical fibers are tapered following a process of heating and pulling until reaching the desired diameter. Heating of the fibers can be done following a few approaches: by using a flame torch, by absorption of laser light, with an electrical micro furnace, and by arc discharge from electrodes [54, 63-65]. In this work, the first two methods were used to fabricate fiber optic micro-resonators and photonic lanterns, and these will be discussed in the following sections.

II.2.1 ADIABATIC TAPERED FIBERS

Losses resulting from the tapering process are originated by a sudden change in the dimensions of the fiber affecting the propagation conditions, and provoking imminent light leaking from the core. To avoid these losses, the changes in the structure must be performed at a very slow rate ensuring an adiabatic change in diameter [55]. An adiabatic taper will prevent the fundamental mode (LP_{01}) to couple to any cladding modes, thereby resulting in zero or negligible loss. Ideally, the transition sections should be extremely long with a progressive minimum change in diameter. However, practical fabrication of these devices does not allow for these conditions since an infinite transition section will be required [54, 66, 67]. In multimode fibers one of the effects is the reduction in the *V*-number, resulting in the conversion of the supported highest order modes into cladding modes.

A criterion typically used to define if a tapered fiber is adiabatic, is defined in terms of the local length-scale of the taper (z_t), and the beat length, z_b, defined as the propagation length required for the LP_{01} and the LP_{02} modes couple [55]. In weakly guiding fibers, such as the case of SMFs, light couples to the cladding material in which the higher order modes can be excited if the tapering process is not adiabatic. Determination of z_t depends on the taper angle $\Omega = \Omega(z)$, and the radius of the core as a function of the length $r = r(z)$, given by [54, 55, 68]:

$$z_t = r/\Omega \qquad \text{<II.41>}$$

$$\Omega(z) = \tan^{-1}\left|\frac{dr}{dz}\right| \qquad \text{<II.42>}$$

For an axially symmetric tapered fiber, the LP_{01} mode will only couple to azimuthally symmetric higher order modes (LP_{0m}) propagating at the cladding material. Hence, z_b depends on the propagation constants of the LP_{01} mode, β_1, and the second mode to couple, β_2, resulting in:

$$z_b = \frac{2\pi}{\beta_1 - \beta_2} \qquad \text{<II.43>}$$

If $z_t \gg z_b$, light coupling from the fundamental mode to other modes is negligible and the taper is considered adiabatic. In contrast, a taper is considered as "lossy" taper when $z_t = z_b$.

As previously said, light confinement in tapers is lost when the core is reduced to a diameter comparable to the wavelength of the signal [54, 55]. A more accurate definition for this condition is given in terms of the core and cladding mode cutoffs. In practice, a simplified method to find this point guiding transition is by directly using the physical parameters of the fiber. Then, a cutoff *V*-number (V_{cc}) depending of the core and cladding radii (r_{cl}) can be defined as [55, 68]:

$$V_{cc} = \sqrt{\frac{2}{Ln\left(r_{cl}/r\right)}} \qquad \text{<II.44>}$$

As an example, for typical step-index SMFs with core and cladding diameters of 8.2 and 125 μm, respectively, a value of $V_{cc} \approx 0.85$ indicates when the light starts to couple from the core to the cladding [46].

II.2.2 FABRICATION USING THE FLAME TORCH APPROACH

The tapering process by flame torch is one of the most widely used techniques owing to its low complexity and high potential to fabricate axisymmetric submicron diameter tapers. A large number of tapering techniques have been developed aiming at achieving full control of the shape of the taper to comply with the adiabatic requirement and thus yielding low-loss devices [54, 61, 63-65, 69, 70]. The heat-brushing technique is the most popular approach, and this relies on a flame torch traveling back and forth across the tapering section of the fiber under tensile stretching [54]. A moving torch allows for defining a desired taper shape with high exactitude, which is hard to obtain using only a stationary flame. Improvements of this technique have been developed in order to achieve a better control, avoid imperfections, and possible mismatch generated by every sweep of the flame [63, 64]. The fuels used for the torch are mainly butane or hydrogen gas; while the former

is a low-cost and widely available option, the latter provides a cleaner flame minimizing the generation of potential impurities affecting the surface of the devices.

In the heat-brushing technique, a heating zone over a section of the fiber is produced by a flame torch; simultaneously, the fiber is pulled at both ends in opposite directions. The heating and pulling processes are usually performed sweeping at constant speed and tension, respectively. However, the hot-zone can vary in length to obtain different transition profiles [54, 63, 64, 69]. Heating of the fibers must ensure the necessary softening of the glass in order to be deformable under the applied tensile force. For silica fibers, a temperature of around 1700 °C is required to make sure that the melting point is reached. A schematic of this process is illustrated in Figure II-6.

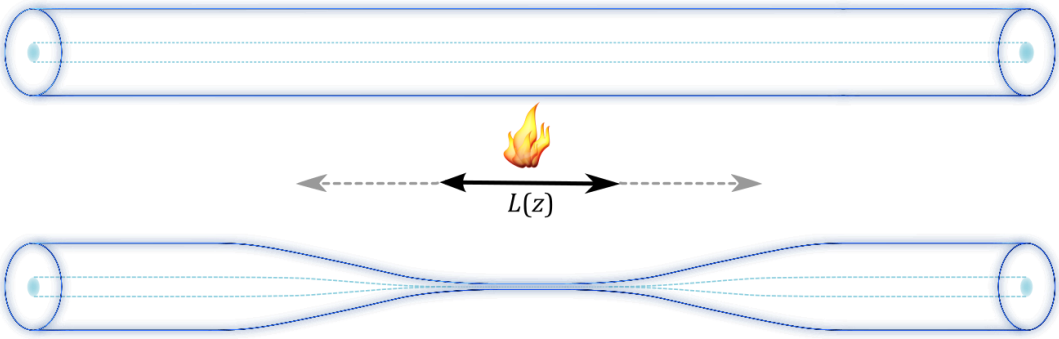

Fig. II - 6. Schematic of the heat-brushing method for tapering optical fibers.

Profiles of the waist radius and transition can be obtained considering conservation of mass as the fiber is stretched over time. The final length of the taper (z_w) will depend on length of the hot-zone (L) and the fiber radius $r(z)$. Initially, the length of the hot-zone is defined as L_0, although this might increase as the process takes place. The condition for an adiabatic process is taken into account upon considering that $\left|\partial r/\partial z\right| \ll 1$. Following the considerations of mass conservation, the variation of the waist radius (r_w) along the total extension of the fiber is given by [54]:

$$\frac{dr_w}{dz} = -\frac{r_w}{2L} \qquad \text{<II.45>}$$

At the end of the process, the length of the waist (l_w) will be the same as the length of the hot-zone or final scanning length of the torch. Thus, the variation of r_w is obtained integrating <*II.45*> with an initial condition $r_w(0) = r_0$, where r_0 is the initial radius of the fiber, and an adjustable hot-zone length $L(z)$. The resulting expression is:

$$r_w(z) = r_0 \exp\left[-\frac{1}{2}\int_0^z \frac{dz}{L(z)}\right] \qquad \text{<II.46>}$$

Further simplifications can be considered from this expression: a *constant hot-zone* is obtained when the swept length of the torch is fixed, and a *linear hot-zone variation* results when the initial and final

torch swept lengths are different. Both practical scenarios can be represented mathematically considering [54]:

$$\begin{aligned} L(z) &= L_0, && \text{constant hot-zone} \\ L(z) &= L_0 + \alpha z_w, && \text{linearly variable hot-zone} \end{aligned} \qquad \text{<II.47>}$$

Using these expression in <*II.46*> and upon integration we obtain:

$$r(z) = \begin{cases} r_{cl} e^{-\left(\frac{z}{L_0}\right)}, & \text{constant hot-zone} \\ r_{cl}\left[1 + \dfrac{2\alpha z}{(1-\alpha)L_0}\right]^{-1/2\alpha}, & \text{linearly variable hot-zone} \end{cases} \qquad \text{<II.48>}$$

where α is a constant indicating the relative rate of the hot-zone change and the taper elongation. It is worth to name special cases for certain values of α resulting in very well defined shapes:

- $\alpha = -0.5$, linear transitions to the waist diameter.
- $\alpha = 0$, exponential transitions (same case as a constant hot-zone).
- $\alpha \to 1$, no transitions, an abrupt change to the waist diameter.

The flame torch tapering approach is ideal for tapering small diameter fibers (e.g., standard SMF with 125 μm) and reaching submicron sizes. However, if thicker fibers or glass elements are to be tapered, other methods have proven to be more effective.

II.2.3 FABRICATION USING THE LASER ABSORPTION APPROACH

An alternative to the flame torch technique is the use of light-induced heating by means of a laser source. This technique is based on absorption of light by the materials of the fiber and the subsequent increase in temperature. For silica-based fibers the most commonly employed type of laser is the CO_2 laser, operating in the mid-infrared wavelengths [71]. Among other advantages, this approach provides highly localized heating, quick adjustment of the temperature, and does not require special operational environments. Because the heat source is a light beam, optical elements such as lenses and mirrors can also be used to reshape the beam spot and adjust the hot-zone.

Until recently, the most popular use for CO_2 lasers in fiber optics was the fabrication of fiber devices such as long period gratings, as well as for collapsing photonic crystal fibers [72]. Due to the capabilities of this approach to obtain a localized heating section, as well as the possibility to control the temperature in a precise manner, CO_2 lasers have recently become an attractive solution for fabrication of tapered-fiber devices. In contrast to the flame brushing technique, the CO_2 laser remains at a fixed position while the fiber is pulled and displaced across the hot-zone to achieve the desired shape in the taper [71, 73]. This is known as the heat-and-pull method.

A reduction in the diameter of the fiber is achieved by pulling and feeding the material at different speeds. This process modifies the diameter of the fiber when passing through the hot-zone, relying on mass conservation. The initial and final diameters of the device, d_1 and d_2 respectively, are related to the pulling and feeding speeds, v_1 and v_2 respectively, as $\left(d_1/d_2\right)^2 = v_1/v_2$. Speed variation profiles will determine the shape of the transitions. An illustration of the heat-and-pull technique is shown in Figure II-7.

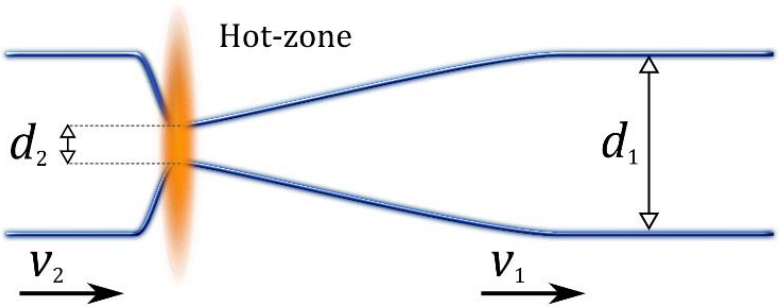

Fig. II - 7. Illustration of the heat-and-pull technique used for fiber tapering.

II.2.4 LIGHT COUPLING IN TAPERED FIBERS

Evanescent wave coupling is typically used to fabricate splitters/combiners, long period gratings, resonators, and nonlinear components [56, 57, 60, 61]. In the context of this work, the operational principle of the fabricated fiber devices is explained in terms of the evanescent coupling effect. Let us begin with the case of two parallel fibers fused and tapered down together. The crucial section of the device to analyze is the transition section as opposed to the waist section, where light will actually be guided by the resulting fused structure. Initially, both fibers are in contact but they are independent waveguides, without light coupling between the cores, as depicted in Figure II-8a.

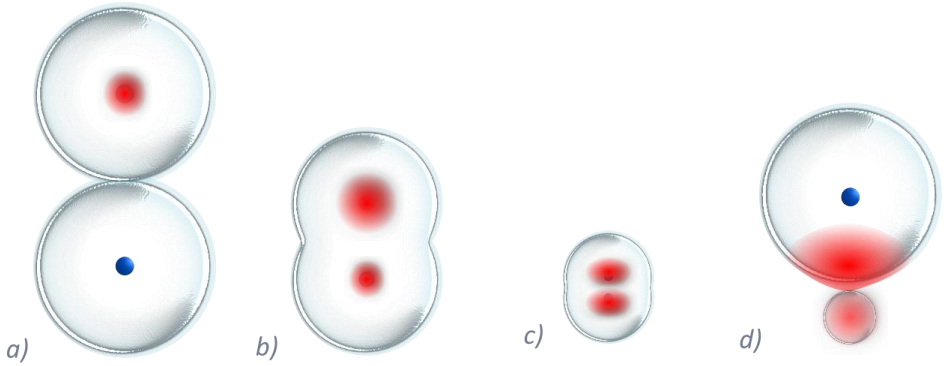

Fig. II - 8. Illustration of the cross section of two optical fibers fused and tapered together: a) both fibers before tapering launching light in one of the fibers, b) transition section with the formation of "supermodes", and c) waist section forming a higher order mode. Light coupling by from a tapered fiber to another proximate non-tapered fiber.

As both fibers are subjected to the heating and pulling processes, they begin to fuse forming a new structure composed by both cores and claddings. Along the transition section, there will be a point at

which light will start coupling from one core to the other. For some adequate length of this section, directional coupling will occur (Figure II-8b) [56, 74]. This particular section of the device will then present a combination of the individual modes (spots) of the cores, resulting in the so-called *supermodes* [75, 76]. The supermodes are a superposition of isolated modes habitually analyzed as light spot arrays. If the tapering process continues, the supermodes evolve into fiber modes at the resulting structure, as shown in Figure II-8c (e.g., the waist of a fused coupler) [56, 75, 76]. Following this example, a larger number of fibers can then be combined together and scaled to a larger number of cores. Similarly, if one fiber is tapered down to the point at which light starts leaking from the core and remains guided in the cladding material, then an external structure can be placed in close contact to transfer the energy, as illustrated in Figure II-8d [70, 77]. These effects are used to fabricate photonic lanterns and fiber micro-resonators, both explained in the following sections.

CHAPTER III: PHOTONIC LANTERNS

The photonic lantern (PL) is a spatial mode converter connecting multiple single-waveguide cores to a multicore array. A more common way to describe a PL is to refer to it as a device capable of coupling light from multiple single-mode fibers (SMFs) to a multimode fiber (MMF), and vice versa [23, 78]. These devices were foremost developed for astrophysics to capture starlight using the multimode end and then decompose it on multiple single-Gaussian modes [79, 80]. Later on, these devices found their use in the telecommunications area serving as multiplexer (MUX) and demultiplexer (DEMUX) for Spatial Division Multiplexing (SDM) applications. This application in particular encouraged the improvement of these devices for achieving a more rigorous control over the modal features obtained at the output end, such as mode selectivity.

Fabrication of fiber photonic lanterns is done by constructing a circular array of multiple fibers, fusing and stretching them together until the multicore fiber array is formed. Different methods have been explored to form fiber bundles to accomplish the creation of PLs. The first method consisted in using a silica cane with an array of air holes, similar to the one employed for photonic crystal fibers fabrication, allocating individual fibers within the cane and the resulting MMF was surrounded by air [79]. Onward fabrication processes made use of low-refractive index glass capillaries to enclose all the fibers, resulting in the creation of a complete few-mode or multimode structure at the tapered end [23, 81, 82]. An extra method to fabricate the PLs was accomplished by making use of multicore fibers fabricating a single structure, where upon tapering the structure the multimode (MM) section was then generated [23]. Alternatively to this last procedure, a photonic crystal fiber with multiple cores was used as well, collapsing the air holes to generate a MM section [23, 83].

This chapter covers the principles of operation, design, and construction of the PLs. Different devices fabricated using the heat-and-pull technique are described and the influence of the fabrication parameters in their modal features are explained. Finally, the characterization of the fabricated PLs and integration to fiber systems is presented.

III.1 PRINCIPLES OF FABRICATION AND OPERATION

The basic principle in which the photonic lanterns are based is in the fusing and tapering of individual fibers. This process generates light coupling among the separate cores of the fibers yielding a characteristic pattern of light in the resulting structure, which depends mostly on the coupling and propagation conditions. For this reason, the fabrication parameters will define the characteristics at the tapered end of the device. Because one of most popular uses for the PLs is in

telecommunications applications, it is of great interest to achieve operation in wavelengths around λ = 1550 nm.

The fabrication method used in this work is based on stacking single-mode optical fibers within a glass capillary. Due to wave guiding conditions, the glass capillary must have a lower refractive index than that of the cladding material of the fibers. Once the fibers are placed inside the capillary, the resulting assembly is then tapered down and fused together until the whole structure collapses. As a consequence, a waveguide with multimode structure is formed at the tapered end, with the low-index glass capillary serving as the new cladding for the SMFs material, which in turn functions as the new core. A schematic representation of a PL can be seen in Figure III-1. The spectral features of the lantern are determined by the following aspects:

- The number and type of fibers used for its construction.
- The position of the fibers inside the capillary.
- The characteristics of the capillary such as refractive index, dimensions, and inner diameter.
- The tapering ratio.

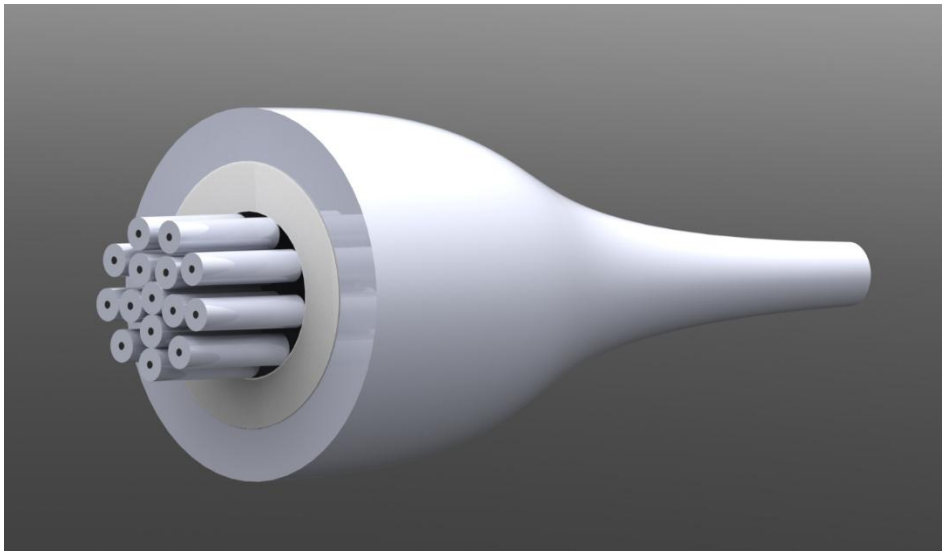

Fig. III - 1. Illustration of a Photonic Lantern formed by N input SMFs at one end, merging to originate a MMF capable of support M number of modes at the output end.

The losses in PLs can be evaluated from the point of view of brightness conservation by analyzing light coupling from the SMFs to the MMF, and vice versa [23]. An ideal device will conserve all the energy when operated in both directions. For accomplishing a low-loss system, the number of input modes (M_{IN}) and output modes (M_{OUT}) requires to fulfill the condition:

$$M_{IN} \leq M_{OUT} \qquad \text{<III.1>}$$

Given this, for a number of input modes larger than those supported at the output, there will be some light that will not couple and will be radiated outside the lantern. An ideal scenario is to have a system

where $M_{IN} = M_{OUT}$. Notice that this condition does not allow a device with a SMF as an input able to excite all the modes supported by a MMF at the output. Conversely, it is not possible to have a device with a MMF input capable of couple all of its modes into a sole SMF. Considering an adiabatic taper and identically SMFs, the number of fibers used (N) will determine the number of excited modes at the output MMF [23, 78, 79]. Therefore, according to the directionality, light propagation in PLs in terms of the individual number modes at the single-mode fibers (M_{SM}) and the multimode side (M_{MM}) can be summarized by [23, 84, 85]:

$$\begin{aligned} M_{SM} &\geq M_{MM}, \quad \text{from MMF to SMFs} \\ M_{MM} &\geq M_{SM}, \quad \text{from SMF to MMFs} \end{aligned} \qquad \text{<III.2>}$$

Determination of the excited transmission modes is given by the fiber positions that match those corresponding to the excitation of the supermodes. For cylindrical geometries, spot arrays originating supermodes and evolving into LP fiber modes capable of couple to FMF has been carried out in previous works by Ryf et al. [84]. These spot positions must follow a very specific configuration depending on the number of LP_{lm} modes. The correct core geometry is formed with a ring equal to the radial index m, adding a spot at the center every time that m increases. Each one of these rings consists of a number of fibers following the rule of $2l_{Max}+1$, where l_{Max} is the largest value of the azimuthal index, l, for each value of m. The positions for the fiber array scaling up to the lowest nine LP fiber modes including one spot for every non-degenerate mode and two spots per degenerate mode, are shown in Figure III-2. It is important to emphasize that a correct configuration of the fibers inside the capillary must be achieved; otherwise the spot array will evolve into different supermodes. Excitation of different supermodes will lead to LP fiber modes that are not supported by the multimode fused structure, leading to losses by radiation modes. The appropriate locations of the spot arrays have been tested by numerical simulations including modal analysis, coupled mode theory, and beam propagation method (BPM) [75, 76, 85,].

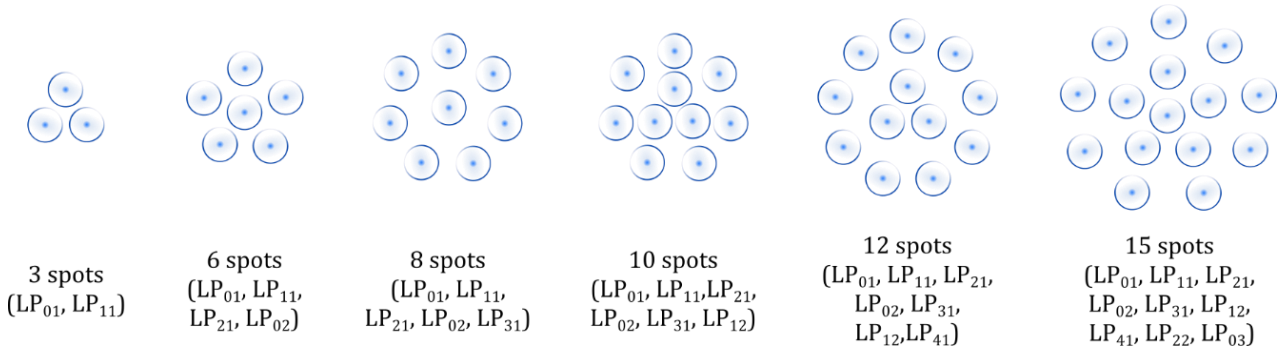

Fig. III - 2. Spot arrangements of supermodes to excite fiber LP modes [84].

The low-refractive index capillary in the PL is a key component serving for a couple of functions. Firstly, it serves as container for the fibers, and the inner diameter must be adequate to contain the required number of the fibers necessary to obtain the desired number of LP modes. The thickness of the capillary is also important to guarantee a complete confinement of the evanescent wave, and the

outer diameter must also be adequate to end up with a proper final diameter compatible with FMFs for further coupling. The second function of the capillary is for the definition of light propagation in the MM tapered end. In this case, the relevant parameter to consider is the difference in refractive index between the glass capillary and the fibers (Δn); this affects the *V*-number and hence, the number of modes allowed at the tapered end.

Given the previous considerations and following the tapering process and adiabatic conditions exposed in sections II.2.1 and II.2.2, formation of the modes takes place at the transition section. For a better description of the process, let us consider the case of a device consisting of two fibers (stage *I*). As the whole structure fuses together and starts to reduce in size, the effective refractive index (n_{eff}) decreases causing a less confined single-mode at each of the SMF cores evolving into *N* degenerate supermodes (stage *II*). When the reduction in the cores is such that light extends considerably into the surroundings, interaction with the neighboring cores starts to take place leading to energy coupling (stage *III*). In this exact stage of the tapering process, the number of supermodes (*N*) starts to split into a number of *N* non-degenerate modes. If the tapering process is continued after this stage (*IV*), the structure will have smaller cores reaching the core-mode cutoff, and a different n_{eff} for each non-degenerate mode depending on the surrounding cores. At this stage light guidance is determined by the low-refractive index capillary. Once this point is reached, the cores will no longer guide light and will couple to the whole structure, causing that each non-degenerate mode will evolve into *N* LP fiber modes [23, 78]. Then, the final diameter of the lantern is obtained from the tapering ratio established during the design stage of the device (stage *V*). Figure III-3 illustrates the energy coupling process and mode evolution along a tapered structure.

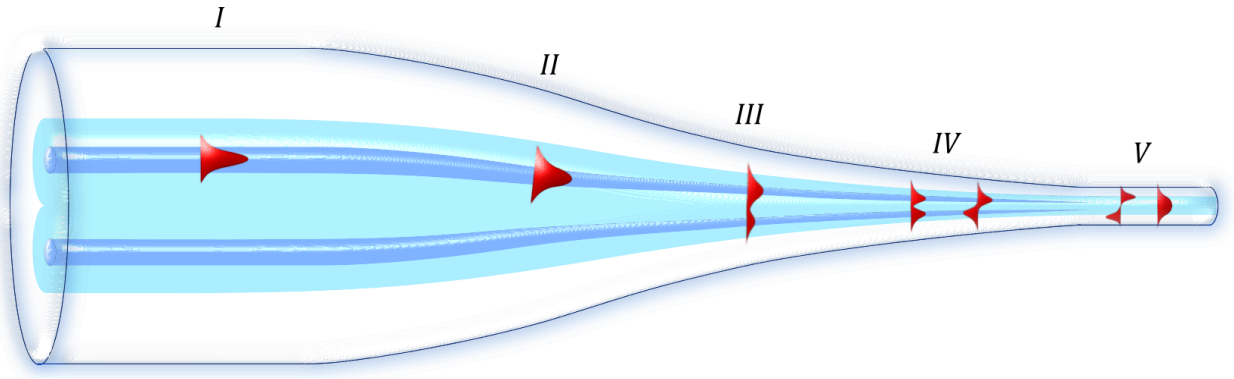

Fig. III - 3. Illustration of the energy coupling and mode evolution at tapering process of the PLs at different stages.

Along with Δn, the final radius of the new core of the MM side of the lantern also plays a role in the number of modes that will propagate. An estimation of the number of modes supported at the multimode side of the lantern can be obtained using Eq. *<II.38>*. The number of fibers used for the construction of the PL also determines the size of the core since the material of each fiber contributes in its formation. Figure III-3 shows light coupling at the different stages of the fabrication process; whereas in Figure III-4, the microscope images of a three fiber PL using identical fibers at different stages of the fabrication process are presented. A more descriptive theory of the power coupling occurring at the transition of a fiber array can be found in [82].

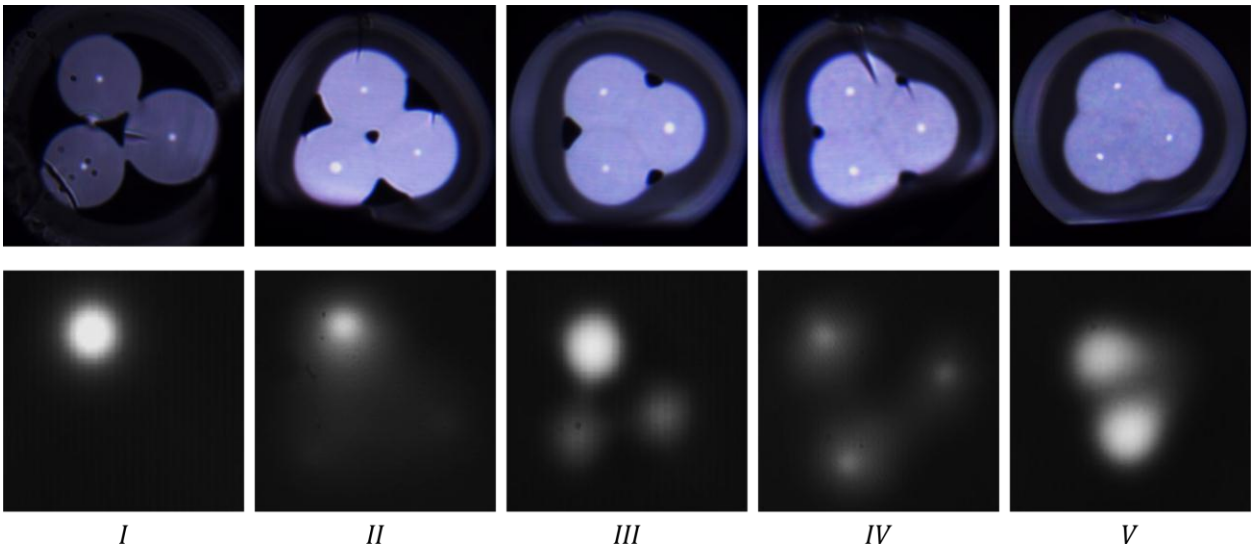

Fig. III - 4. Microscope pictures of the cleaved end facet from a three fiber PL showing the energy coupling and mode evolution at different stages of the tapering process.

III.1.1 MODAL FEATURES

A better understanding of how light evolves from a SM to a MM signal requires modal analysis. Works performed by León-Saval et al. [78, 86] and Fontaine et al. [87] demonstrate how mode evolution takes place along the tapered region upon considering a change in the modal effective refractive indices, n_{eff}. The simplest scenario illustrated in the previous section is when all the SMFs are identical and thus, the propagation constants for each core are the same along the whole structure. Under these conditions, light will start to couple from each fiber to the multimode structure in the same region of the taper. Then, the allowed degenerate modes will start to originate almost simultaneously and propagate through the fused part. Eventually, at certain point of the tapered section the mode effective index splits for each mode group, originating a break in the degeneracy of the modes. To exemplify this, Figure III-5 shows a plot illustrating the mode evolution for a photonic lantern fabricated with three identical SMFs [86].

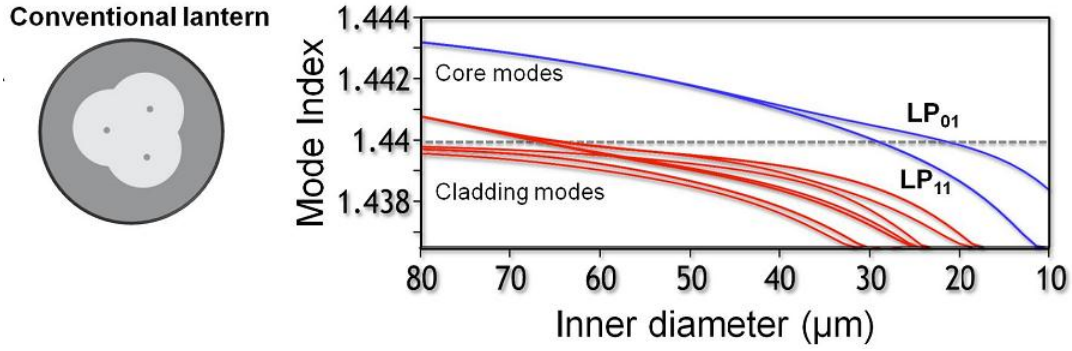

Fig. III - 5. Modal evolution simulations for a PL formed by three identical SMFs. Blue and red lines indicate the modes propagating through the core and the cladding, respectively. Taken from [86].

PLs fabricated with identical fibers will present a certain degree of coupling to all the possible modes of the MMF upon launching light into each of the SMF cores. Therefore, the output signal will be a light pattern composed by the superposition of all the modes. Depending on the core position inside the fiber array, preferential coupling can also occur since the light coupling will take place at different positions within the fiber array. Also, scrambling among the modes is caused by structural imperfections that may occur during the fabrication process [78, 86].

III.1.2 MODAL SELECTIVITY

Control over mode generation is a desirable feature in multimode devices and systems. Mode-selective photonic lanterns (MSPLs) are devices in which each individual input fiber excites only one LP mode at the MM tapered end without any mixing among the supported modes [86, 88]. Devices with such a feature require different coupling condition for each individual core along the transition of the tapered section, thereby providing a different evolution of the propagated modes. To obtain MSPLs, it is necessary to break the degeneracy between the modes of the uncoupled cores, as well as to provide different propagation constants for each mode. Both of these conditions must be maintained across the entire transition section of the PLs [86].

Mode selectivity in PLs can be accomplished during the fabrication process by generating different propagation constants in each fiber. This generates different propagation conditions for the fundamental mode in each SMF, which in turn will determine the mode to be excited at the MM output. In other words, each propagation constant (β) in the SMFs will become the propagation constant of one LP mode at the MM end. This difference in propagation constants must be adequate to excite different LP modes in the PLs. For these devices, the largest β will correspond to the lowest order LP mode of the structure, and the smallest β will correspond to the highest LP mode [86]. A way to achieve this condition is to use dissimilar fiber cores for the construction of the fiber array, which can be accomplished in the following ways:

- Using identical core diameters but different Δn.
- Using different core diameters but the same Δn.
- Using a combination of both.

In principle, addressing each of the LP modes, including the two degenerate modes *a* and *b* when this is the case, will require one fiber per mode. This of course would require a large number of fibers for the lantern assembly. Thus, a simplification to achieve this objective consists in only employing a core size for every LP mode, and breaking the degeneracy of the LP_{lma} and LP_{lmb} modes with a proper tapering ratio in the MM end structure. Therefore, the required tapering length is also decreased since the degeneracy of the modes is broken. To illustrate the modal evolution of a MSPL, a plot from [86] is shown in Figure III-6, demonstrating the modal refractive indices from a PL constructed with

different sizes for the fiber cores. In this instance, a large core size is used to excite the LP_{01} mode and the small core sizes are used for the LP_{11} modes.

Another kind of mode-selective photonic lanterns can be obtained generating selectivity by mode groups, leading to the generation of mode-group-selective photonic lanterns (MGS-PLs). These devices contemplate modes contained in the same group mode that can be addressed using only one fiber core diameter. The capability to excite all the corresponding modes in that group arise due to the similar propagation constants in the modes within the same group mode (see Figure II-2 and Table II-2) [89]. MGS-PLs are useful when the fibers in transmission systems generate mixing among all the modes contained in the same mode group, and independent excitation of each degenerate mode is unnecessary.

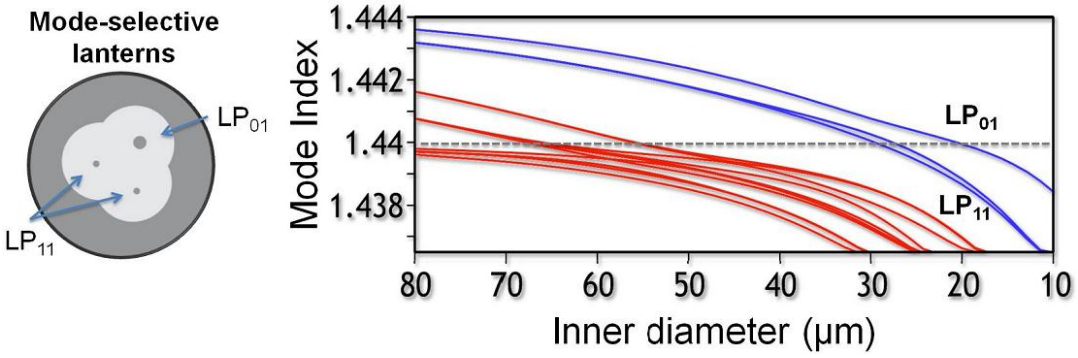

Fig. III - 6. Modal evolution simulations for a mode-selective PL formed by dissimilar fibers. Blue and red lines indicate the modes propagating through the core and the cladding, respectively. Taken from [86].

The modal evolution of the modes propagated inside the core of a PL and a MSPL can be observed in Figures III-5 and III-6. By comparing both plots, a difference in the mode effective index at the beginning of the tapering process, caused by different values of β, is notorious when dissimilar fibers are used for a MSPL. The use of different fibers avoids the mixing of the propagation constants between both LP modes and the LP_{11a} and LP_{11b} modes are separated at the end of the tapered section. For this reason, individual excitation for each of the three modes is accessible through different fibers without the generation of modal mixing.

Construction of the MSPLs requires two fibers for the excitation of the corresponding degenerate modes for each LP mode, with exception of the LP_{0m} modes. Excitation of each non-degenerate mode is successfully achieved by only one corresponding fiber core size. Given the vertical symmetric distribution of the fibers inside the low-index capillaries, the fibers intended for excite the same LP mode are expected to be placed in reciprocal positions, considering as a reference a vertical axis crossing through the center of the fiber array. This can be observed in the MSPL schematic shown in Figure III-6.

In some cases, fibers with larger cores can also be used with the purpose to generate different propagation constants and obtain mode selectivity in the PLs. However, this results in multimode propagation within these fibers. Hence, care must be taken in order to excite only the fundamental mode and thus obtain proper single-mode coupling within the PL. Nonetheless, excitation of the

fundamental mode is achieved by carefully alignment, considering their operation in the single-mode regime.

III.2 FABRICATION AND MODE PROFILES

Fabrication and characterization of PLs devices were done in two laboratories: the Microstructured Fibers and Devices Laboratory, under the supervision of Dr. Rodrigo Amezcua-Correa and Dr. Axel Schülzgen, at CREOL, the College of Optics and Photonics at the University of Central Florida (UCF), USA; and in the Optics Communications Laboratories under the supervision of Dr. Nicolas Fontaine and Dr. Roland Ryf, at Bell Laboratories/Alcatel–Lucent, USA. The relevant details of the fabrication process of these devices will be covered in the following sections.

III.2.1 ASSEMBLY AND TAPERING STATIONS

Assembly of the photonic lanterns starts by placing the required number of SMFs inside the capillaries. These must be placed in the correct positions according the desired number of modes at the output of the PL. An assembly station consisting of positioning and visualization systems was built to carry out these actions. The capillaries or microstructured preforms are placed in a special holder serving also for protection and transportation of the assembled structure (A). The fibers are inserted without the polymer coating and are fixed on a V-groove on top of the positioning system. The latter is further contained in an XYZ-translation stage with fine movement (B). An optical microscope with a long work distance objective comprises the visualization system (C); this is intended to achieve the correct placement of each fiber within the structure. Once the fibers are set on the correct position, an additional long-travel linear translation stage (D) is used to insert completely the fibers inside the capillaries. Additional elements enhancing the station capabilities include adequate illumination (E) and an electrostatic suppressing system (F). A photograph of the system is shown in Figure III-7.

Some of the advantages using this station include the visual inspection of the capillaries and microstructured preforms for identifying possible structural defects. Also, examination of the correct positioning of the fibers along the entire length of the capillary allows finding bends, twists, or obstructions of the fibers, which originate mode mixing and losses. Another advantage of the station is that it minimizes the hand manipulation of the bare fibers within the capillaries, thereby reducing contamination sources for the assemblies.

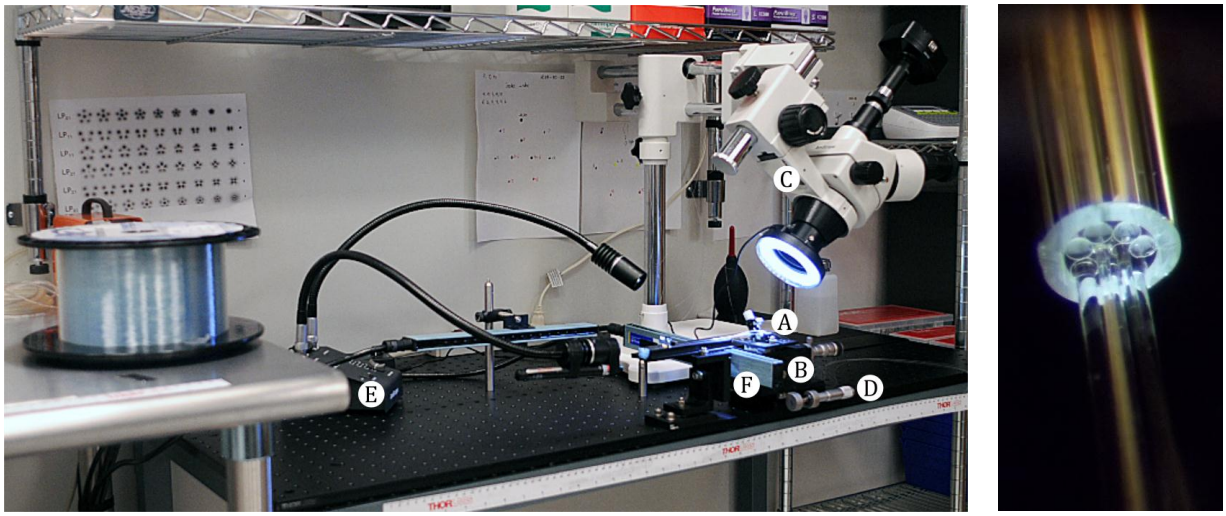

a) *b)*

Fig. III - 7. PLs assembly station. a) Photograph of the system, and b) fibers being placed inside a microstructured preform.

After assembling the fibers/capillary structures these were cleaned and placed inside a glass processing station. Figure III-8 shows images of the tapering station used to fabricate the PLs. This is an AFL Fujikura LZM-100 LAZERMaster that uses a CO_2 laser to fuse and taper optical fibers and glass rods/capillaries, and is able to taper cylindrical glass elements with diameters of up to 2 mm [90, 91]. The operational principle of the station is based on the heat-and-pull method, incorporating a thermal imaging system, which allows for real-time monitoring of the element under heating. Operation of the system is carried out by computer control allowing to set the relevant fabrication parameters, such as initial and final diameters (d_1, d_2), pulling speeds (v_1, v_2), taper section lengths, and laser power. Upon programing these parameters in the control software results in a repeatable process and hence allows the production of devices with the same features. After the PLs are tapered to their final diameter, the section of the second transition has to be removed. This is done in the same tapering station with an in situ cleaving process performed by scribe-scratching and pulling at a controlled velocity.

In the subsequent sections, the general procedure for the assembly of PLs with 3, 6, 10, and 15 fibers is described. The requirements to obtain modal selectivity with these devices are also covered.

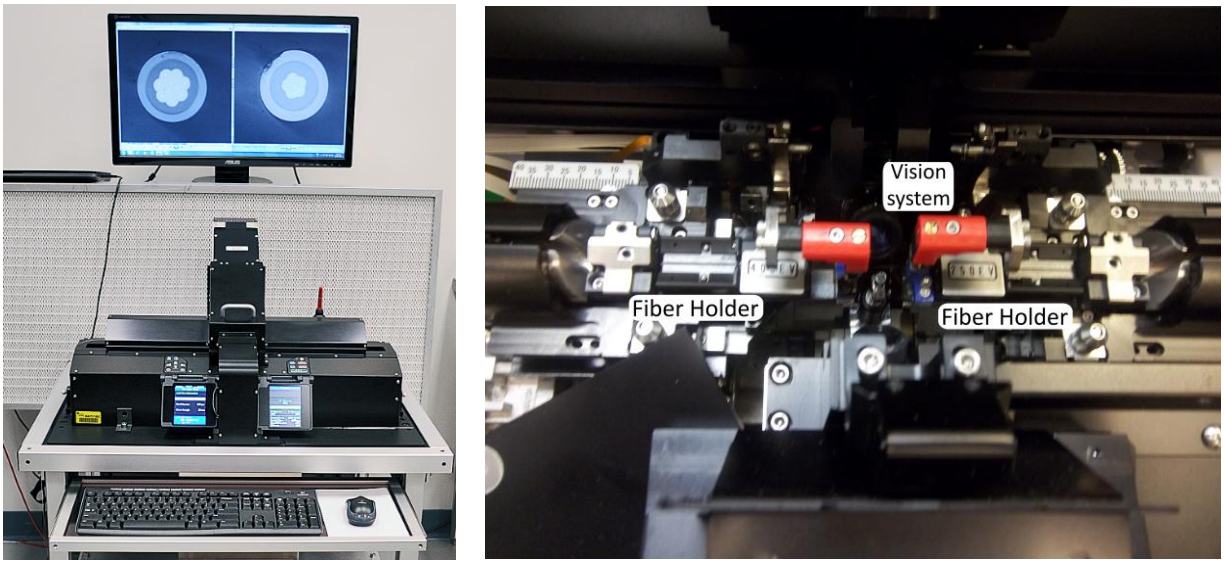

a) *b)*

Fig. III - 8. CO_2 laser tapering station: a) AFL LAZERmaster LZM-100, and b) internal system.

III.2.2 CAPILLARIES AND MICROSTRUCTURED PREFORMS

The glass capillary in the PLs provides support and adequate enclosing for the optical fibers within a lower refractive index material (Figure III-9). Low-refractive index capillaries include an inner fluorine-doped layer, which has a refractive index lower than that of silica. Typically, the fibers are placed in the capillary forming a hexagonal array; however, some configurations to obtain specific modal patterns require fiber positions that will not fit in a hexagonal pattern (see Figure III-2) [80, 84]. This limitation is overcome using capillaries with custom inner structures capable of holding the fibers with the required geometrical arrangements. PLs requiring these *microstructured capillaries* arrangements are those with two or more fiber rings and more than one fiber at the center of the array [92]. In general, PLs with eight or more optical fibers require the use of these microstructured capillary arrays. In this work, we fabricated PLs with ten and fifteen optical fibers.

Construction of the microstructured preforms is based on stacking synthetic silica capillaries within the fluorine-doped tube. These are placed according to the theoretically estimated positions for ten and fifteen supermodes [84]. Thin silica glass capillaries with high air filling fraction (ID/OD > 0.95) were used to minimize the inclusion of additional silica material around the fibers, and preserving the distance between cores for subsequent coupling. The structure of a preform with ten fibers consists of a central array of three capillaries (ID = 110 μm) forming a triangular geometry. These are then surrounded by a ring array of seven capillaries with an ID = 170 μm. The resulting preform is then a structure with an OD of 900 μm (see Figure III-9b). For the preform using fifteen fibers, the structure requires two arrays of capillaries (ID = 145 μm) forming concentric rings of nine and five capillaries for the outer and inner rings, respectively. This preform also includes additional silica rods to fill any air gaps between the capillaries and the central region is left empty to hold the fifteenth

fiber. The resulting structure is a preform with an OD ~ 2 mm. Optical microscope pictures of the ten and fifteen microstructured preforms can be observed in Figure III-9 compared with a normal fluorine-doped capillary.

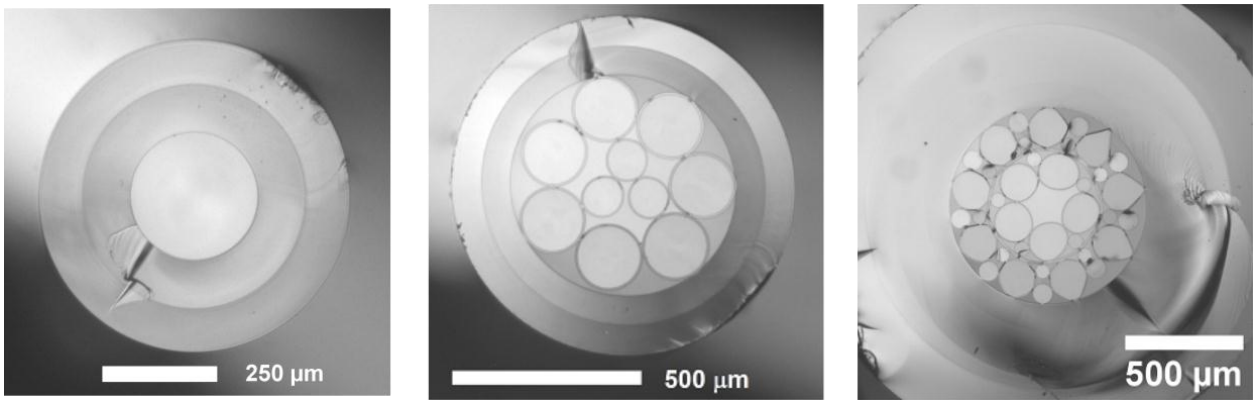

a) *b)* *c)*

Fig. III - 9. Optical microscope images from the glass capillaries used in the construction of PLs: a) capillary with a fluorine-doped inner layer used in low-order modes photonic lanterns, and microstructured preforms for higher-order modes lanterns, b) ten and c) fifteen modes.

Along with the special capillaries, a collection of fibers with different outer and core diameters were fabricated intended to fit special places within the fiber array in order to generate mode-selective lanterns. An increase in the number of modes requires increasing the tapering length and as a consequence the fabrication complexity also increases [83]. Graded-index fibers (GIFs) allow for larger core sizes with smaller effective mode areas for the LP_{01} mode compared to step-index fibers. Thus, the use of GIFs for PL fabrication reduces mode coupling along the tapered transition, shrinking the length required to achieve an adiabatic transition [23, 93]. For this reason, all the PLs fabricated used GIFs with $\Delta n = 16\times10^{-3}$, unless it is mentioned otherwise. The effects of using step- or graded-index fibers for PLs fabrication are demonstrated for MSPLs of three and six modes in subsequent section. All the fibers and capillaries used in this work were fabricated in the fiber draw facilities at CREOL.

III.2.3 THREE FIBERS PLS – 2 LP MODES

The basic situation when constructing photonic lanterns requires using only three fibers inserted in the capillary. Distribution of the fibers takes place in a triangular fashion resulting in a symmetrical pattern; in this case, fibers with identical outer diameters fit adequately within the capillary. PLs formed by only three fibers are capable of exciting only two LP modes: LP_{01} and LP_{11}. Assembly of these PLs consisted in placing fibers with an outer diameter of 125 µm in no particular order within the capillary and then tapering the structure to its final diameter. The fluorine-doped capillary had a $\Delta n = -9\times10^{-3}$ and an ID = 275 µm, resulting in a PL with NA = 0.16. The fabrication parameters to successfully obtain three modes PLs required a tapering ratio of 10 with a transition

section of 50 mm. The end facet of a three modes lantern cleaved at the waist section can be seen in Figure III-10a, showing the triangular geometry of the core with an approximate diameter of 22 μm.

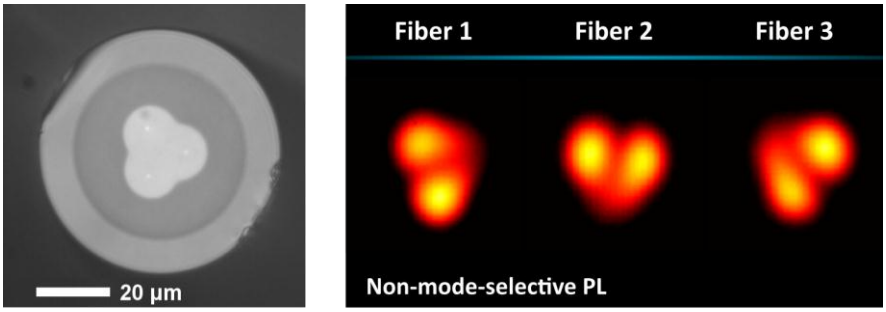

Fig. III - 10. Three fibers photonic lantern. a) End facet cleaved at the waist section. b) Near filed mode profiles from a non-mode-selective PL at 1550 nm.

Upon coupling light from a superluminiscent diode centered at 1550 nm into each of the input fibers, it was possible to observe the near field mode profiles at the output end. As expected, the devices fabricated using standard step-index SMFs yielded a response with no modal selectivity. As shown in Figure III-11b, the same light patterns are observed when exciting each of the fibers. This is because each fiber shares the same neighboring conditions (i.e., each fiber has two nearest neighbors). A triangular shape in the output mode profiles is noticeable owing to the geometry of the PL core obtained when the capillary collapses and the air gaps within the fibers are filled.

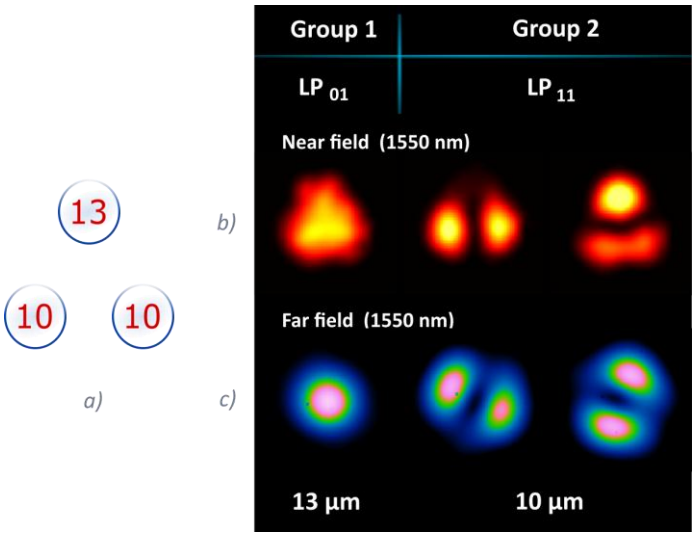

Fig. III - 11. Three modes mode-selective photonic lantern. a) Fiber core positions, b) near field mode profiles, and c) far field mode profiles at 1550 nm.

To generate mode selectivity in this kind of PLs, only one of the cores must have a different size. Using GIFs and a fiber with larger diameter than the ones of the other two fibers, a mode-selective photonic lantern was thus fabricated. The fiber cores for this device were 13 and 10 μm, aiming at exciting the LP_{01} and LP_{11} modes, respectively. The near field mode profiles at the output of the PL and the fiber

positions inside the capillary are shown in Figure III-11a and 11b. The evolution of the mode profiles is observed in the far field mode profiles shown in Figure III-11c.

The mode profiles clearly show that the two identical fibers used to excite the same LP_{lm} mode, produce the corresponding degenerate modes at the output of the PL. In this particular case, the LP_{11a} mode is generated by one of the 10 μm fiber, whereas the LP_{11b} mode is obtained upon launching light through the other 10 μm fiber.

III.2.4 SIX FIBERS PLS – 4 LP MODES

Handling a larger number of modes in photonic lanterns demands the use of more optical fibers inside the capillary. The LP modes that can be excited in PLs with six fibers include the LP_{01}, LP_{11}, LP_{21}, and LP_{02}. For these PLs, the arrangement includes a central fiber with a smaller diameter than the surrounding five fibers used to complete the array. Hence, the fibers inserted in the fluorine-doped capillary include five 125 μm OD fibers surrounding an 83-86 μm OD fiber. The 375 μm inner diameter fluorine-doped capillary had a $\Delta n = -9\times10^{-3}$, yielding a photonic lantern with NA = 0.16. A tapering ratio of 11.3 with a transition section of 60 mm was required for obtaining these devices. The core diameter for these PLs was around 27 μm, as observed in the cleaved end facet shown in Figure III-12a. The near field mode profiles from non-mode-selective PLs constructed using fiber core diameters of 13 μm are shown in Figure III-12b. Notice that the excitation of each fiber produces a different mode profile in spite of using identical core diameters. The reason of this effect is due to the different number of neighboring fibers for each one of the fibers forming the PLs.

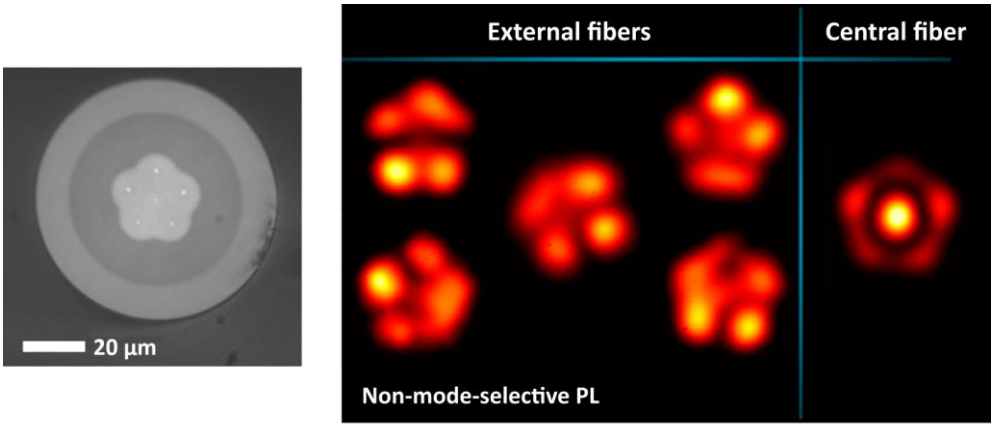

Fig. III - 12. Six fibers photonic lantern. a) End facet cleaved at the waist section. b) Near filed mode profiles from a non-mode-selective PL at 1550 nm.

For the fabrication of MSPLs, four different core diameters (20, 18, 15, and 6 μm) were used for exciting the LP_{01}, LP_{11}, LP_{21}, and LP_{02}.modes. The horizontally symmetrical location of the fibers within the arrangement is depicted in Figure III-13a. Typically near and far field mode profiles for a wavelength of 1550 nm obtained at the output of these MSPLs are shown in Figure III-13. For this

case, the core geometry shows a pentagonal distribution, defining the output light patterns observed in the near field mode profiles.

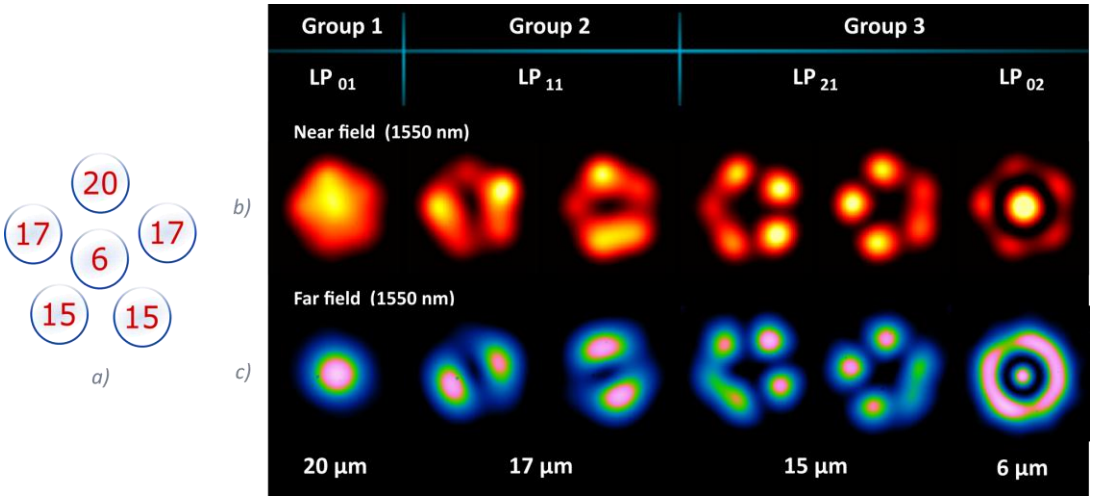

Fig. III - 13. Six modes mode-selective photonic lantern. a) Fiber core positions, b) near field mode profiles, and c) far field mode profiles at 1550 nm.

III.2.5 TEN FIBERS PLS – 6 LP MODES

As mentioned in a previous section, scaling to higher order modes PLs involves more elaborated fiber arrangements. For ten or more fiber devices, the use of microstructured preforms is mandatory due to the complexity of the fiber arrangements (see Figure III-9). For the ten fibers preform, two different fibers were used: 125 µm and 83 µm outer diameters. While the fibers with larger diameter were inserted into capillaries (170 µm ID) forming the outer ring of the preform, the fibers with the smaller diameter were inserted in the three remaining capillaries (110 µm ID). The fabrication parameters used for these PLs include a tapering ratio of 16 and a transition length of 57.5 mm to reach the desired reduction in diameter.

The preform was assembled within a fluorine-doped capillary with a $\Delta n = -16\times10^{-3}$, and with an inner diameter big enough to house the set of smaller capillaries holding the optical fibers. Thus, the resulting PL yielded a MM output with a NA = 0.216 after the fusing and tapering process. As shown in Figure III-14a, the tapered end of the PL exhibits a core size of 27 µm with a more rounded shape when compared to PLs with a smaller number of fibers. As for the devices described previously, a non-MSPL was fabricated using fibers with identical core diameters of 13 µm. The near field mode profiles at the output end are shown in Figure III-14b. As seen in the figure, similar light patterns at the PL output are obtained when the central fibers are excited. In contrast, mode mixture can be clearly observed when light is launched into the surrounding fibers.

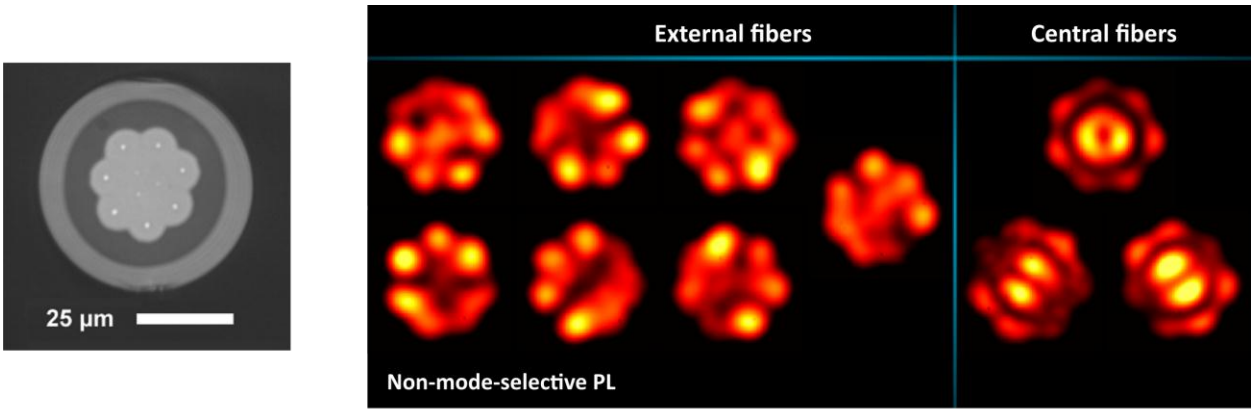

Fig. III - 14. Ten fibers photonic lantern. a) End facet cleaved at the waist section. b) Near filed mode profiles from a non-mode-selective PL at 1550 nm.

The construction of a MSPL with ten fibers results in a device capable of producing the LP_{01}, LP_{11}, LP_{21}, LP_{02}, LP_{31}, and LP_{12} modes. The fibers needed to generate this type of lantern involved core diameters of 23, 20, 17, 9, 13, and 6 µm, exciting respectively the LP modes listed before. For a successful excitation of the LP modes, a specific fiber position was necessary, yielding the core distribution illustrated in Figures III-15a. The light patterns generated at the output of the MSPL can be observed from the near and far field mode profiles shown in Figures III-15b and III-15c, respectively.

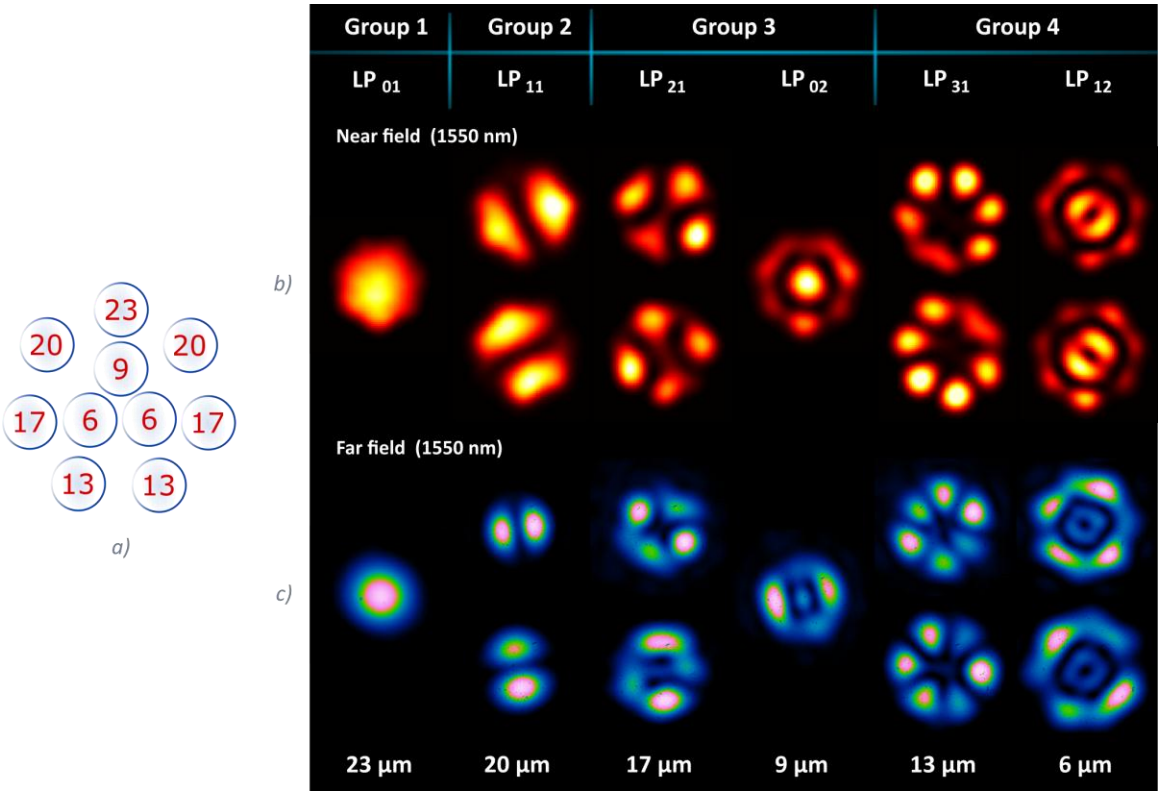

Fig. III - 15. Ten modes mode-selective photonic lantern. a) Fiber core positions, b) near field mode profiles, and c) far field mode profiles at 1550 nm.

A point to highlight for this particular device is the need of a larger core diameter for exciting the LP_{31} compared to the core size used for the LP_{31}. Intuitively, one would expect that the LP_{31} mode would require a smaller core diameter than that used to excite the LP_{02} mode; however, experimental results showed that the opposite was necessary for generating these modes at the MSPL output using these microstructured preforms. This may be due to the fact that dissimilar cladding fiber diameters were used for this device, which in turn may affect light coupling conditions. Numerical studies have shown that the distance among the fiber cores within the structure affect the evolution of the modes propagating along the MSPL [78, 75]. The use of different microstructured preforms, optical fibers, or a combination of both, will change the fabrication parameters.

III.2.6 FIFTEEN FIBERS PLS – 9 LP MODES

The most complex devices to fabricate were the mode-selective photonic lanterns with fifteen fibers. This sort of PLs was also constructed using a microstructured preform capable of allocating all the required fibers, forming an array of three concentric layers (see the 15-spot array shown in Figure III-2). The fabricated preform had a $\Delta n = -9\times10^{-3}$ and the glass capillaries had the proper dimensions to enclose fibers with 125 μm cladding diameter. Fabrication parameters for these PLs comprised a tapering ratio of 20, requiring a 6 cm-long transition section. With these parameters, the output end of the device is multimodal with 35 μm core diameter, as shown in Figure III-16a. Notice that in contrast with previous devices, the fifteen fiber array yields a PL with circular core geometry.

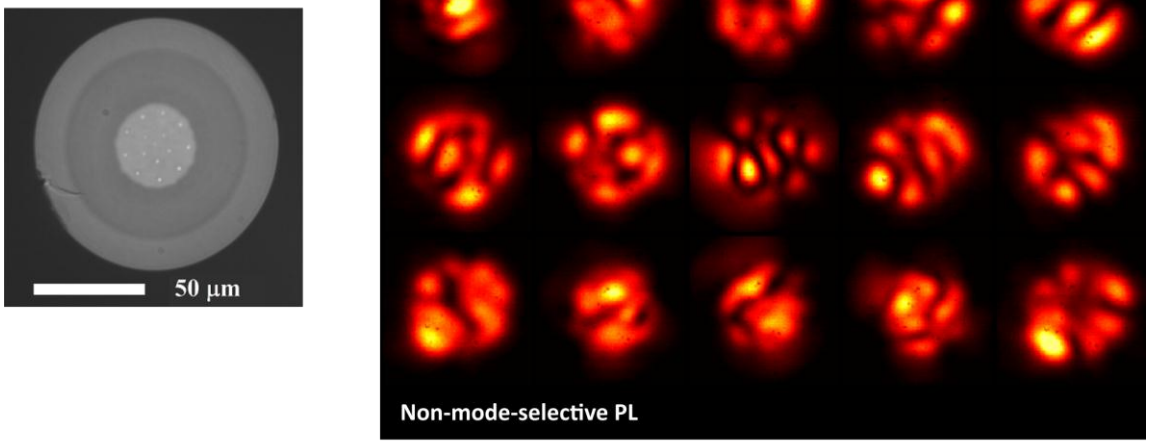

a) *b)*

Fig. III - 16. Fifteen fibers photonic lantern: a) End facet cleaved at the waist section. b) Near filed mode profiles from a non-mode-selective PL at 1550 nm.

As in previous cases, we first fabricated a PL without modal selectivity, using fifteen fibers with the same core size (13 μm). The near field patterns obtained with this device are shown in Figure III-16b. As expected for non-MSPL, modal mixing occurs at the output of the device, showing a response

comparable to a standard MMF. Evidently, such a device would not provide any significant advantages for SDM applications or for controlled generation of specific light patterns.

The fifteen fiber MSPLs allowed for the excitation of nine different LP modes and the corresponding degenerate modes. For these PLs, the accessible modes were the LP_{01}, LP_{11}, LP_{21}, LP_{02}, LP_{31}, LP_{12}, LP_{41}, LP_{22}, and LP_{03}, respectively excited using fibers with core diameters of 30, 28, 23, 20, 17, 15, 13, 10, and 6 μm. To obtain modal selectivity and independent excitation of all the LP fiber modes, the fibers were allocated within the preform as shown in Figure III-17a. Characterization of these lanterns was performed observing the near and far mode profiles produced upon launching light into each of the different cores. In Figure III-17, the mode profiles obtained from a series of fifteen fiber MSPLs are shown (the degenerate modes are not included).

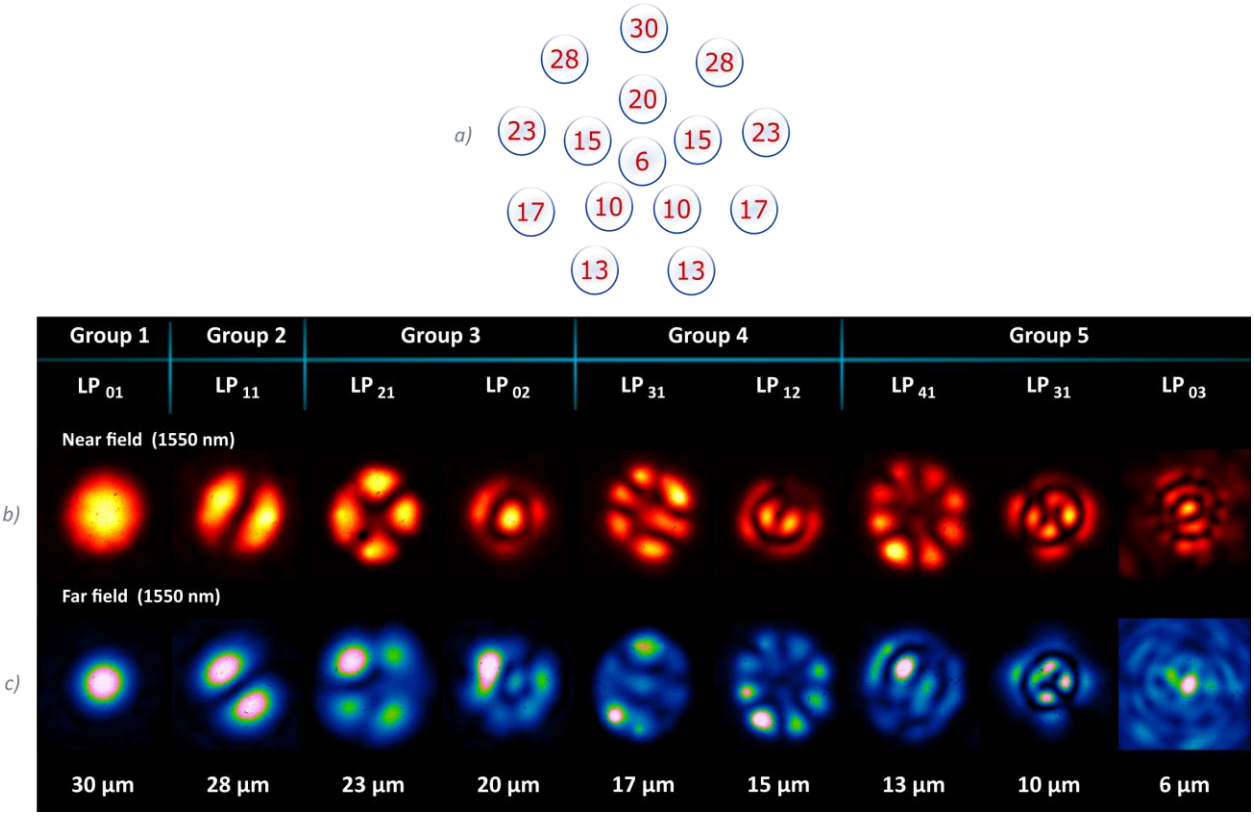

Fig. III - 17. Fifteen modes mode-selective photonic lantern. a) Fiber core positions. b) Near field mode profiles, and c) far field mode profiles at 1550 nm (only one degenerate mode per fiber core size is shown).

Although these devices were successfully fabricated and showed good modal selectivity, the scalability to obtain full-modal selectivity exciting each of the available LP modes individually, involves an increase in fabrication complexity. For instance, fabrication of MSPLs with a large number of LP modes will require an equal number of fibers with different core diameters. It must be pointed out that higher order modes will be more susceptible to mixing in the presence of minor imperfections due to the similarity in propagation constant. For this purpose, the available range of β values for the fiber cores needs to be large enough to completely avoid mode mixing; a larger transition section in the taper will also be required. An additional aspect is related to the

microstructured preforms, which involves the fabrication of more elaborated structures; nonetheless, the same fabrication technique can be used.

An alternative to manufacture PLs with a large number of fibers is to address each mode through group modal selectivity (MGS-PL). In contrast to the MSPLs, this approach requires a smaller difference in propagation constants or fiber core diameters in order to address each mode group. In this case, the structure allows isolating the modes by groups, although mixing can occur among the modes within the same group. Isolation of the modal group is achieved upon using fibers with different core sizes, one size for each modal group. This sort of PL is suitable for applications where mixing between modes comprised in the same group mode is acceptable (e.g., in telecommunications using FMFs in which mode mixing usually occurs).

The construction of the MGS-PLs for 5 mode groups was accomplished using core diameters of 30, 28, 23, 17, and 8 μm corresponding to the mode groups 1, 2, 3, 4, and 5. The fiber core distribution inside the preform illustrated in Figure III-18a follows the same order in core diameters used in the case of the MSPLs, with the larger core diameters in the outer ring of the fiber array and the fiber with the largest core at the top position. The characteristic near field-intensity profiles obtained at the output of the device demonstrates an evident mode mixing (Figure III-18b). The resulting light patterns are composed by the superposition of the available LP fiber modes and their corresponding degenerate modes within the mode group; this can be readily observed in groups 2, 3, and 4.

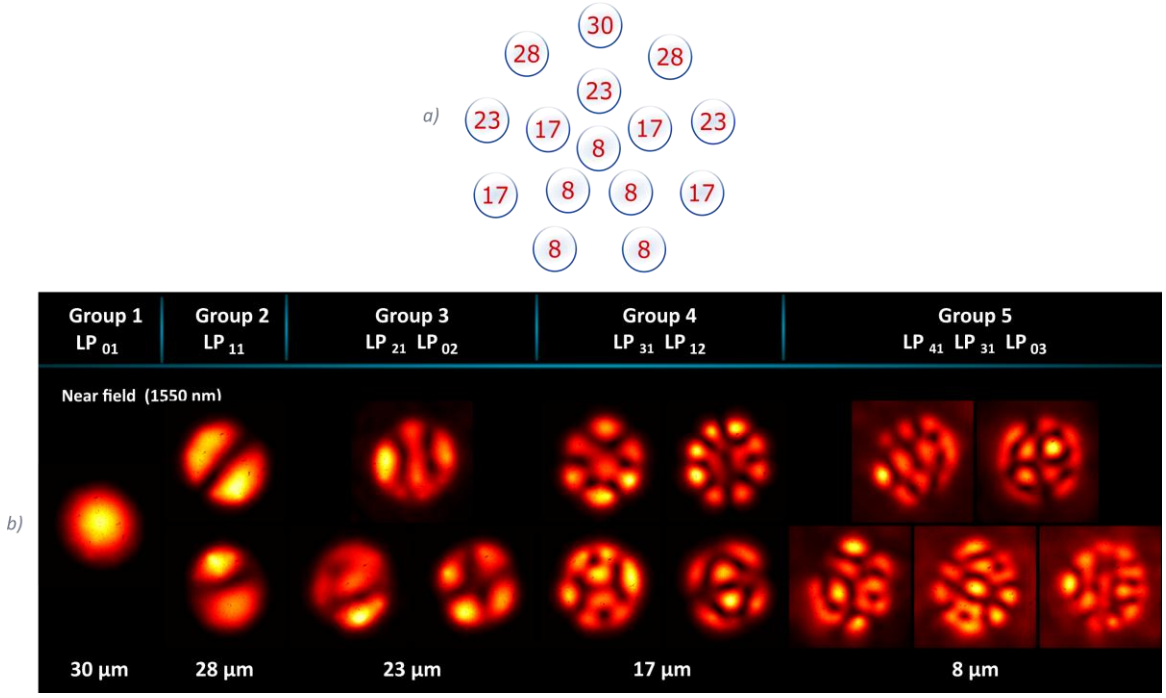

Fig. III - 18. Group-mode-selective photonic lantern. a) Fiber core distribution and b) near field mode profiles at 1550 nm.

III.3 ADDITIONAL CONSIDERATIONS FOR PL FABRICATION

The optimal fabrication parameters for the described PLs and their characteristics were covered in the previous sections. However, some variations in the fabrication processes will produce device with different features that might be important for particular applications or needs. In this section, we will discuss a few important variations in the fabrication process parameters and their effect on the resulting PLs.

III.3.1 STEP-INDEX VS GRADED-INDEX FIBERS

Given the nature of the fabrication process for all-fiber photonic lanterns, the details involving the adiabatic tapering and fusing of the device are crucial. Increasing the number of modes, increases the required taper length and thus the PL fabrication complexity [83]. This is evident from the increased tapering ratio required for the PL as the number of fibers is increased as well. As explained in section II.2.1, the transition lengths in a device ultimately determine the mode coupling and losses of a device, as analyzed for the case of step-index fibers. Graded-index fibers offer the advantage of low-mode coupling of the fundamental mode to higher order modes over shorter distances [89, 94]. Therefore, using GIFs reduces mode coupling along the transition zone of the device allowing for a better confinement of the fundamental mode, yielding shorter devices with improved losses.

To demonstrate the effect of using graded- and step-index fibers, several photonic lanterns of six fibers were fabricated. For the PLs fabricated with step-index fibers, well defined mode profiles were observed for a 6 cm transition length. In contrast, a PL with a transition length of 5 cm showed some scattered light in the modes, as typically observed in devices with non-adiabatic transition sections. In comparison, PLs constructed with GIFs preserved the quality of the mode profiles when the taper transition length was reduced from 6 to 3 cm. Hence, a reduction by a factor of ~ 2 in the tapering length is obtained when using GIFs, compared to PLs fabricated using step-index fibers. These results are illustrated in Figure III-19, showing the LP_{02} mode from lanterns fabricated using both types of fibers with different transition lengths.

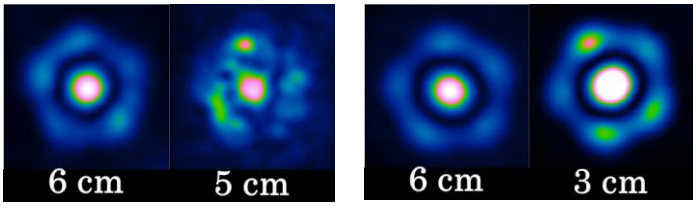

a) *b)*

Fig. III - 19. Near-field LP_{02} mode profile from MSPLs with different transitions lengths: (a) step-index and (b) graded-index fibers.

An important parameter that provides information about the performance of the PLs is the mode purity. This parameter is obtained upon analyzing the intensity distribution of the near field mode

profiles, quantifying the ratio between the minimum and maximum peak intensities of the lobes. For the PLs fabricated with step-index fibers, the mode purity changed from -11.76 to -6.73 dB when the transition length was reduced from 6 to 5 cm. In contrast, for the devices with graded-index fibers a length reduction in the transition section from 6 to 3 cm only diminished the mode purity from -17.67 to -16.28 dB. Furthermore, this mode purity was preserved even for transition lengths of ~ 4 cm.

III.3.2 WAVELENGTH DEPENDENCE

The main use of PLs is targeted for telecommunication applications operating in wavelengths centered at λ = 1550 nm. Nonetheless, operation of the PLs at different wavelengths is desirable for diverse applications. The wavelength dependence of the devices was evaluated using light sources operating at wavelengths of 980 and 1310 nm. These light sources were launched in the input fibers of the MSPLs, and the near field mode profiles were obtained for lanterns formed by three, six, ten, and fifteen fibers. A typical pattern obtained at the tapered end of the MSPLs for λ = 980 nm is shown in Figure III-20. While the output mode profiles for the higher order modes are well defined at the output, the lowest order modes appear like supermodes formed by the light coupled among all the fiber cores.

From the response of the MSPLs, it is obvious that this behavior is caused due to the small tapering ratio used to fabricate the device. At this wavelength, light is significantly confined and propagates inside each independent core in the fiber array, thus yielding an output composed of independent spots [75, 78]. A similar behavior is observed for a wavelength of λ = 1310 nm. Thus, the geometry of the devices, such as the final diameter, must be chosen adequately for proper operation at shorter wavelengths.

As a proof of concept, a three fiber MSPL was fabricated by tapering down with a ratio of 14.4. The near field mode profiles at the output obtained for wavelengths of 980, 1310, and 1550 nm are shown in Figure III-21. While well-defined mode profiles can be appreciated for shorter wavelengths, the output pattern at 1550 nm shows a partial light leaking from the tapered end due to the small size of the resulting waveguide.

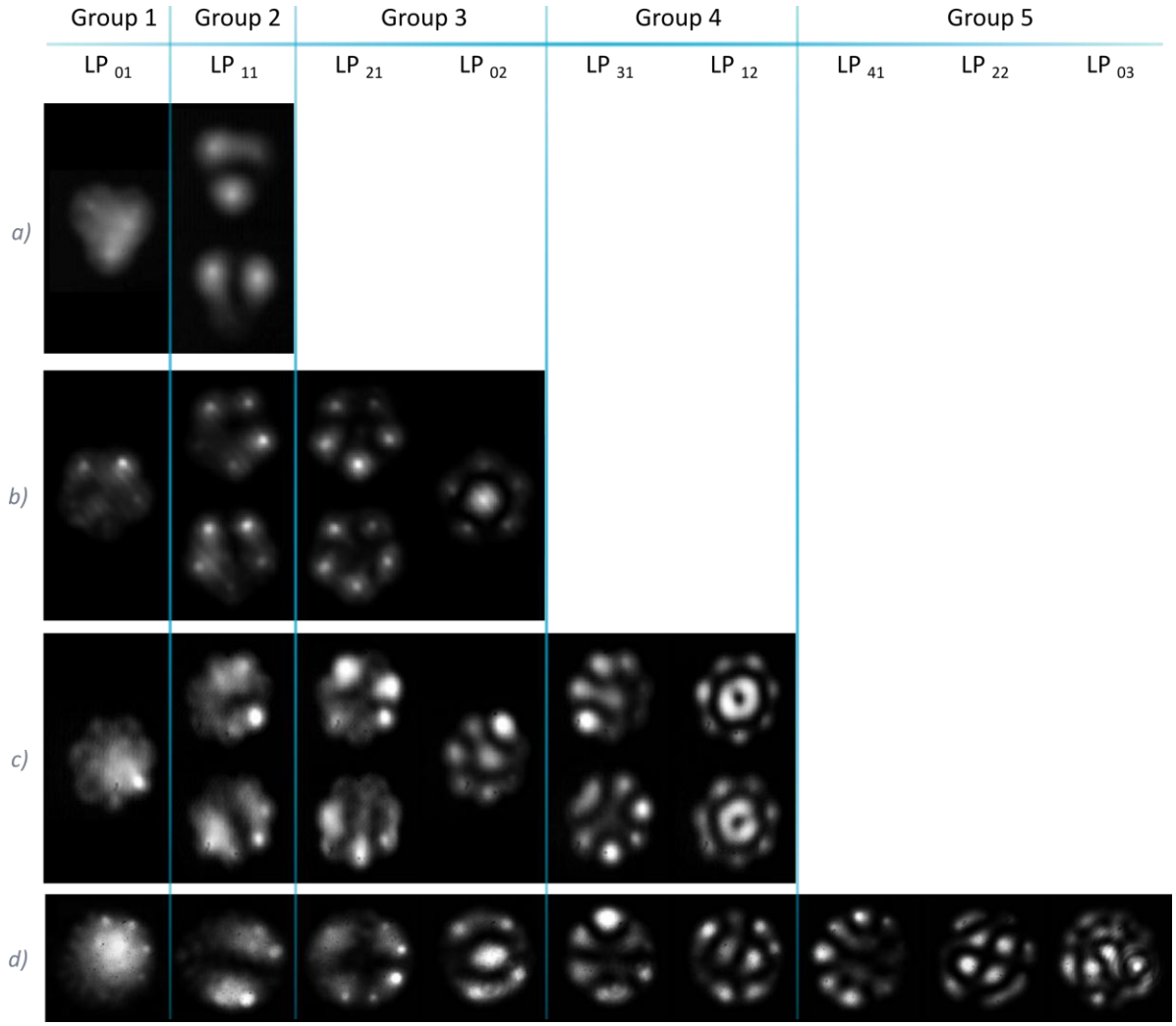

Fig. III - 20. Near field mode profiles at a wavelength of 980 nm from: a) three, b) six, c) ten, and d) fifteen fiber MSPLs.

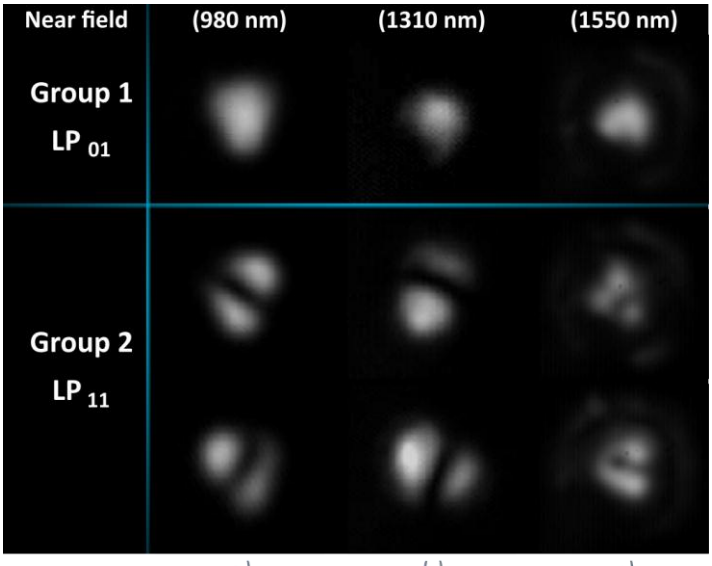

Fig. III - 21. Near field mode profiles from a three fibers MSPL with a tapering factor of 14.4 at a wavelengths of: a) 980 nm, b) 1310 nm, and c) 1550 nm.

III.3.3 FIBER POSITIONS AND DEFECTS

Photonic lanterns can produce diverse light patterns originated by mode mixing. An example of this behavior can be found in the mode profiles from MGS-PLs, like those presented in Figure III-18. These light patterns can be generated when the fiber core diameters used for the PLs construction are similar in dimensions, thus yielding similar propagation constants in the device resulting in mode mixing. Another possibility to generate this effect is to use fibers with different diameters but placing them in different positions inside the low-index capillary or microstructured preform (as in the MSPLs); hence, the coupling among the different fiber cores will change. Owing to the wide variety of combinations available during the fabrication process, a large diversity of mode patterns can be obtained through mode mixing.

To explore this situation, two ten fiber PLs were fabricated using similar fiber core diameters located at similar positions as those used for the ten fiber. Both modified PLs were based on the structure shown in Figure III-15: one was fabricated keeping the same fiber positions but reducing the sizes of two of the fiber cores (one changed from 20 to 17 μm and the other from 17 to 15 μm); for the second PL, only one fiber core was reduced (from 17 to 15 μm) and two fibers were swapped from their original positions. The locations of the fibers in the resulting devices are illustrated in Figure III-22a and III-22c. Both of these PLs were constructed using the same fabrication parameters (e.g., tapering ratio, length, etc.) as those used for the regular ten fiber PLs described earlier.

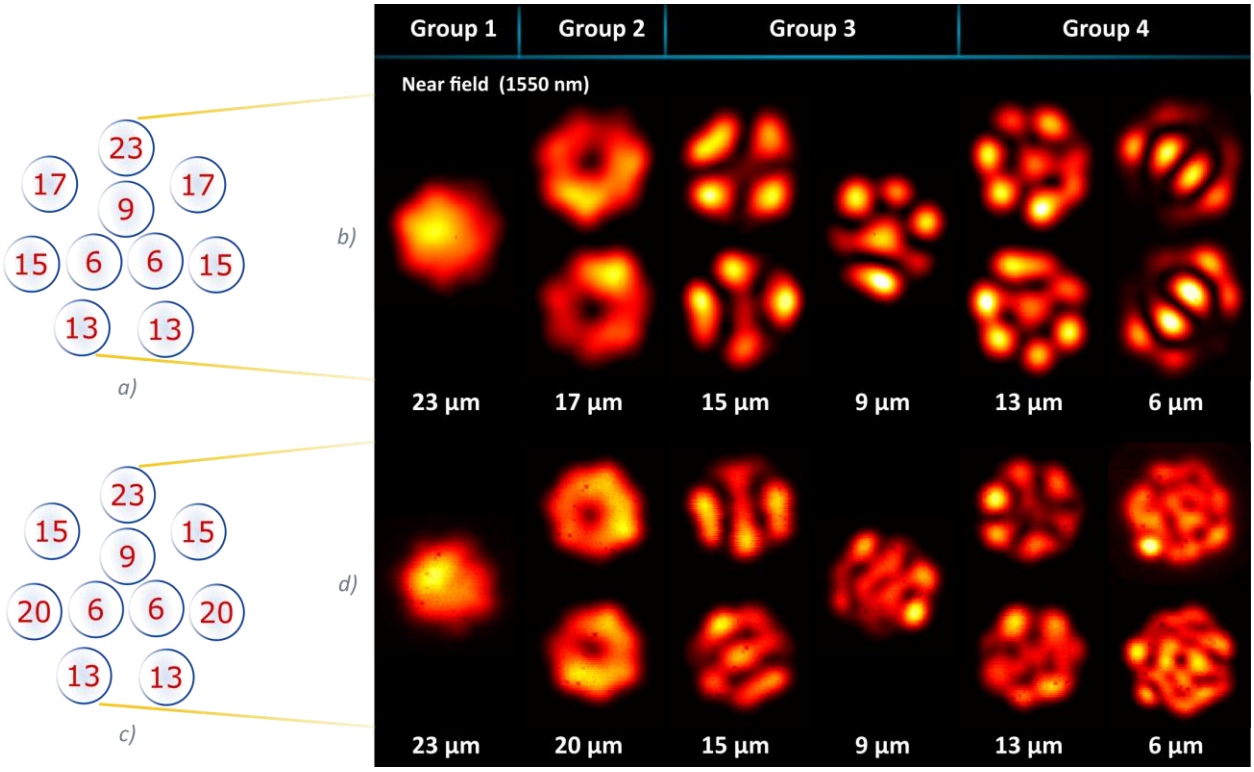

Fig. III - 22. Ten fiber PLs with different light patterns at the output. Different fiber diameters: a) fiber core distributions and b) near field mode profiles. Different fiber positions: c) fiber core distributions and d) near field mode profiles.

Near field patterns obtained at the output of both devices are shown in Figure III-22. The first PL shows a slight but clear mode mixing, causing the characteristic bright spots of the LP modes to look as "connected" spots; nonetheless, each LP fiber mode can still be identified. The second type of PL shows stronger mode mixing effects, yielding very different light distributions at the output. Generation of such responses can be originated from the different light coupling among the different fiber core diameters. Light exposed from a fiber core will couple first to a neighboring core with a larger diameter, rather than to one of a smaller diameter. These devices clearly demonstrate that the choice of diameters for the fiber cores, as well as their position within the fiber array provide a means for tuning the light patterns generated at the output of these devices.

Defects and imperfections generated during the fabrication process are an important factor to consider. The most common defects arise from fiber twisting/bending, ellipticity when tapering the structure, air bubbles, or cracks in the glass capillaries. Figure III-23.a shows the image of an air bubble encapsulated in the transition section of a PL. The presence of any of these defects results in mode mixing at the output of the devices. As an example of this situation, the near field mode profiles of a fifteen fiber MSPL with imperfections at the fabrication stage are shown in Figure III-23 in which mode mixing is clearly noticeable.

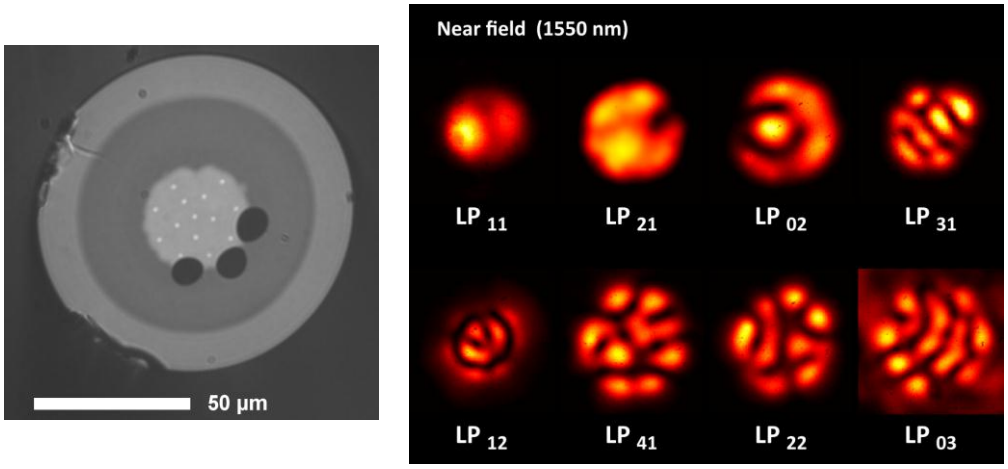

a) *b)*

Fig. III - 23. Defect present during the PLs fabrication process: a) image of an air bubble encapsulated in the transition section, and b) near field mode profiles from a fifteen fiber MSPL with defects.

III.4 CHARACTERIZATION

Evaluation of the performance of photonic lanterns requires additional characterization. One aspect to cover includes the analysis of the intensity distribution of the mode profiles. Also, the evaluation of the PLs when coupled to transmission fibers is a key aspect, since these devices are designed for their integration in fiber transmission systems. This last feature is generally achieved by obtaining the transfer matrix of the transmission system, measuring the crosstalk of the devices. Both aspects are described in the following sections.

III.4.1 MODE-INTENSITY PROFILES

Quantification of the mode purities was carried out for each type of MSPL fabricated by analyzing the intensity distribution from the near field and far field mode profiles. Numerical results of the mode purities measured for the MSPLs are listed in Table III-1. Typical results for the energy distribution for each LP mode are presented in Figure III-24, showing the near field (blue) and far field (orange) intensity profiles; theoretical mode profiles are also included for a direct comparison of the intensity distribution.

Table III - 1. Near field mode purity analysis of the MSPLs.

LP mode	Mode Purity (dB)							
	3 fiber MSPL		6 fiber MSPL		10 fiber MSPL		15 fiber MSPL	
	Near field	Far field	Near field	Far field	Near field	Far field	Near field	Far field
LP_{11}	-13.0	-13.4	-10.5	-8.9	-12.2	-8.9	-11.3	-11.0
LP_{21}			-14.4	-17.7	-10.2	-15	-11.2	-10.6
LP_{02}			-19.4	-17.7	-14.2	-10.9	-13.4	-9.7
LP_{31}					-12.6	-13.4	-11.4	-11.3
LP_{12}					-11.6	-12.4	-10.9	-12.4
LP_{41}							-9.75	-12.9
LP_{22}							-12	-10.1
LP_{03}							-13.1	-12.9

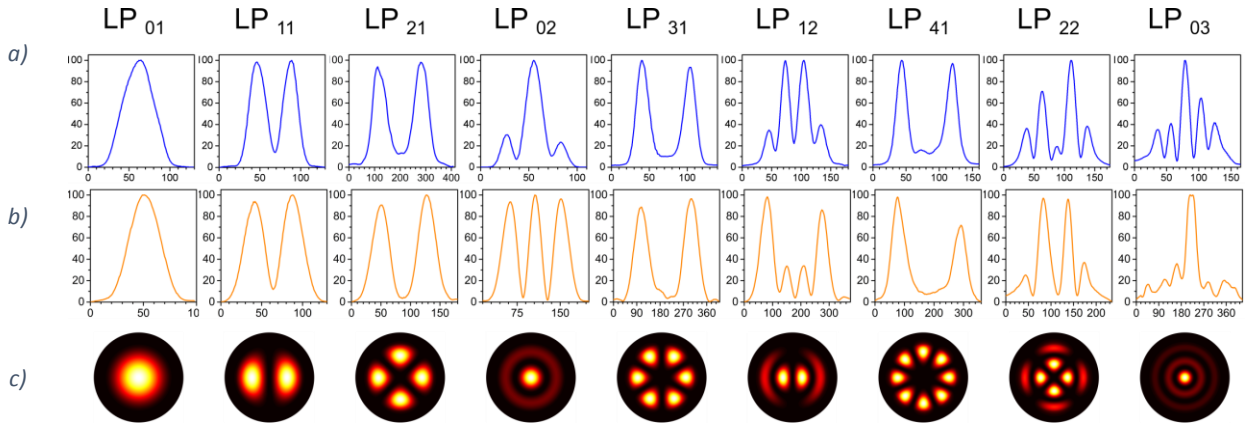

Fig. III - 24. Mode-intensity profiles from the MSPLs: a) near field and b) far field mode profiles. c) Theoretical light distributions of the fiber LP modes included for direct comparison.

Measured light maxima of the experimental mode-intensity patterns show a good agreement with the theoretical light distributions. From analyzing the near and far field-intensity profiles, the peaks remain within the same spatial allocation indicating mode preservation. However, for some modes the peak intensity contrast change; specifically for the LP_{02} and LP_{12} modes. A relevant feature visible in the far field mode-intensity profiles is a smoother distribution for the peaks in the plots, as in contrast for the near field case.

III.4.2 FIBER COUPLING: LOSSES AND TRANSFER MATRICES

One of the attractiveness of photonic lanterns is their ease of integration to fiber systems for signal transmission. A correct pairing between the cores of the PL and the transmission fiber is a critical factor for a successful alignment and for a full excitation of all the modes supported by the fiber. Recent research in few-mode fibers (FMFs) has been developed aiming at reducing mode coupling [49, 95, 96] during transmission as well as at minimizing the differential group delay (DGD) of the modes [51-53]. FMFs were created for their use in telecommunications but they are also attractive for sensing applications due to its increased sensitivity to perturbations of higher order modes [97, 98]. Integration and performance of PLs in fiber systems are commonly tested by coupling and splicing the lanterns to FMFs, and consecutively evaluating their capabilities to excite and transmit each of the supported modes. The PLs described in the previous sections were tested with FMFs supporting 2, 6 and 9 LP fiber modes [52, 53].

Coupling of the PLs to the FMFs was performed in the tapering system, which possesses the capability of splicing a wide variety of fibers. The PLs are first butt coupled to the FMF and a correct alignment is verified upon observing the mode profiles at the output end of the fiber. Splicing is then performed by means of the CO_2 laser of the tapering system. A thorough evaluation of the PLs/FMFs coupling is achieved using mode-selective devices since each LP mode can be analyzed independently. The features of the graded-index FMFs coupled to each of the fabricated MSPLs are listed in Table III-2.

Table III - 2. Characteristics of the graded-index fibers coupled to MSPLs.

Fiber	ID/OD [μm]	Spliced to
2 LP modes	14/125	3 fiber PLs
6 LP modes	28/125	6 and 10 fiber PLs
9 LP modes	30/125	Tapered MMF
MMF	50/125	15 fiber PLs

Particular attention was paid in splicing the fifteen fiber PLs due to the low Δn housing capillary used for the microstructured preforms. This resulted in a small NA restricting the final diameter of the device and impeding a direct splice to a 9 LP modes FMF due to modal mismatch. Because the resulting core diameter of the fifteen fiber PLs is greater than the 9 LP-FMF core (35 μm vs. 30 μm) and the different refractive index profile (step-index vs. graded-index, respectively), an intermediate standard MMF of 50 μm core diameter had to be spliced in between in order to reduce the difference in core sizes.

The MMF for core matching is further adapted by tapering process, thus reducing the core diameter to 30 μm. Additional tapering of the MMF restricts the propagation of unnecessary modes, thereby allowing the transmission of only the desired 9 LP modes. Near field mode profiles at the output of the FMFs spliced to 3, 6, 10, and 15 fiber MSPLs are shown in Figure III-25. As seen in these mode profiles, conservation of the light patterns generated by the MSPLs is apparent after 2 m of propagation along the FMF. However, mode mixing of the LP modes within the same group mode is

evident in the modal patterns. This modal mixing occurs among the radial order modes with the same azimuthal order between the step-index and the graded-index fibers. Also, this effect can be provoked due to the use of the intermediate MMF for core size matching.

Further characterization of the devices included measuring the fabrication and coupling losses after splicing a meter of FMF to the MSPLs. Fabrication losses measured in all the devices were usually in the range of 0.1 – 0.5 dB. Due to the FMF splice, an increase in losses occurs as the mode group increases; this effect is known as mode-dependent loss (MDL) [99]. Table III-3 summarizes the measured coupling losses from splicing the MSPLs to FMFs. For the fifteen fiber devices, MGS-PLs were used instead of a MSPL because of the additional losses caused by the low-NA preform and mode mixing.

Table III - 3. Coupling losses resulting from MSPLs and FMFs splices.

LP mode	FMF Splicing Losses [dB]			
	3 fiber MSPL	6 fiber MSPL	10 fiber MSPL	15 fiber GMS-PL
LP_{01}	0.3	0.17334	0.405	0.34
LP_{11}	--	0.22998	0.46	0.96
LP_{21}		0.15619	0.82	1.11667
LP_{02}		0.54167	1.52	
LP_{31}			1.4275	1.41708
LP_{12}			2.3	
LP_{41}				4.576
LP_{22}				
LP_{03}				

The PLs performance as MUX and DEMUX devices was tested upon splicing pairs of lanterns onto the opposite ends of FMFs. Light from a swept wavelength interferometer (SWI) with spatial diversity was then launched into every single-mode fiber of the MUX, and the output power at each of the output fibers of the DEMUX was measured with a photodetector. This arrangement allows obtaining the transfer matrix along the entire C- and L-bands, commonly used in the optical fiber communications [100]. The transfer matrix of a SDM transmission system plots the normalized intensities at the inputs and outputs of the PLs used for MUX/DEMUX purposes. An important feature of this graphic representation is the capability to provide information about crosstalk among the spatial channels, as well as information regarding mode mixing.

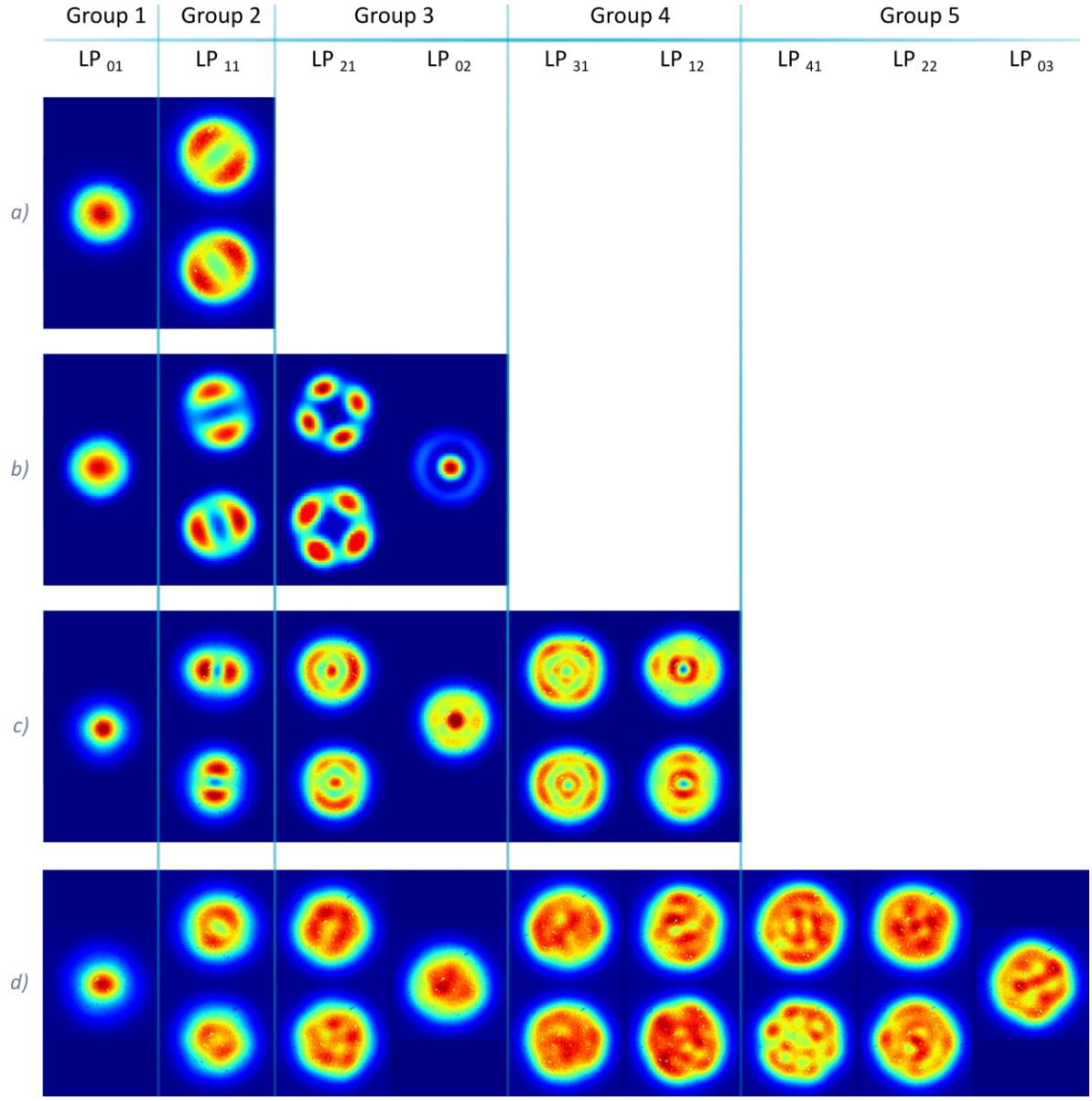

Fig. III - 25. Near field mode profiles of the MSPLs spliced to FMFs. a) Three fiber MSPL spliced to a 2 LP mode FMF. b) Six fiber MSPL spliced to a 6 LP mode FMF. c) Ten fiber MSPL spliced to a 6 LP mode FMF. d) Fifteen fiber MSPL spliced to a MMF and then to a 9 LP mode FMF.

Ideally, a system with modal selectivity should present zero mixing between modes and crosstalk should be negligible. For ideal MSPLs and FMF, neither LP modes of the fiber nor their corresponding degenerate modes should mix, and light launched into a single fiber should exit only at its reciprocal output fiber [100, 101]. This is illustrated in Figure III-26a, showing the transfer matrix for this ideal case. If modal mixing is present at the level of group modes, the total power launched in any single fiber will be equally distributed only among the fibers corresponding to the same group mode (see Figures III-26b and III-26c). In contrast, for a system with no modal selectivity at all, the light launched at any input fiber will spread evenly among all of the output fibers.

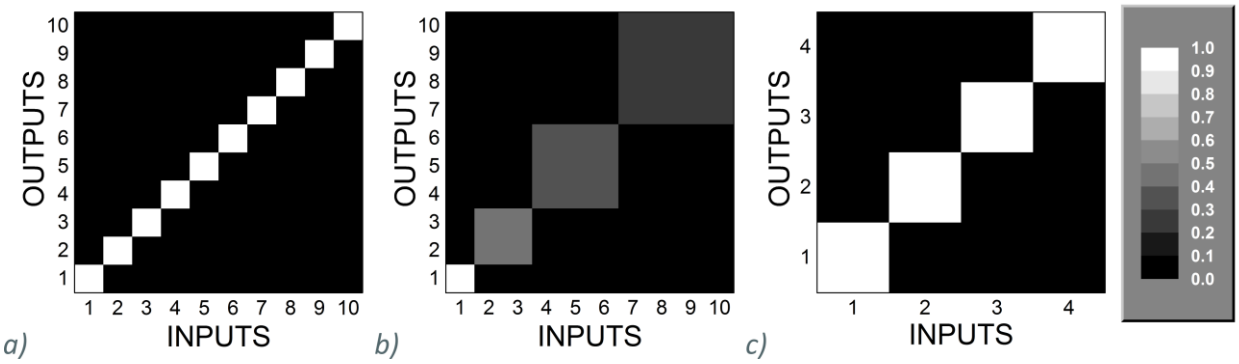

Fig. III - 26. Theoretical transfer matrices for ideal mode-selective ten fiber PLs. a) Perfect mode-selective fiber transmission system without group or degenerate modal mixing. Perfect mode group-selective fiber transmission system: b) fiber to fiber and c) mode-group blocks representations. Fiber No. 1 correspond to the lowest order mode, whereas fiber No. 10 correspond to the highest order mode.

The transfer matrices for the fabricated lanterns were obtained for two cases: one using a transmission arrangement with mode-selective lanterns (ten fiber MSPLs), and another using devices without any modal selectivity (fifteen fiber PLs). Experimental data obtained for both scenarios is plotted in the transfer matrices shown in Figure III-27. As clearly seen in the transfer matrix of the MSPLs, light is mainly confined in regions corresponding to the mode groups, as delimited by the square areas marked in dashed lines. For the PLs without modal selectivity, a random distribution of light is obtained in the transfer matrix.

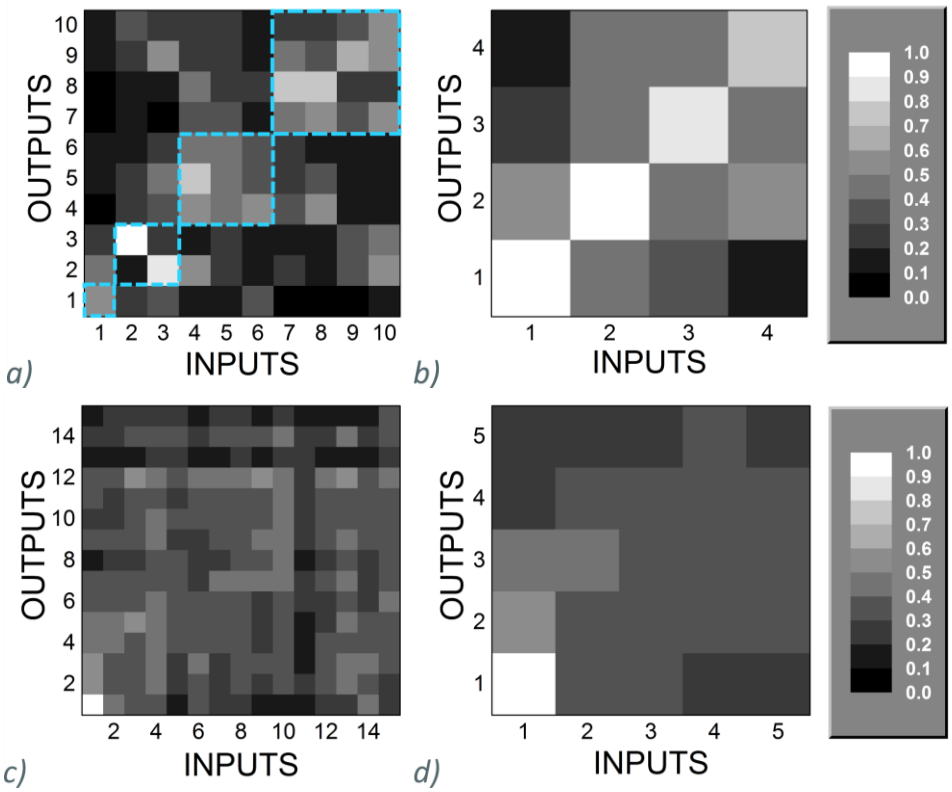

Fig. III - 27. Transfer matrices showing the normalized light intensity. Ten fiber MSPL with a) fiber-to-fiber and b) mode-group blocks representations. Fifteen fiber PL without modal selectivity with c) fiber to fiber and d) mode-group blocks representations.

A useful parameter for crosstalk evaluation is the mode selectivity factor. This is defined as the ratio of the power contained in the desired mode to that obtained for all of the remaining modes within a mode group. In other words, this parameter compares the light confinement in a mode group in a MSPL and a non-mode-selective PL. The plot in Figure III-28 shows the comparison of the results between the two analyzed scenarios. For MSPLs, clear mode selectivity of around 3 dB is achieved for the second, third, and fourth mode groups. In contrast, for the common PLs the mode selectivity is negligible, with the exception of the first group mode, which presents mode selectivity similar to that obtained for a MSPL. This can be attributed to the graded-index of the transmission fibers, which tend to favor the propagation of the fundamental mode.

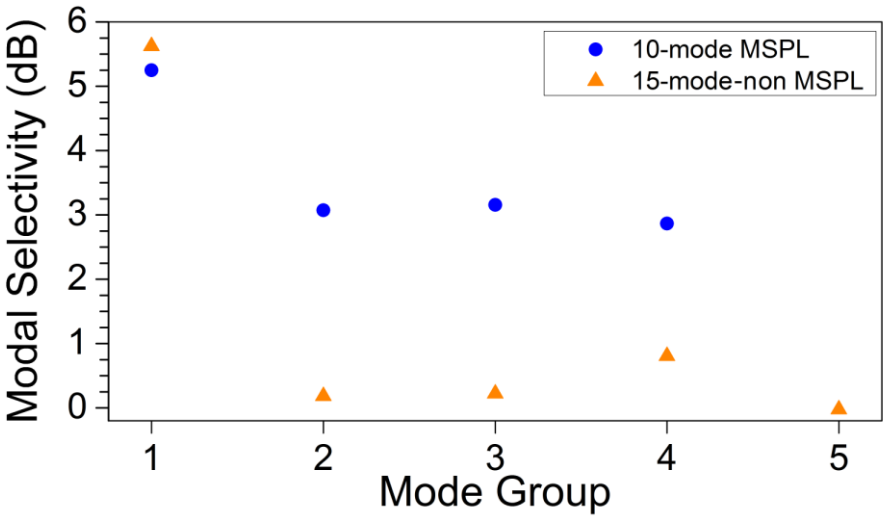

Fig. III - 28. Comparison between experimental results obtained for photonic lanterns with and without modal selectivity.

The performance of the photonic lanterns indicates how this developing technology possesses the capabilities to generate specific light patterns. Specific light patterns at the output of these devices can be obtained by the appropriate selection of the fabrication parameters and fibers characteristics. An amazing advantage of these all-fiber PLs over other existing technologies is the minimum losses achievable if the tapering process is completely adiabatic; in fact, all-fiber devices for SDM are hypothetically lossless. Furthermore, all-fiber PLs can directly be integrated into fiber systems, avoiding the use of free-space optics or other materials. Notice also that scalability to a larger number of modes with these PLs is more straightforward than other fiber approaches [62]. Other applications for these devices will surely emerge as this technology evolves.

CHAPTER IV: MICRO-RING RESONATORS

Micro-ring resonators (MRRs) are a popular technology for sensing applications nowadays because they offer outstanding sensitivity to external perturbations. These typically affect the refractive index of the device leading to changes of the resonance conditions, hence modifying the transmission spectrum [25, 28-31]. The use of reconfigurable materials in the fabrication of MRRs allows for the adjustment in their spectral features. Fabrication of devices working on this principle has been explored with acusto- and electro-optic materials [102, 103]. The use of polymeric materials has also been demonstrated for fabricating micro–ring resonators, yielding devices with lower fabrication costs, ease of processing, and showing adequate performance for sensing applications [104]. An advantage of utilizing polymers, is the possibility of further functionalization using additional materials such as doped polymers, which are capable of modifying their refractive index with external signals [105-108]. These capabilities have proven to be useful for optics and photonics applications [106-108].

An approach for fabrication of tunable MRRs is the use of cylindrical elements coated with thin layers of functional polymers. Coating films in optics are required to be smooth and uniform, in order to achieve good quality devices. A crucial factor in optical coatings is the control of thickness as it defines the interaction of light with the coated material. Usually thin layers of solid materials are preferred for coating optical elements requiring highly controllable deposition process (e.g., PVD, CVD, sputtering, etc.) [109-111]. The use of fluidic materials represents an alternative to create coating layers, making use of the physical properties of the coating material to define the resulting coatings. This approach usually implies a simpler fabrication, where the most common methods include spin coating, dip coating, and roll coating [112-114]. However, all of these methods are limited to planar surfaces and are not the most suitable options to apply on other geometries, such as cylinders.

Uniform coating of wires or fibers is normally performed upon pulling them through a container with the liquid solution to be deposited. The thickness of the resulting coating is given by the diameter of the output aperture of the container. However, this technique requires large lengths of fiber to work properly and induces strain over the elements to be coated, thus representing a problem when fragile optical devices are used or when coating short elements [115, 116]. Adapted techniques based on variations of the dip and wire coating processes, have been efficiently accomplished for fabrication of small diameter photonic devices incorporating thin and uniform layers of polymeric materials [117-119]. These approaches are based on displacing a small reservoir or drop of the coating fluid along the cylindrical element, leaving a layer of the material on the surface of the element.

In this chapter we demonstrate the fabrication and characterization of MRRs fabricated with cylindrical elements coated with thin layers of polymeric materials. Characterization of the coating process using two different polymers is described for the single-layer and multiple-layer approaches. The use of polymers incorporating photoluminiscent, absorbent, and birefringent materials is studied with the purpose to generate an optically tunable response. We further explore the use of multilayer resonators aiming at improving the tuning effect achieved in these MRRs.

IV.1 MICRO-RESONATORS PRINCIPLES AND FABRICATION

In general, a micro-resonator is formed by a waveguide which conducts light in a closed loop trajectory in the micrometric scale size. When the light waves propagated through the loop build up a phase shift equal to a multiple integer of 2π in a round trip, constructive interference of the waves takes place and generates a resonant effect yielding intense confinement of light within a small volume [28-30, 120]. Normally, this loop trajectory can be formed by different circular-like geometrical configurations, such as rings, disks, spheres, racetracks, or ellipses. Micro-ring resonators are formed by a closed circular waveguide, confining light inside by conventional total internal reflection (TIR). The supported transverse and azimuthal modes in these waveguide structures are defined by their physical dimensions [28-30]. Since MRRs are very small, they offer great potential for integration with other technologies and/or components such as fiber optics [30, 31]. These optical devices have been used for a wide variety of applications, and the most common include filters, switches, modulators, sensors, wavelength division multiplexers (WDMs), and micron-size lasers [29-31, 120]. Photolithographic processes compatible with the electronics industry are normally used for the fabrication of micro-ring resonators. However, fiber approaches have been studied presenting the advantage of direct coupling to fiber optic technologies.

A special case of resonance commonly found in micro-disks and micro-spheres are the whispering gallery modes (WGM). In WGM, the resonances are originated by the waves propagated azimuthally at the boundary of the resonator and the surrounding media [29-31]. This particular type of resonance is considered only when the outer boundary plays a role in the confinement of the wave, usually present in single material micro-resonators [29]. Therefore, in WGM light does not penetrate inside the material of the resonator. When an inner boundary exists, the requirement for generating WGM is that the caustic radius of the inner material lies between the other two interfaces. Otherwise, the waveguide is multimode and several modes will couple at different resonance wavelengths [29, 30, 31, 121].

The most common method for coupling light into resonating cavities is through evanescent waves from another optical waveguide [28-30]. The use of tapered optical fibers is the most popular approach for light coupling [30]. To fully describe the resonance features of the MRRs it is useful to consider a straight single-mode waveguide close to a circular single-mode waveguide. Light traveling through the straight waveguide couples to the resonant cavity, as depicted in Figure IV-1. The

complex mode amplitudes interacting in the coupling process include the input (E_{I1} and E_{I2}) and output (E_{O1} and E_{O2}) signals in the straight and curved waveguide, respectively.

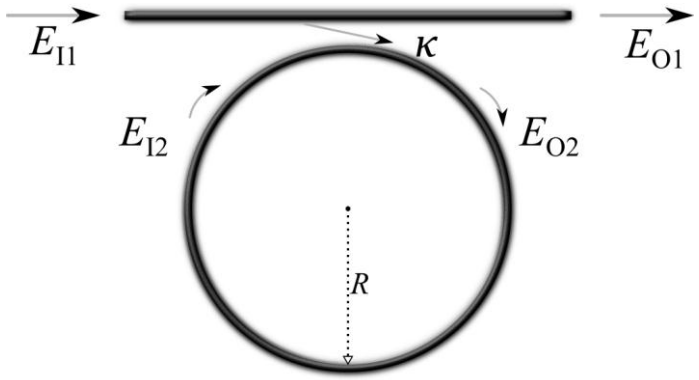

Fig. IV - 1. Micro-ring resonator scheme. A light signal (E_{I1}) is launched through a single-mode waveguide and coupled to the resonant cavity (radius R), yielding a resonant response (E_{O1}).

The relationship between the inputs and outputs of the system can be obtained from coupled mode theory analyzing the interaction between both guiding structures. For this analysis the propagation constants for the straight and resonant waveguides are assumed to be identical $\left(\beta = \beta_1 = \beta_2\right)$. Taking into account the parameters of the directional coupler such as the coupling length (ℓ), the mode-coupling coefficient (κ), and intensity-insertion-loss coefficient (γ), the output signals are defined as [2]:

$$E_{O1} = (1-\gamma)^{1/2}\left[E_{I1}\cos(\kappa\ell) - jE_{I2}\sin(\kappa\ell)\right] \qquad \text{<IV.1>}$$

$$E_{O2} = (1-\gamma)^{1/2}\left[E_{I2}\cos(\kappa\ell) - jE_{I1}\sin(\kappa\ell)\right] \qquad \text{<IV.2>}$$

Considering the circular geometry of the waveguide of radius R, the light travels a total trajectory $L = 2\pi R$ presenting a single-pass shift ($\phi = \beta L$), the losses can be accounted with the intensity attenuation coefficient (ρ). Then, the energy coupling back to the straight waveguide after a round trip in the resonator is [2]:

$$E_{I2} = E_{O2}e^{\left(-\frac{\rho}{2}L - j\beta L\right)} \qquad \text{<IV.3>}$$

Given these relationships, determination of the amplitude transmittance through the straight waveguide can be defined as [2, 28, 29]:

$$\frac{E_{O1}}{E_{I1}} = (1-\gamma)^{1/2}\left[\frac{\cos(\kappa\ell) - (1-\gamma)^{1/2}e^{\left(-\frac{\rho}{2}L - j\beta L\right)}}{1-(1-\gamma)^{1/2}\cos(\kappa\ell)e^{\left(-\frac{\rho}{2}L - j\beta L\right)}}\right] \qquad \text{<IV.4>}$$

Redefining the parameters of the previous equation, the parameters x and y are defined as:

$$x = (1-\gamma)^{1/2} e^{\left(-\frac{\rho}{2}L\right)} \qquad \text{<IV.5>}$$

$$y = \cos(\kappa \ell) \qquad \text{<IV.6>}$$

The condition $\phi = 2\pi m$ is required for resonance to occur, where *m* is an integer; hence, <*IV.4*> can be rewritten as [2, 28, 120]:

$$T(\phi) = \left|\frac{E_{O1}}{E_{I1}}\right|^2 = (1-\gamma)\left[1 - \frac{(1-x^2)(1-y^2)}{(1-xy)^2 + 4xy\sin^2\left(\phi/2\right)}\right] \qquad \text{<IV.7>}$$

This expression shows that coupling into the cavity occurs only at certain wavelengths. A typical transmission spectrum for these devices is shown in Figure IV-2.

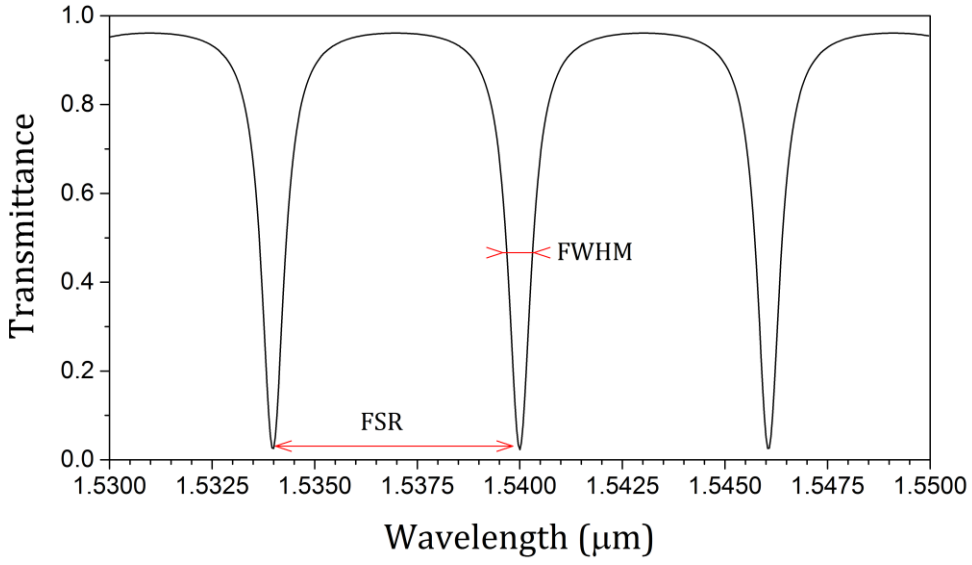

Fig. IV - 2. Typical transmission spectra from a micro-ring resonators (R = 62.5 μm).

As illustrated in Figure IV-2, resonance occurs at wavelengths with a separation given by the features of the micro-ring, which is inverse to the time delay in a round trip. The separation between these resonant wavelengths ($\Delta\lambda$) is known as the Free Spectral Range (*FSR*), defined as [28, 29]:

$$FSR = \Delta\lambda = \frac{\lambda^2}{n_g L} = \frac{\lambda^2}{n_g 2\pi R} \qquad \text{<IV.8>}$$

$$n_g = n_{eff}(\lambda_0) + \lambda_0 \left.\frac{\partial n_{eff}}{\partial \lambda}\right|_{\lambda_0} \qquad \text{<IV.9>}$$

where λ_0 is the central wavelength between both resonances, and n_g is the group refractive index given in terms of the effective refractive index (n_{eff}).

Another important parameter in MRRs is the Full Width at Half Maximum (*FWHM*), indicating the half of the power measured from the peak intensity, or 3 dB bandwidth. Measurement of the *FWHM* allows defining the width of the resonance peaks, a useful parameter when MRRs are used as filters or for lasers [30, 40, 120]. This parameter is given by [28, 29]:

$$FWHM = 2\delta\lambda = \frac{\kappa^2\lambda^2}{\pi L n_{eff}} \qquad \text{<IV.10>}$$

The ratio between the *FSR* and the *FWHM* is known as the Finesse (F), indicating the quality of the resonance at a specific wavelength. Using the above expressions the Finesse can be estimated as [28, 29, 120].

$$F = \frac{FSR}{FWHM} = \frac{\Delta\lambda}{2\delta\lambda} \qquad \text{<IV.11>}$$

A similar parameter is the quality factor (Q), which measures the sharpness of the resonance at the central resonance wavelength. This parameter indicates the capacity of the resonator to confine energy per optical cycle, and is defined as:

$$Q = \frac{\lambda}{FWHM} = \frac{n_{eff}L}{\lambda}F \qquad \text{<IV.12>}$$

All the above expressions are valid when considering a single-mode straight waveguide and a ring waveguide. However, when using spheres or cylinders to implement resonators, a larger surface is available and excitation of multiple modes is therefore possible. In addition, if the straight waveguide used to couple light into the resonator supports more than one mode, these could favor the excitation of additional modes inside the loop waveguide. An aspect noteworthy to mention is the different resonance wavelength associated for every mode with different linewidth, representing different coupling conditions for each resonant mode [30, 31]. This effect is present for modes guided by conventional TIR as well as for the WGM, and can be described upon analyzing the resonator as a curved waveguide. To exemplify multiple resonances, an illustration showing the fundamental mode and the second order modes (azimuthal and radial) for a spherical WGM resonator can be observed in Figure IV-3 [31].

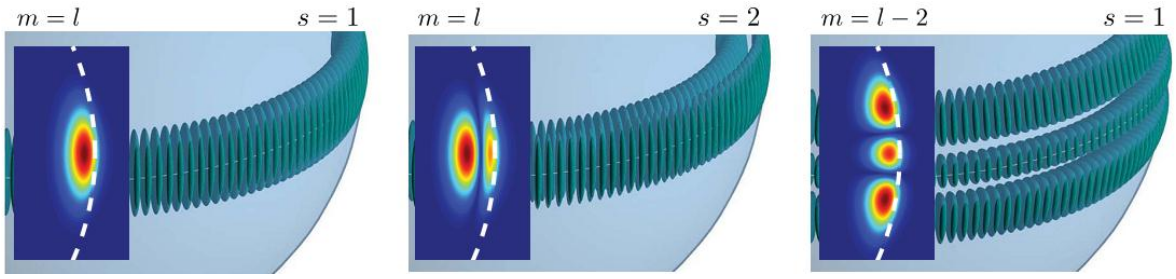

Fig. IV - 3. Example of a multimode WGM resonator in a sphere. Top: intensity distributions at the surface of the sphere; the insets show the intensity at the cross-section of the sphere for the fundamental mode and second-order radial and azimuthal mode, respectively. Bottom: the corresponding effective potentials and wavefunctions. Taken from [31]

IV.1.1 SENSING WITH MICRO-RING RESONATORS

The principal mechanism for sensing with MRRs consists on the modification of resonance conditions. Mainly, the cavity dimensions and the refractive index of the materials used for their fabrication define the spectral response of the resonators. Detection in micro-resonators is usually performed analyzing the spectral changes in the resonance. Changes in the resonance wavelengths can be categorized as follows (see Figure IV-4) [30]:

- *Resonant wavelength (or frequency) shift*.- this effect is originated by changes in the refractive index or resonator dimensions.
- *Change in the quality factor*.- this is provoked by changes in absorption of the resonator materials affecting the broadening of the resonance.
- *Change in peak transmission*.- this effect is generated by variations in the coupling conditions between the straight waveguide and the micro-resonator.

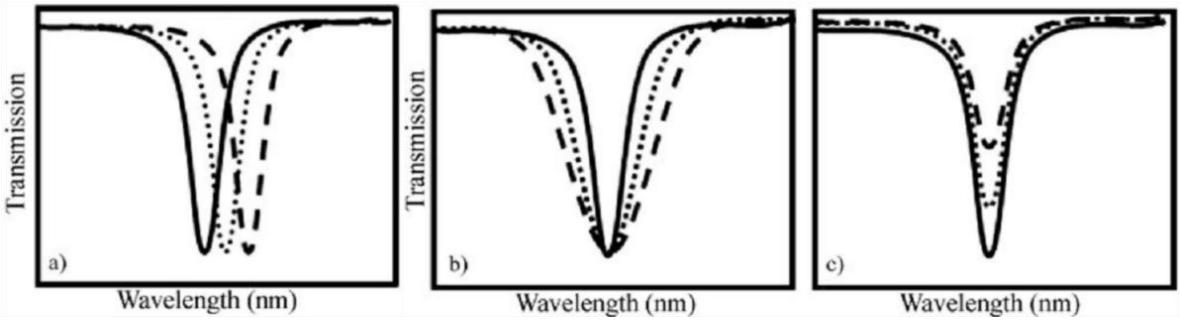

Fig. IV - 4. Sensing responses in micro-ring resonators. a) Change in the resonance wavelength. b) Change in the quality factor. c) Change in the peak transmission. Taken from [30].

Light coupling into resonators of circular cross section, such as micro-spheres or rods, commonly give place to WGM resonances. In contrast, micro-ring resonators make use of elements with thin walls (e.g., thin wall glass capillaries), resulting in light confinement due to conventional TIR. Deposition of thin layers on the cylindrical elements further leads to light confinement conditions analogous to those obtained for optical waveguides. When the material used as coating possess a higher refractive index than the cylindrical element, light is confined mostly within the coating layer. In contrast, the use of a material with lower refractive index yields light propagation within the coating and the cylindrical element, and some modes will be confined in the cylindrical element. The use of multiple layers in this kind of resonator thus offers the potential for customizing light confinement and the spectral features of devices upon selecting adequate materials. As an example, micro-ring resonators formed with two coating layers may offer the capability to confine most of the light either within the outer layer or allow for it to extend to both layers, depending on the choice of refractive indices. Such a feature can lead to devices with tunable resonances upon the use of reconfigurable materials. Furthermore, these may render useful for sensing applications as well.

Micro-resonators operating under these schemes are illustrated in Figures IV-15a to IV-15c, showing how light is confined and propagates depending on the number of layers used for the structure.

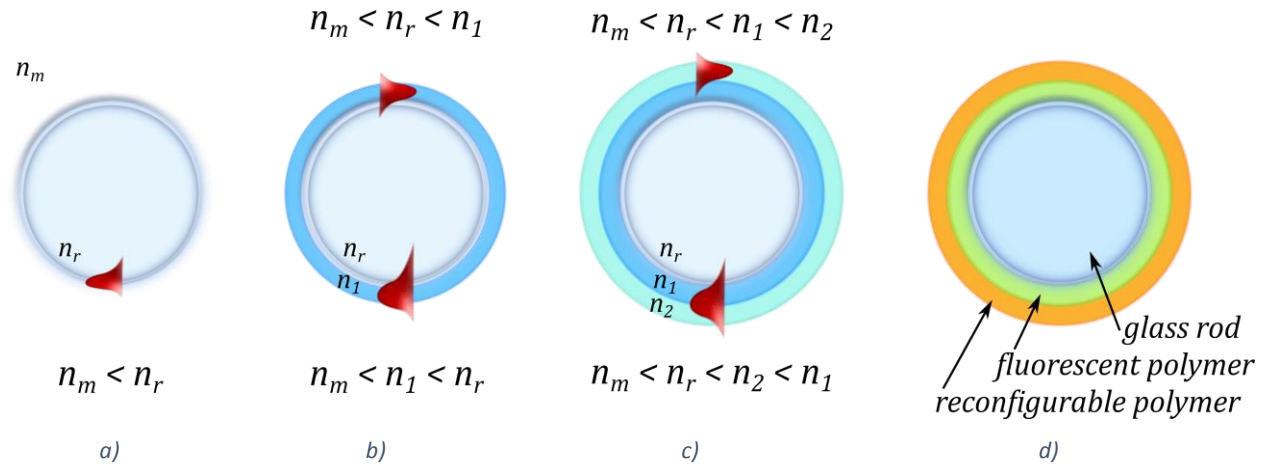

Fig. IV - 5. Light confinement in MRRs with circular cross-section: a) bulk materials (WGM resonances), b) single-layer coating, c) multilayer coatings, and d) functional polymer multilayer coated MRR.

New approaches for fabricating micro-ring resonators formed by distinct layers of functionalized materials can yield versatile devices for a wide variety of applications. Under this approach, the combination of reconfigurable layers can be used (i.e., materials capable of change the refractive index under an external signal or by the interaction with external objects/substances). As an example, tunable devices may be obtained upon appropriately selecting the materials forming the layers of the resonators. This can be realized by depositing two different polymeric thin coatings on solid glass rods as illustrated in Figure IV-5d. While the inner layer of the MRR may contain a fluorescent material activated by infrared light, the outermost coating may include a material whose optical features change upon absorption of the light emitted from the inner layer. Thus, the combination of these coating layers provides a means to modify the refractive indices of the materials, thereby changing the spectral features of the MRR. Fabrication details and characterization of these multilayer-coated MRRs are provided in the following sections.

IV.2 THIN-LAYER COATINGS

Coating of cylindrical optical elements to generate the functional MRRs is based on the wire coating technique first described by Landau, Levich, and Derjaguin (LLD theory). The dynamics of this process were later defined by Ryck and Quéré [122, 123]. The principle of this technique relies on pulling a wire of constant diameter with smooth and uniform surface through a liquid solution; during the pulling process, a small amount of the liquid is left on the surface of the wire. As a result, a wire (radius r) can be coated with a thin-layer of liquid (see Figure IV-6). The thickness of the coating layer (h) is given by the speed at which the process takes place (V), and the intrinsic properties of the liquid, such as the viscosity (η) and surface tension (γ). These parameters conform the capillary number (Ca), defined as:

$$Ca = \eta V / \gamma \qquad \text{<IV.13>}$$

For $h < r$, $Ca \ll 1$ and the thickness of the coating layer can be obtained as:

$$h = 1.34 r Ca^{2/3} \qquad \text{<IV.14>}$$

If $Ca \approx 1$, it is necessary to adjust <*IV.14*> replacing r by $r + h$ resulting in [124]:

$$h = \frac{1.34 r Ca^{2/3}}{1 - 1.34 r Ca^{2/3}} \qquad \text{<IV.15>}$$

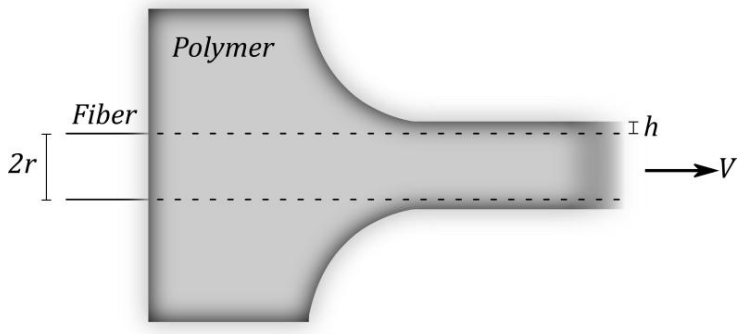

Fig. IV - 6. Wire coating technique scheme. A layer of coating material (thickness h) is left on the surface of the wire (radius r) by pulling the coating material at a constant velocity (V) through a liquid container

Coating of glass optical fibers, both, tapered and of standard diameters, was realized through a modified version of the wire coating technique. A coating system was specifically design for this task, capable of housing cylindrical devices to be coated with liquid polymers [117]. Polymer-coated MRRs were fabricated with this system, which maintains the cylindrical element fixed and moves the coating fluid along the section to be coated. Using this approach, only a small section of the element to be coated is fully immersed in the liquid, thus avoiding the rupture or deformation by strain of the element. The reservoir containing the liquid is displaced at a controlled velocity along the cylindrical element by activating a stepper motor. This capability allows for generating a uniform thickness in the coating. The system can also accommodate devices ranging from one micron in diameter (e.g., single-mode tapered optical fibers) up to a millimeter (e.g., glass capillary tubes). An additional feature of this coating system is the capability of placing up to ten cylindrical elements for simultaneous coating, granting similar fabrication conditions for multiple devices. A more detailed description of the coating system can be found in [117].

Selection of the polymeric materials for the fabrication of photonic devices is based on their properties such as refractive index, hardness, thermal features, just to name a few. Usually, the polymers used for photonic applications are based on acrylate, styrene, carbonate, and silicone compounds [125]. In our case, we used two different polymers: polydimethilsiloxane (PDMS, Sylgard 184) which is thermally curable, and an acrylate UV-curable polymer (Efiron PC-414, further denoted

as UVpoly). Characterization of the coatings for single and multiple layers, as well as the generation of coating instabilities, are discussed in the following sections.

IV.2.1 COATING INSTABILITIES

Under certain conditions, the coating on a wire can present undulations owing to liquid instabilities. Such an effect is described by the Plateau-Rayleigh instability, resulting in the generation of a series of periodic droplets [126]. The characteristic growth of the periodic droplets occurs at a characteristic time (t_0), which depends on the wire and the coating thicknesses as follows:

$$t_0 = 12\frac{\eta\left(r+h\right)^4}{\gamma h^3} \qquad \text{<IV.16>}$$

Another factor to take into consideration is gravity, which may cause radial variations in the coating. This effect can be gauged upon comparing the capillary and gravity forces, determined by the density of the liquid polymer $\left(\rho\right)$ and the gravitational acceleration $\left(g\right)$. A common dimensional parameter used to evaluate this is the Bond number, given by:

$$Bo = \frac{\rho g r^2}{\gamma} \qquad \text{<IV.17>}$$

A criterion used is for a value of $Bo \ll 1$, where gravity effects on the coating material can be neglected given the characteristics of the fluid and thus radial uniformity on the coating layer can be assumed. Otherwise, the thickness and geometry of the deposited coating layer will depend on the capillary and Bond numbers [123].

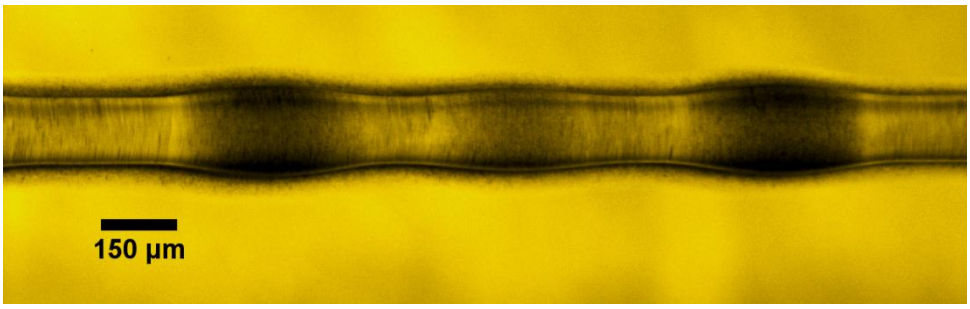

Fig. IV - 7. Optical microscope image from the coating instabilities produced when coating an optical fiber with PDMS containing a colorant.

From Eq. <*IV.16*>, it can be inferred that for $h < r$, the required time for formation of instabilities will be large. Conversely, for thick coatings the instability will appear after short periods of time once the coating layer has been deployed, thus producing a non-uniform coating. The formation of instabilities is a very important factor to consider in the wire coating process since its characteristic growth time limits the dimensions of a uniform layer. If polymers are sought as coating materials, the instability growth time must be larger than the time required for curing the polymer and hence obtain a uniform

coating layer. Figure IV-7 shows an unstable layer obtained in a PDMS coating deposited onto a glass capillary using a coating velocity of 2.5 mm/min.

IV.2.2 SINGLE-LAYER COATINGS

To evaluate the performance of single-layer coatings, standard single-mode optical fibers with a diameter of 125 μm (Corning SMF-28e) were coated at different speeds with thin-layers of PDMS and the UVpoly in 35 mm long sections. Prior coating, the protective polymer of the optical fibers was removed; the glass cladding was then cleaned with laboratory grade isopropyl alcohol and acetone, and finally they were placed in the coating system.

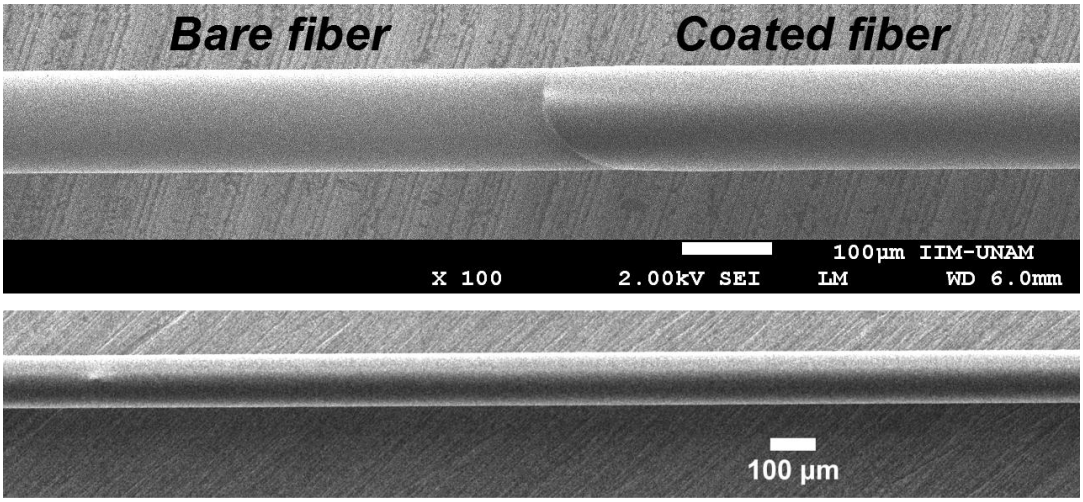

Fig. IV - 8. Scanning electronic microscopy (SEM) images of an optical fiber coated with a layer of UVpoly of approximately 1.15 μm at a speed of 1 mm/min: a) initial section of the coating, and b) uniformly coated optical fiber (bright dot caused by sample preparation-manipulation for SEM imaging).

Once the coating process was finished, the thickness of the deposited coating was measured using scanning electron microscopy (SEM). Thickness measurements were performed analyzing the SEM images in sections of 215 μm of length, every 5 mm along the entire coated section of the fiber. A direct comparison between the images obtained from the coated sections and those obtained from an uncoated section of the fibers yielded the increase in diameter due to the coating layer. In order to ensure uniform polymer thin coatings and avoid fluid instabilities, the fibers were coated at low velocities (< 2 mm/min). An example of an optical fiber coated with the UVpoly is shown in Figure IV-8. A noticeable difference between the bare fiber and the coated section is appreciated in Figure IV-8a, whereas the uniformity of the resulting coating is demonstrated in Figure IV-8b.

Thin layers of UVpoly were deposited at velocities of 0.5, 0.75, 1.0, and 1.5 mm/min., curing the polymer after the coating process was finished. Curing was carried out with a single sweep across the coated section with an UV curing LED system (Thorlabs CS2010, 365 nm) with a power density of 6 W/cm^2 for a period of time of 2 minutes. The thicknesses of the single-layer UVpoly coatings are

plotted in Figure IV-9 with their corresponding coating velocities. For comparison, the measured thicknesses are plotted along with the curve experimentally obtained using the LLD theory.

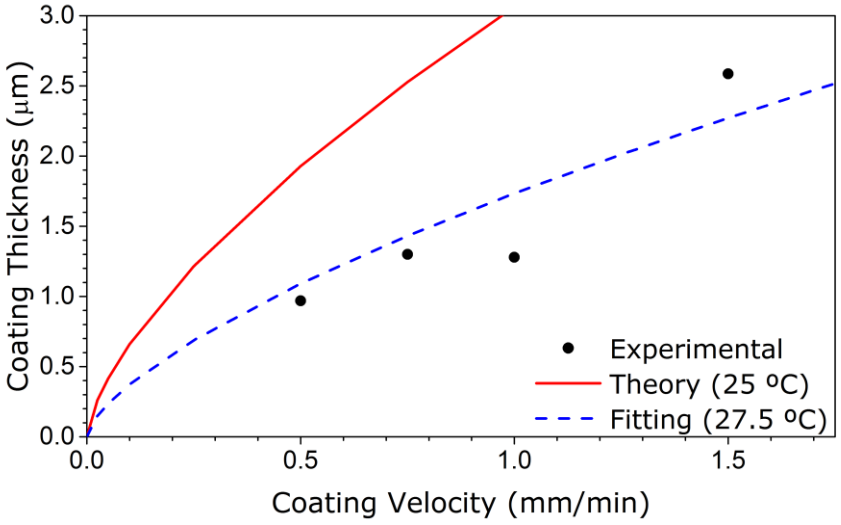

Fig. IV - 9. Measured layer thicknesses for the UVpoly at different coating velocities and calculated thickness for two different temperatures.

Since the data sheet of the UVpoly only includes the values of the viscosity as a function of temperature, the surface tension was estimated by fitting Eq. <*IV.14*> with the experimental data. The coatings in this experiment were performed at a room temperature of 27.5 °C, which yields an estimated viscosity of 6.45 Pa·s according to the data sheet. Based on this estimated value, we obtained a surface tension of 36.09 mN/m, which is in good agreement with previous reports for acrylate polymers [126]. It is important to notice that the surface tension and viscosity are highly affected by temperature, and this consequently affects the resulting coating thicknesses. Thermal variations during the coating process are thus accounted in the error bars included in the plot. To illustrate the temperature effects on the coating thickness, a plot of Eq. <*IV.14*> for a room temperature of 25 °C is also included in Figure IV-9.

PDMS is a thermally curable material composed by a silicone base polymer and a crosslinking agent. Owing to its curing mechanism (thermal), the surface tension and the viscosity vary with time, and the coating and characterization are thus more complex than the UVpoly. An additional factor to take into consideration is the mixture ratio of base polymer and curing agent affecting the properties of the cured PDMS. As an example, the data sheet specifies a η = 5.1 Pa·s for the base polymer and a η = 3.5 Pa·s for a mixture ratio of 10:1, for which a γ = 19.8 mN/m is reported elsewhere [128, 129]. In our experiments, the coatings were made of a polymer to curing agent mixture ratio of 8:1 to ensure complete solidification of the composite. In order to consider appropriate values for the PDMS viscosity, a time-dependent rheological characterization was carried out with a rheometer (ARG2, TA Instruments, cone-plate geometry 60 mm, 2 °). The results from this characterization yielded a nearly Newtonian viscosity of 0.5 Pa·s for a temperature of 27.5 °C during the first half hour after the mixture was done. However, four hours later, the viscosity of the mixture was measured to be η = 10 Pa·s, clearly showing that the rheological properties of PDMS vary considerably during the curing process.

Several bare optical fibers were coated with PDMS mixed in an 8:1 ratio at velocities ranging from 0.375 to 1.5 mm/min. As for the UVpoly case, the coatings were measured via SEM images. As illustrated in Figure IV-10, different thicknesses were obtained for the same coating velocity when using different PDMS viscosities. The fitting curves shown in the figure were obtained considering a γ = 19.8 mN/m. From these results, it is clear that an increase in the layer thickness occurs as the polymer viscosity increases as a consequence of thermal effects. In some of these cases, the polymers were prepared and deposited as coatings in different days and under different environmental conditions. Nonetheless, the results are consistent with the predictions of wire coating theory.

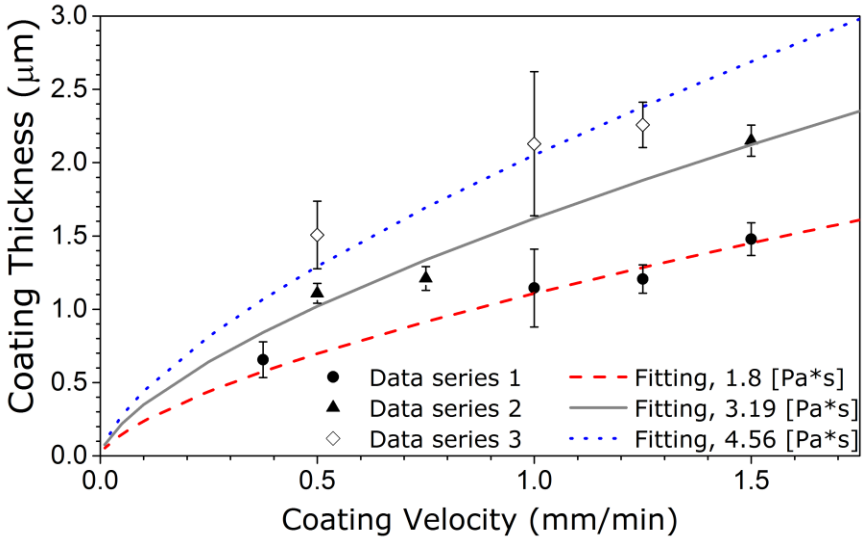

Fig. IV - 10. Characterization of the coating layer thickness for PDMS at different coating velocities and viscosities.

Optical losses induced by the coatings are an important factor to consider in photonic devices. These were evaluated on the transmission spectra of tapered optical fibers fabricated with standard single-mode fibers using the flame-brushing technique [54]. Optical fiber tapers with a total length of 4 cm and with a constant waist diameter of approximately 6 μm along 1 cm were coated at a speed of 1.5 mm/min using both materials, UVpoly and PDMS; the resulting coating layers were estimated to had thicknesses of 200 and 110 nm, respectively. As the radius of the tapered section is significantly reduced, light propagation in occurs in the cladding material of the fiber. As a consequence, light confinement is then defined by the surrounding material.

Typical attenuation losses on the transmission spectrum after depositing the polymer coatings onto the tapered section of the fibers are shown in Figure IV-11. While PDMS coating layers can present losses from 1.8 to 0.75 dB, the UVpoly coatings losses are below 0.75 dB. The attenuation slope over the spectral range observed for PDMS layers is attributable to wavelength dependent power confinement or mode field extension due to the effective refractive index of the coating. Similarly, the spectral modulation registered in the spectra is most likely due to the refractive index and due to variations in mode confinement when a layer with similar *n* value surrounds the optical fiber. Small fluctuations with maximum amplitude of 0.3 dB observed for both coatings may be attributed to

modal beating typically observed in non-adiabatic tapered structures [130, 131]. Therefore, these results suggest that small non-uniformities are present along the coating layers, probably caused by polymer impurities and growth of imperceptible instabilities in the tapered sections of the fibers, as well as the a change in light confinement generated by the thin-layer coatings.

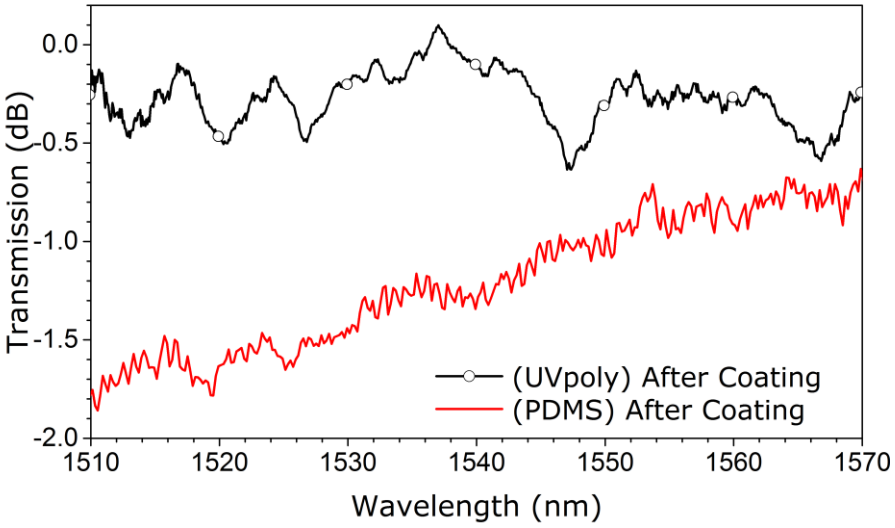

Fig. IV - 11. Transmission losses registered after coating with tapered optical fibers polymer thin-layers.

Since the curing process for thermally activated polymeric materials evolves in time, it is recommended to always start the coating process immediately after adding the curing agent. This will ensure a constant viscosity and homogeneity of the polymer during the lapse of time of the coating process. Aside from thermal effects, other sources that may contribute to the alteration of the coatings thickness and uniformity include external vibrations, inadequate sample preparation, and humidity. These factors must therefore be minimized and particularly addressed during coating process.

From the SEM images analysis we observed uniform coatings over the entire length of the fibers, even for coatings of a few centimeters in length. For the thin layers deposited on the fibers, and using the fitted values of the surface tension, the Bond numbers calculated for our experiments yielded values of 1.6×10^{-3} for the UVpoly, and 4.9×10^{-3} for the PDMS. Hence, gravity effects on the coatings were negligible for both cases and radial uniformity can be assumed for the deposited layers. All the listed results prove the suitability of the coatings produced by this method for the development of polymer coated photonic and optic devices with small diameters, in particular for tapered fiber devices.

IV.2.3 MULTIPLE-LAYER COATINGS

Deposition of thicker uniform polymer layers can be achieved upon performing a multiple coating process. The coating layer thickness (h) is commonly limited in the single-layer deposition by the growth time of the surface instability. Deposition of multiple layers prevents the growth of

instabilities provided that *h* is decreased in every step of the deposition process. This approach was explored by applying multiple layers of the described polymers onto optical fibers and glass capillaries.

An important factor to consider during the deposition of multiple layers is the solid polymer–liquid polymer interface (i.e., liquid polymer over a cured polymer, instead of having a glass-liquid polymer interface). This is important because such an interface favors the slippage of the liquid upon applying the second polymer layer [132]. Thus, the LLD thickness model (Eq. *<IV.14>*) requires adjustments to account for this slipping condition during the coating process. This is addressed by using an *apparent viscosity* (η_{app}) defined as [133]:

$$\eta_{app} = \frac{\eta h}{\left(h + \lambda_{slip}\right)} \qquad \text{<IV.18>}$$

where λ_{slip} is the slip length, which accounts for the non-zero velocity at the interface.

Standard single-mode optical fibers were coated at a speed of 1.5 mm/min with one layer of UVpoly and cured with UV light irradiation; subsequently, a second coating layer of the same polymer was deposited and cured. Thickness results exhibit an increase in fiber diameter for a two-layer coating, as shown in Figure IV-12. Using Eqs. *<IV.14>* and *<IV.18>* we obtained a η_{app} = 2.93 Pa·s. The experimental thickness measured after deposition of the second layer coating agrees well with the value predicted by the LLD model.

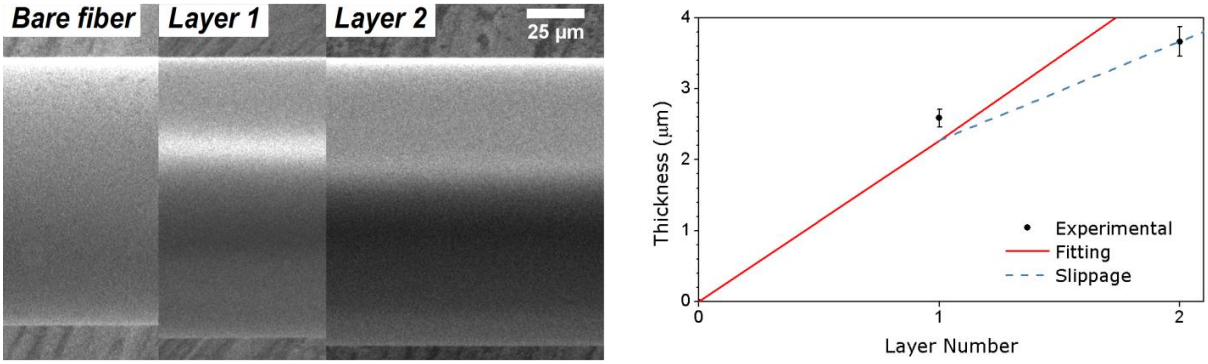

a) *b)*

Fig. IV - 12. Characterization of the layer thickness of UVpoly for multiple layers on optical fibers: a) SEM images of the bare and coated fibers; b) measured thicknesses for the layers and fitting using the slipping condition (see text).

Coating of cylindrical elements with bigger dimensions is also of interest for diverse applications which may require thicker layers. Several applications have arisen based on glass capillaries in the fields of optofluidics and photonics [134, 135]. An example of this is the use of photoresponsive polymer layers on glass capillaries proposed as a novel approach for inducing thermocapillary flow [134].

Evaluation of the multilayer approach was performed in [117], coating 20 µL glass capillary tubes (Drummond, 450.85 µm radius) with the UVpoly at a velocity of 5.21 mm/min. These results were

then compared with those previously reported in [134], where multiple layers of PDMS with carbon nanopowder (PDMS+CNP) were deposited at the same velocity. Measurements of layer thicknesses exhibited a lower slippage for the UVpoly in glass capillaries than for the coated optical fibers, with a η_{app} = 5 Pa·s. As for the PDMS+CNP composite, the measurements and fitting yielded a η_{app} = 2.7 Pa·s [134]. As expected from Eq. *<IV.18>*, thicker coatings will be less affected by the variations caused by the apparent viscosity and hence slippage will decrease (i.e., $\eta_{app} = \eta$). The resulting Bond numbers for the capillaries were 0.085 for the UVpoly and 0.1 for the PDMS, respectively; as before, gravity effects on the coating layers are minimum.

As shown above, multiple layer coatings can be readily deposited on devices ranging from the micrometric to millimetric diameter scales. It is important to notice that the desired thickness of each layer can be easily adjusted upon controlling the coating process velocity following the guidelines provided by simple wire coating theory. Adjustment of the coating thickness allows for the definition of the final diameter of micro-resonators using cylindrical elements.

IV.3 FUNCTIONAL POLYMERIC MATERIALS

A long list of different polymer based materials has been developed for optics and photonics applications [106-108, 136]. Polymers grant a simpler processing and fabrication processes compared to other materials. Moreover, a wide diversity of functional materials can arise from their flexibility for hosting additional materials. As an example, PDMS is a polymer extensively used in MEMS, electronics, optics, and biomedical applications due to its mechanical, rheological, thermal, and optical properties. The use of PDMS in optics has grown due to its transparency over a wide spectral range and its ease of use in replica-molds fabrication processes [137].

Incorporation of different materials into PDMS has been successfully demonstrated for the creation of reconfigurable composites. Examples of these include the addition of azobenzenes, carbon nanoparticles, metallic powder, etc. [107, 138]. For our experiments, light activated composites were obtained upon mixing azobenzenes and fluorescent materials with PDMS as a host polymer matrix. A detailed description of the mixing procedure for these composites can be found in Appendix A. The relevant characteristics of these photoactive composites are discussed in the following sections.

IV.3.1 AZOPOLYMERS

Azopolymers are functional polymers originated from the inclusion of azobenzenes in a polymeric matrix. Azobenzenes are chemical molecules commonly used as colorants or dyes, although the most attractive feature of these materials for photonics is the photoisomerization process. This can generate physical changes in the azobenzene molecules through light irradiation. Typically, the photoisomerization process leads to the *trans-cis* transformation as well as to the

realignment of the molecules when interacting with linearly polarized light [108, 139]. These changes originate optical anisotropy, which is of interest for the fabrication of photonic devices.

MRRs with azopolymer coatings were fabricated using Disperse Red 1 (DR1) obtained from Sigma-Aldrich (CAS: 2872-52-8) as azobenzene. As shown in the spectrum of Figure IV-13a, the absorbance of DR1 lies within the range of 410 – 555 nm. This azobenzene has been proved to generate birefringence under irradiation with linearly polarized light when contained in polymeric matrices [108, 139]. In our experiments, the concentration ratio used for the mixture of DR1 with PDMS was of 0.1 % in weight; this composite is denoted as PDMS+DR1. Removal of DR1 clusters was done through filtering with two syringe polytetrafluoroethylene (PTFE) filters: first a 1 μm filtering stage followed by a second stage of 0.4 μm. This filtering process yielded a red-translucent composite.

Photoinduced birefringence in the azopolymer mixture was tested with an array of crossed polarizers [139, 140]. A probe beam is launched through a film of a given thickness (d), measuring the change in the beam intensity at the input (I_0) and output (I) of the sample. The probe beam used for this experiment must be of a wavelength (λ) where the material under study presents null absorbance. Change in refractive index (Δn) generated in the azopolymer can be described by [139]:

$$\Delta n = \frac{\lambda}{\pi d}\sin^{1}\sqrt{\frac{I}{I_0}} \qquad \text{<IV.19>}$$

A 138 ± 11 μm layer of PDMS+DR1 was deposited on a glass substrate and subsequently irradiated with a semiconductor laser (λ = 532 nm, 5 mW). A HeNe laser (λ = 632.8 nm) was used as a probe signal to measure the birefringence, and the change in optical power transmission through the polarizers was measured with a silicone photodiode (S150C, Thorlabs). The change in power transmission registered with this arrangement is shown in Figure IV-13b. Using this result, the change in refractive index for this composite was estimated according Eq. <*IV.19*> yielding a result of $\Delta n = 2.41\times10^{-5}$, which in good agreement with previous reports for similar compounds [139].

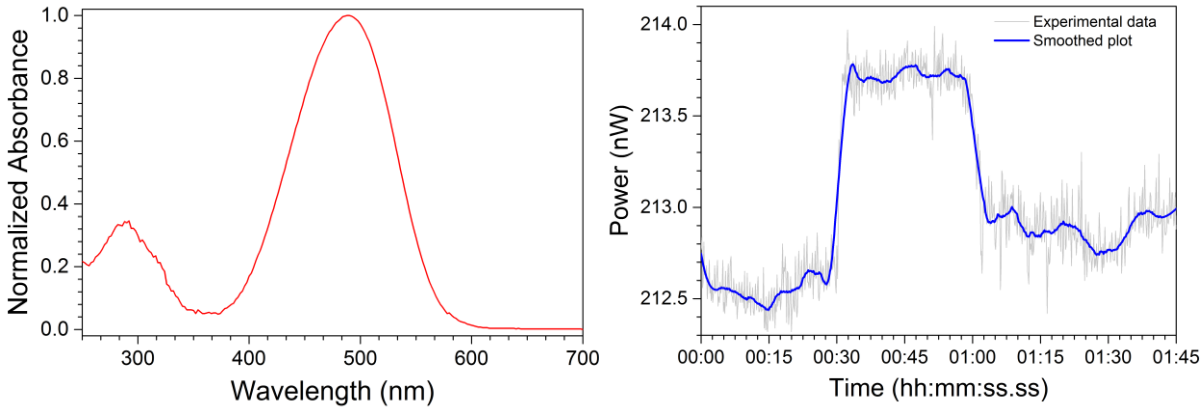

a) *b)*

Fig. IV - 13. PDMS+DR1 azopolymer characterization. a) Absorbance spectrum. b) Photoinduced birefringence with a laser beam of 475 nm and measured at 633 nm.

IV.3.2 FLUORESCENT COMPOSITES

Upconversion process is an attractive feature in some materials that can be used to trigger different effects activated by light. As an example, emission of visible light can occur in materials such as erbium and ytterbium, owing to IR light absorption and subsequent electron transition to higher electronic states. The radiative decay of these electrons will thus lead to the emission of photons within the visible spectrum. Erbium and ytterbium, which are among the most popular materials used with optical fibers, can thus radiate visible light (typically green-like) through upconversion [142]. An improved composite to generate fluorescence in visible wavelengths under IR irradiation is the ytterbium and erbium-doped sodium yttrium fluoride (NaYYbErF). Commercially available NaYYbErF powder (Sigma-Aldrich, CAS: 753489-02-0) was used for doping PDMS with a weight ratio of 1 %; this composite was labeled as PDMS+Yb. A typical fluorescence spectrum generated with this material is shown in Figure IV-14. As seen in the figure, upon irradiation with a laser diode (λ = 975 nm), the fluorescence peaks occur at wavelengths of 539.5 nm and 653.5 nm.

The PDMS+Yb composite offers the possibility to generate changes in its optical properties by means of an optical signal, a feature desired in photonic devices. Specifically, the incorporation of PDMS+Yb in fiber optic devices use an excitation signal with λ = 975 nm, and a signal with λ = 1550 nm can be used as a probe beam, for instance, as a carrier for data transmission. Thus, the required optical signal to generate fluorescence in this material can have a different wavelength than that used for signal transmission. Both wavelengths are normally used in optical telecommunications applications. Another possibility is the combination with other layers of different materials, where the emission generated by the upconversion process may be absorbed to induce further changes, as occurs in azopolymers.

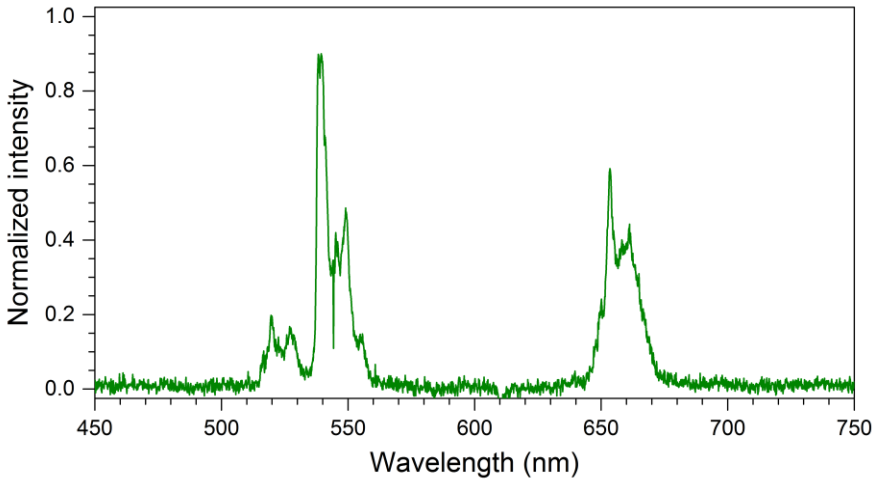

Fig. IV - 14. Emission spectrum from the PDMS+Yb composite upon irradiation with a λ = 975 nm laser diode.

IV.4 MICRO-RING RESONATORS WITH FUNCTIONAL POLYMERS

Micro-ring resonators coated with layers of PDMS+Yb and a PDMS+DR1 were fabricated using the wire coating technique described earlier. The MRRs were excited by coupling light from the waist section of a single-mode tapered optical fiber, with a waist diameter of approximately 3.5 μm, along 1 cm section, and total length of 5.5 cm. Coupling was generated by setting the resonator perpendicularly to the tapered fiber aiming to generate a circular-cross section for the resonances instead other geometries (i.e., elliptical-cross sections for tilted resonators). Analysis of the MRRs features was performed upon recording the transmission spectra with an Optical Spectrum Analyzer (OSA, Agilent 86140B); further details of the spectra were obtained through the Fast Fourier Transform (FFT). A broadband probe signal coming from an amplified stimulated emission (ASE) from an erbium doped fiber amplifier (EDFA, Pritel LNHPFA-27-IO) centered at a wavelength of 1550 nm was used, which was launched into the tapered fiber. The spectral features of the polymer coated MRRs are described in the following sections.

IV.4.1 ALL-GLASS RESONATORS

Standard single-mode silica (SiO_2) fibers were used as the building blocks for the MRRs. In these experiments the resonator is constituted only by the cylindrical-glass rod. The typical transmission spectrum of a resonator using a bare single-mode fiber (125 $\pm$ 0.7 μm diameter) is shown in Figure IV-15a. The resonances are periodic dips with a FSR = 4.26 nm (delimited by the red dashed-lines) and a FWHM = 0.1 nm. With the measured values and by using Eq. <*IV.8*>, a group refractive index of 1.4361 was determined for the 125 μm diameter fiber MRR. As seen in Figure IV-15a, the spectrum shows multiple resonant peaks within a single period, indicating that several resonant modes are excited in the resonator due to light penetration in the bulk material. The response obtained was repeatable under the same coupling conditions, whereas changing the position of the resonator or parameters of the tapered fiber resulted in similar responses but different resonant wavelengths. The strongest resonance peak corresponds to the fundamental mode, showing a contrast of 2 dB. For these all-glass MRRs, the registered average losses were in the range of 1.5 – 4 dB.

Further details of the registered spectra were obtained using the FFT. In particular, the magnitude of the FFT indicates how many periodic signals are present in the transmission spectrum, and each point indicates the number of periods of each component. For the spectrum shown in Figure IV-15a, the FFT shows a strong single low-order component, corresponding to the number of periodic lobes for the fundamental mode component, shown in Figure IV-15b. Higher order components indicate the multimodal resonances obtained in the cylindrical structure decaying in a gradual fashion.

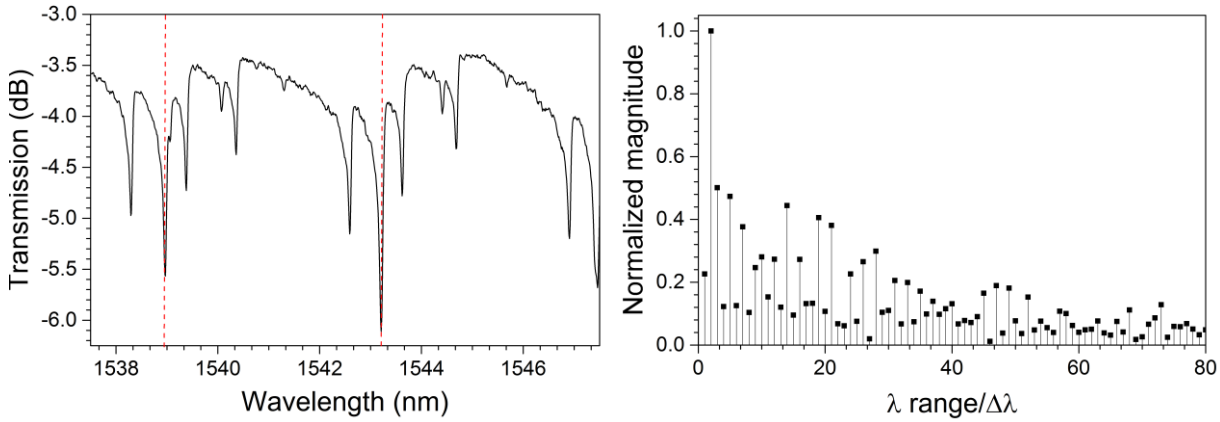

Fig. IV - 15. a) Typical transmission spectrum for an all-glass MRR. The resonant element is a SMF silica fiber (125±0.7 μm diameter); b) FFT obtained from the transmission spectrum.

Polarization effects in MRRs are an important and these have to be considered when analyzing the spectral response. This is because light coupling to the resonator will depend on the orientation of the electric field (i.e., TE or TM polarization) [28, 29]. Hence, a change the polarization of the signal sent through the tapered optical fiber will favor light coupling into certain resonant modes. This effect is illustrated in Figure IV-16, showing the transmission spectra for the same resonator but for two states of polarization (SOP) launched into the tapered fiber.

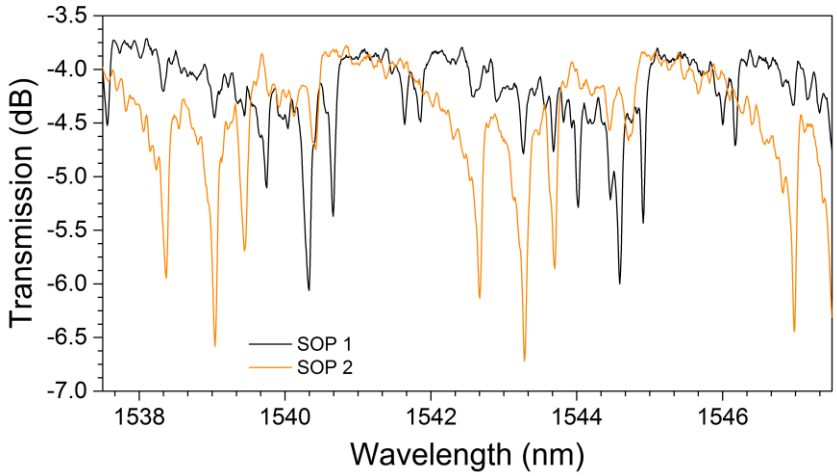

Fig. IV - 16. Transmission spectra for two different states of polarization (SOP) coupled into the SMF-based MRRs.

IV.4.2 RESONATORS COATED WITH A SINGLE MATERIAL

The spectral features of MRRs based on a composite polymer/glass structures will depend on the thickness and refractive indices of the polymer and glass fiber used for their construction. Single-layer MRRs were fabricated upon the deposition of thin layers of PDMS, PDMS+DR1, and PDMS+Yb polymer coatings on standard single-mode fibers (SMFs). In order to solidify the composites, each of the base mixtures were mixed with a crosslinking agent in a weight ratio of 9:1 and then heated at

85°C during a period of time of 2 hours [117]. These coatings were deposited using the same coating system described earlier (see section IV.2), using a coating velocity of 0.935 mm/min for all cases. The resulting coating thicknesses were approximately 1.55 μm and these were excited with a tapered fiber. Obtained normalized transmission spectra and the corresponding FFT for each of these coated resonators are shown in Figure IV-17.

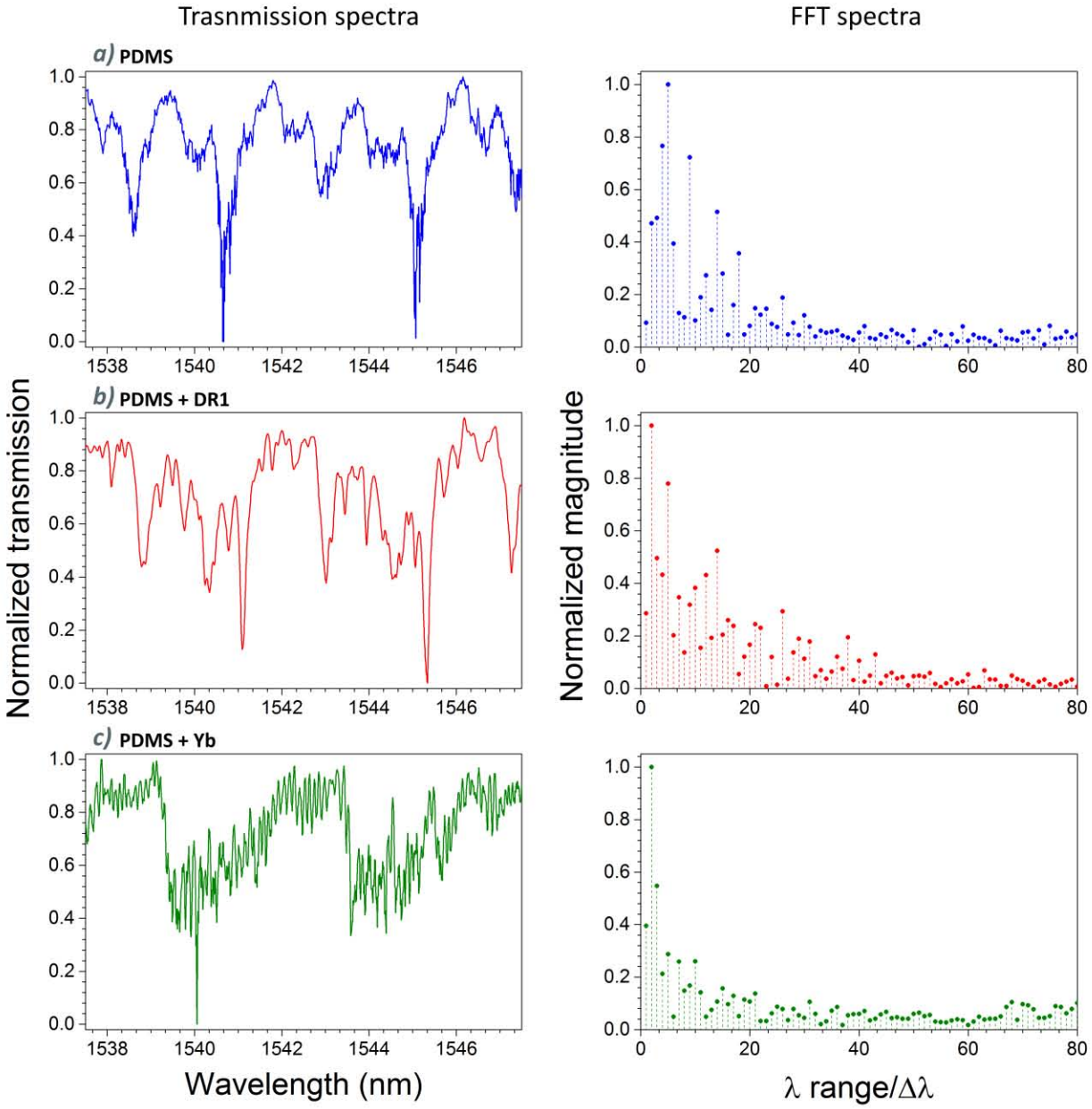

Fig. IV - 17. Transmission spectra and FFT for the MRRs using single-layer coatings (1.55 μm thicknesses) of: a) PDMS, b) PDMS+DR1, and c) PDMS+Yb.

Analysis of the PDMS coated resonator provides information of the effects generated only by the polymeric matrix, which is further used to host the active materials. Since PDMS possesses a smaller refractive index than that of silica, light confinement in this structure is similar to the case illustrated

in Figure IV-5c. Hence, light does not get confined completely in the PDMS layer and light interacts mostly with the silica fiber. Nonetheless, the addition of this layer allows for the propagation of fewer modes in the resonant structure due to coupling from the PDMS into the silica, but not in the reverse direction. This can be noticed upon comparing the FFT for the SMF (Figure IV-15b) and the single-layer PDMS (Figure IV-17a); notice that the latter spectrum does not show the higher order components.

As shown in Figure IV-17b, the spectrum for the PDMS+DR1 show similar resonances to those obtained with PDMS. Also, a notorious increase in the contrast of the dips corresponding to the lower order components contained within a single period can be observed. This indicates better propagation of the lower order modes excited in the resonator coated with PDMS and PDMS+DR1. FFT analysis indicates a reduction in the higher order spectral components, which agrees with the features of the transmission spectra. For the PDMS+Yb coatings, the quality of the resonance decreases drastically, showing a noise-like spectrum and without a clear contrast of resonance wavelengths (see Figure IV-17c). The FFT for this composite shows that most of the spectral components disappear with this coating, with the exception of a few lower order modes. This is however an expected feature due to the optical absorption of Yb and Er within this wavelength range.

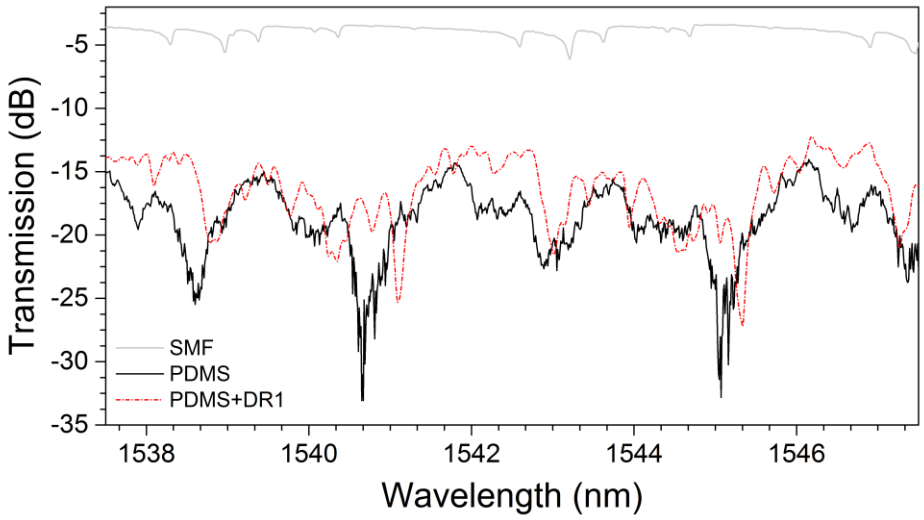

Fig. IV - 18. Insertion losses and resonance features in the transmission spectra for the MRRs.

An effect observed for the resonances when polymer coatings are used for the MRRs is the broadening of the FWHM to approximately 0.41 and 0.18 nm for the PDMS and PDMS+DR1, respectively. A feature of interest when using polymeric coatings is the contrast enhancement generated at the resonance wavelengths, which can reach attenuations of 15 dB. However, coupling losses increase for polymer resonators when compared to the bare SMFs. A comparison of the transmission spectra for all the single-layer coated and the bare SMF micro-ring resonators is shown in Figure IV-18. Notice that the insertion losses are much larger for the polymer-based MRRs owing to the difference in refractive indices. These could be improved upon reducing the refractive index

contrast between the polymer and the glass fiber, or by using an additional index-matching coating layer.

IV.4.3 MULTILAYER COATED RESONATORS

Multilayer micro-ring resonators were fabricated with standard single-mode optical fibers coated with alternating thin films of PDMS+Yb and PDMS+DR1 composites. Deposition of the coating layers was performed using the same procedure than for the single-layer case. The multilayer resonator was fabricated using a first layer of the PDMS+Yb mixture, and a second layer using the PDMS+DR1 composite. The main purpose of this layer was to induce changes in the refractive index by means of an optical signal. These were induced by a 975 nm laser diode launched through the tapered fiber. This "pump" beam was combined with the probe signal by means of a 980/1550 nm fiber wavelength multiplexer (WDM). An illustration of the excited multilayered micro-resonator and the experimental setup to test these devices are shown in Figure IV-19. The excess of excitation light not coupled to the resonator was filtered with a 980/1550 nm WDM.

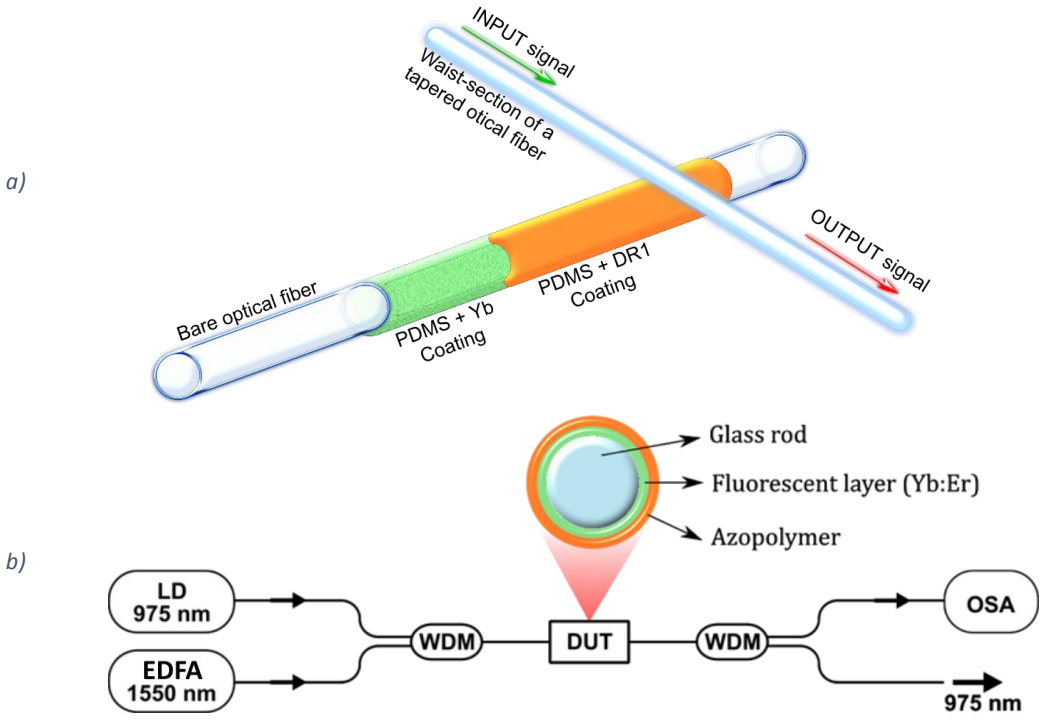

Fig. IV - 19. a) Illustration of the multilayer coated micro-ring resonator. b) Experimental setup to excite and analyze the multilayer MRRs.

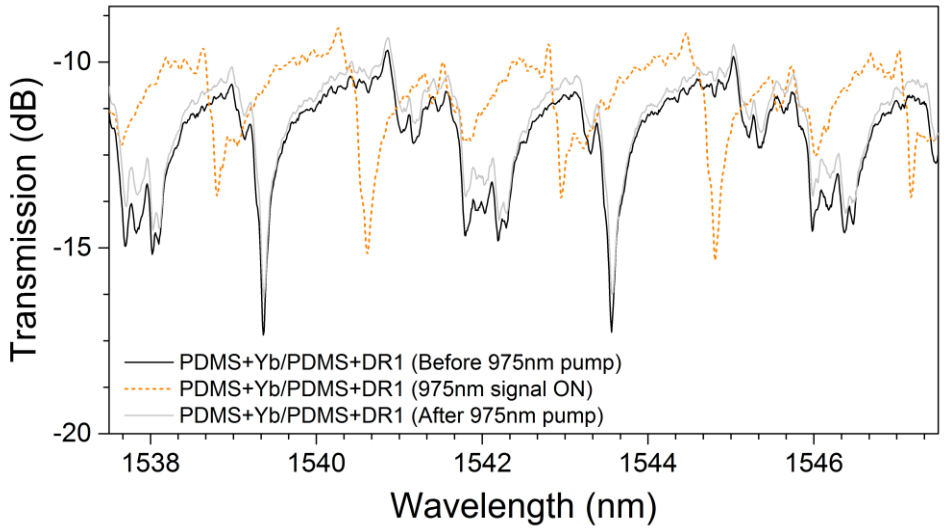

Fig. IV - 20. Transmission spectra of the multilayer MRRs coated with photoactive materials.

The transmission spectrum of the device and the effects generated when the pump signal is launched are shown in Figure IV-20. For this arrangement the pump light is absorbed mostly by the PDMS+Yb layer and the resonance features are only shifted towards longer wavelengths. Notice that for this configuration, resonance occurs at outermost polymer layer, which incorporates the azobenzene. Excitation of the PDMS+DR1 layer is realized by the green luminescence generated in the PDMS+Yb layer. This is produced through upconversion effects when this polymer layer is pumped with the 975 nm signal. The green fluorescence signal is thus absorbed by the DR1 molecules and an additional change in the refractive index is therefore obtained. Larger wavelength shifts were observed upon increasing the power of the 975 nm pump laser. This is due to the infrared light absorption of the PDMS+Yb layer and reabsorption of the green light by the PDMS+DR1, generating a continuous change in the refractive index. This effect will cease once the saturation point of the Yb and Er is reached. In our experiments, we did not observed any saturation effects. Finally, upon turning the pump signal off, the original spectral features are readily obtained.

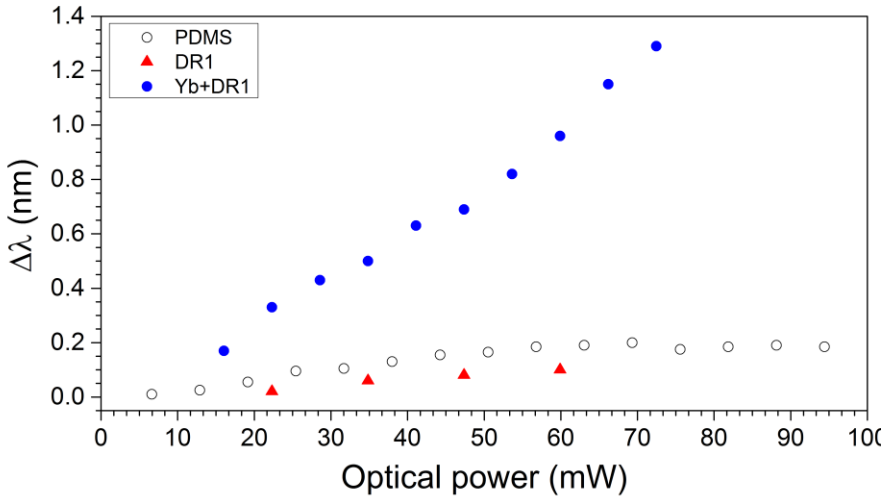

Fig. IV - 21. Wavelength peak shift upon 975 nm laser signal excitation in different polymer coated micro-ring resonators.

When using only PDMS as coating material, a slight displacement is gradually induced until a saturation point is reached. A similar response is generated when DR1 is added into the PDMS matrix, indicating no interaction of infrared light with the azobenzene. In contrast, for the PDMS+Yb resonators (not included in the plot), absorption of the 975 nm laser signal induces a larger modification in the refractive index. However, this leads to a distortion in the transmission spectra and the resonance peaks are lost. Notice that for the multilayer arrangement, no saturation point was observed and a maximum wavelength shift of 1.6 nm was registered. The addition of a second layer (PDMS+DR1) thus contributes to an enhanced tuning response, without distorting the resonance effects.

IV.5 DEVICE PACKAGING

As exposed earlier, applications of wavelength tunable MRRs devices include sensor development and filtering for signal conditioning. An important factor to be addressed for these devices resides in the packaging procedure. Proper packaging of MRRs is a challenge that commonly limits their use in real-life applications [30, 142]. A simple way to alleviate this problem is to encapsulate the devices in a polymeric matrix. This approach allows ensuring a fixed position of the optical elements composing the MRR, thus yielding a stable spectral response. PDMS has proven suitable for packaging and fabricating optical elements with low losses. Therefore, packaging may contemplate entirely or partially embedding the MRRs in PDMS [143]. An example of the multilayer MRRs enclosed in PDMS is shown in Figure IV-22.

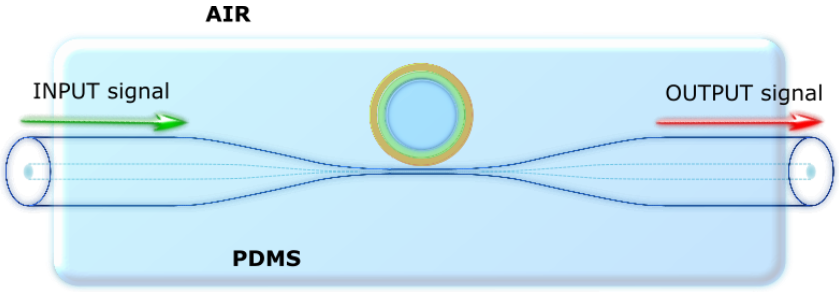

Fig. IV - 22. Illustration of a multilayer coated MRR packed in PDMS

It is important to recognize that the packaging process modifies the surrounding medium of the MRR and thus changes the number of resonant modes. This effect is illustrated in Figure IV-23, showing the transmission spectra for a MRR before and after being embedded in a PDMS housing. An improvement in the total losses is observed due to the reduction of the refractive index contrast of the materials. Notice however that the contrast in the resonant dips decreases; hence, optimization in the refractive index difference is required in order to obtain adequate spectral features for a specific application.

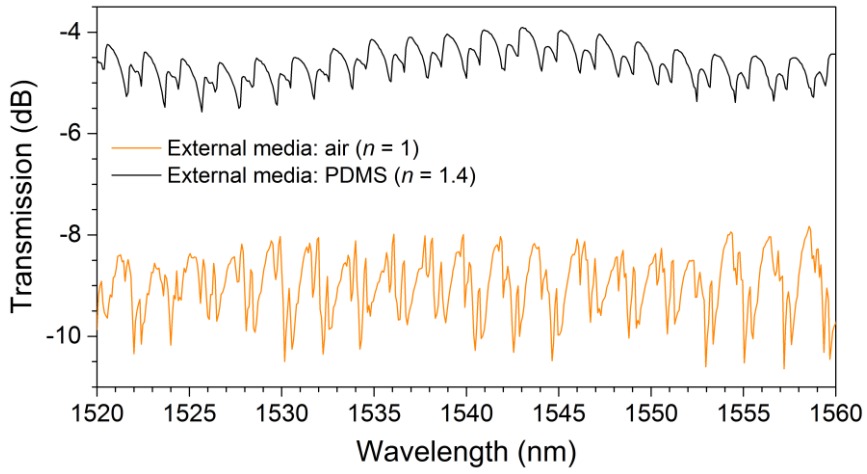

Fig. IV - 23. Pure silica rod used as micro-resonator packed entirely in PDMS.

The use of multiple polymer layers for the construction of micro-ring resonators clearly represents an attractive option the fabrication of low-cost devices. Their ease of fabrication and the possibility to incorporate different materials provide a versatile platform for developing photonic devices.

CHAPTER V: CONCLUSIONS

All-fiber photonic lanterns formed with multiple fibers were fabricated exhibiting the capability of produce diverse light patterns at the output in a controlled fashion. The fabrication process followed to obtain adequate devices was fully described. Also, the relevant parameters and aspects needed for the realization of these devices were also defined. Modal selectivity granted independent excitation of linearly polarized fiber modes through separate input fibers. This feature was achieved by a correct selection and positioning of the optical fibers during the assembly process of these devices. For the arrangements and methodology followed in this work, it was possible to address the first nine LP fiber modes without additional requirements other than a proper design of mode-selective photonic lanterns.

Fabrication of PLs able to generate a larger number of modes was accomplished by using microstructured preforms specifically tailored for this purpose. These preforms simplified the fabrication process of the PLs, resulting in a straightforward and repeatable method. Additionally, the use of this approach allows for overcoming the intrinsic fabrication complexity when scaling to a larger number of fibers. Nonetheless, there is still room for improvements in the preforms used for fabrication of these devices since novel designs may lead to generate specific light patterns, devices with lower losses, and compatibility with other multimode fibers.

Integration of the PLs to fiber systems was tested upon splicing them to fibers supporting multiple modes (i.e., few-mode fibers, FMFs). Transmission of the generated mode profiles through these fibers was verified further showing low-coupling losses. The use of the PLs as MUX/DEMUX devices showed to be a viable application, directly compatibility with FMFs that have been developed for the upcoming generation of fiber optics telecommunications systems. Additional information obtained from this study corroborated the modal selectivity of these devices, as observed from the output mode profiles. Hence, a proper design of photonic lanterns can allow for a correct match with FMFs and successful transmission of each particular light pattern.

Careful analysis of the intensity distributions at the output of the mode-selective PLs revealed remarkable mode purity values. Complementary examination of MSPLs demonstrated that following the correct fabrication procedure, it is possible to obtain operation in a broadband wavelength range, preserving the same light intensity distribution. This feature proved the suitability of these devices for multiple applications aside the telecommunications area. Therefore, a significant number of research areas using complex devices to generate specific light patterns could be simplified with the use of passive and compact devices, such as mode-selective PLs.

A simple methodology to fabricate reconfigurable micro-ring resonators was also proposed in this work. This may offer a viable option for developing reconfigurable devices with potential use in

sensing applications. The use of polymeric materials as coatings allowed for easily incorporate different compounds. Such a capability offers the possibility to include different functionalities in a single device, and thus address diverse needs. Furthermore, the incorporation of multiple layers of material serves as a mechanism to control light confinement in these devices. Therefore, the interaction of light with multiple layered materials can be adjusted upon the appropriate choice of refractive indices. As shown in this work, control of the coating process is key feature for successfully producing resonators with a specific thickness. In this sense, the coating system used for this purpose offered the necessary means for obtaining well defined thicknesses of polymer coatings by varying the speed of the coating process.

The fabrication of polymeric multilayer resonators is an attractive proposal as it employs low-cost materials, with high commercial availability and ease of fabrication. Adjustments in the coating thickness allows for the definition of the final diameter of the micro-resonators, which in turn defines the resonance conditions. Another attractive aspect of this method is the use of standard cylindrical elements as a building block for the micro-resonators, avoiding the need of specialized substrates or materials, typically requiring additional processes to fabricate resonant structures.

Incorporation of light-activated materials prevents the use of electrical signals to activate specific functions of the materials used as coatings for the resonators. On this basis, activation and monitoring of the proposed devices can be achieved through a single optical fiber. As an example, devices using a layer of photoluminiscent material, in combination with a photoactivated material, yielded a device capable of tuning its spectral response by means of an optical signal.

The achievements and progress presented in this work comprise contributions on the area of fiber optic devices fabrication. The most relevant aspects of the fabricated devices can be summarized as:

- The relevant fabrication parameters to obtain mode-selective photonic lanterns, able to excite several number of LP fiber modes, were defined.
- A new method to fabricate micro-ring resonators, based on multiple coatings of reconfigurable polymeric materials, was demonstrated.

Future work on these devices may address improvements in photonic lantern design, aiming at obtaining LP modes of a superior quality. Further efforts are also required in order to obtain direct compatibility between the PLs and the FMFs, in particular for spatial division multiplexing applications. As for the MRRs, the next step is their use in a specific application; this will define the number of layers, coating materials, and thicknesses required to achieve the desired performance. Evidently, packaging must be improved on both devices in order to grant stability in their spectral responses as well as robustness. This will lead to rugged devices which may find direct application in a wide variety of photonic related areas.

REFERENCES

[1] B. Saleh y M. Teich; "Fundamentals of Photonics," Wiley Interscience, 2nd Edition, 2007.

[2] Katsunari Okamoto, "Fundamentals of Optical Waveguides," Academic Press, 2nd Edition, 2005.

[3] S. Sudho and K. Okamoto, "New Photonics Technologies for The Information Age: The Dream of Ubiquitous Services," Artech House optoelectronics library, 2006.

[4] E. Udd, "Fibre Optic Sensors," Wiley Interscience, 2002.

[5] Chen Sun,Mark T. Wade, Yunsup Lee, Jason S. Orcutt, Luca Alloatti, Michael S. Georgas,Andrew S. Waterman, Jeffrey M. Shainline, Rimas R. Avizienis, Sen Lin, Benjamin R. Moss, Rajesh Kumar, Fabio Pavanello, Amir H. Atabaki, Henry M. Cook, Albert J. Ou, Jonathan C. Leu, Yu-Hsin Chen, Krste Asanović, Rajeev J. Ram, Miloš A. Popović & Vladimir M. Stojanović, "Single-chip microprocessor that communicates directly using light," Nature 528, pp. 534–538, 2015.

[6] Jeffrey J. Fielda, Keith A. Wernsing, Scott R. Domingue, Alyssa M. Allende Motz, Keith F. DeLuca, Dean H. Levi, Jennifer G. DeLuca, Michael D. Young, Jeff A. Squier, and Randy A. Bartels, "Superresolved multiphoton microscopy with spatial frequency-modulated imaging," PNAS, vol. 113 No. 24, 2016

[7] Meng-Tsen Ke, Yasuhiro Nakai, Satoshi Fujimoto, Rie Takayama, Shuhei Yoshida, Tomoya S. Kitajima, Makoto Sato, Takeshi Imai, "Super-Resolution Mapping of Neuronal Circuitry With an Index-Optimized Clearing Agent," Cell Reports, Volume 14, Issue 11, pp. 2718 – 2732, 2016.

[8] Paras N. Prasad, "Introduction to Biophotonics," J. Wiley & Sons, Inc, 2003.

[9] Maria Dienerowitz, Michael Mazilu, and Kishan Dholakia, "Optical manipulation of nanoparticles: a review," Journal of Nanophotonics, Vol. 2, 021875, 2008.

[10] J. Bland-Hawthorn, "Astrophotonics: The Future of Astronomical Instrumentation," in *CLEO: 2015*, OSA Technical Digest (online), paper STu4L.1, 2015.

[11] P. J. Winzer, "Spatial multiplexing: the next frontier in network capacity scaling," in 39th European Conference and Exhibition on Optical Communication (ECOC), pp. 372–374, 2013.

[12] D. J. Richardson, J. M. Fini, and L. E. Nelson, Space-division multiplexing in optical fibres," Nat. Photonics 7, 354, 2013.

[13] Guifang Li, Neng Bai, Ningbo Zhao, and Cen Xia, "Space-division multiplexing: the next frontier in optical communication," Adv. Opt. Photon. 6, pp. 413-487, 2014.

[14] Roland Ryf, Sebastian Randel, Alan H. Gnauck, Cristian Bolle, Alberto Sierra, Sami Mumtaz, Mina Esmaeelpour, Ellsworth C. Burrows, René-Jean Essiambre, Peter J. Winzer, David W. Peckham, Alan H. McCurdy, and Robert Lingle, "Mode-Division Multiplexing Over 96 km of Few-Mode Fiber Using Coherent 6 × 6 MIMO Processing," J. Lightwave Technol. **30**, pp. 521-531, 2012.

[15] H. Chen, V. Sleiffer, B. Snyder, M. Kuschnerov, R. van Uden, Y. Jung, C. M. Okonkwo, O. Raz, P. O'Brien, H. de Waardt, and T. Koonen, "Demonstration of a Photonic Integrated Mode Coupler With MDM and WDM Transmission," IEEE Photon. Technol. Lett. 25(21), pp. 2039–2042, 2013.

[16] Andrew Forbes, Angela Dudley, and Melanie McLaren, "Creation and detection of optical modes with spatial light modulators," Adv. Opt. Photon. 8, pp. 200-227, 2016.

[17] R. G. H. van Uden, R. Amezcua-Correa, E. Antonio-Lopez, F. M. Huijskens, C. Xia, G. Li, A. Schülzgen, H. de Waardt, A. M. J. Koonen, and C. M. Okonkwo, "Ultra-high-density spatial division multiplexing with a few-mode multicore fibre," Nat. Photonics 8, 865, 2014.

[18] Benyuan Zhu, John M. Fini, Man F. Yan, Xiang Liu, S. Chandrasekhar, Thierry F. Taunay, Michael Fishteyn, Eric M. Monberg, and Frank V. Dimarcello, "High-Capacity Space-Division-Multiplexed DWDM Transmissions Using Multicore Fiber," J. Lightwave Technol. **30**, pp. 486-492, 2012.

[19] R. Ryf, S. Randel, N. K. Fontaine, M. Montoliu, E. Burrows, S. Chandrasekhar, A. H. Gnauck, C. Xie, R. Essiambre, P. Winzer, R. Delbue, P. Pupalaikis, A. Sureka, Y. Sun, L. Gruner-Nielsen, R. V. Jensen, and R. Lingle, "32-bit/s/Hz Spectral Efficiency WDM Transmission over 177-km Few-Mode Fiber," in Optical Fiber Communication Conference/National Fiber Optic Engineers Conference 2013, OSA Technical Digest (online) (Optical Society of America, 2013), paper PDP5A.1.

[20] Haoshuo Chen, Roy van Uden, Chigo Okonkwo, and Ton Koonen, "Compact spatial multiplexers for mode division multiplexing," Opt. Express **22**, pp. 31582-31594, 2014.

[21] Jeffrey B. Driscoll, Richard R. Grote, Brian Souhan, Jerry I. Dadap, Ming Lu, and Richard M. Osgood, "Asymmetric Y junctions in silicon waveguides for on-chip mode-division multiplexing," Opt. Lett. **38**, pp. 1854-1856, 2013.

[22] Liang Fang and Hongzhi Jia, "Mode add/drop multiplexers of LP_{02} and LP_{03} modes with two parallel combinative long-period fiber gratings," Opt. Express **22**, pp. 11488-11497, 2014.

[23] T. A. Birks, I. Gris-Sánchez, S. Yerolatsitis, S. G. Leon-Saval, and R. R. Thomson, "The photonic lantern," Adv. Opt. Photon. 7, pp. 107-167, 2015.

[24] Jiangang Zhu, Şahin Kaya Özdemir, Lina He, Da-Ren Chen, and Lan Yang, "Single virus and nanoparticle size spectrometry by whispering-gallery-mode microcavities," Opt. Express **19**, pp. 16195-16206, 2011.

[25] Carol E. Soteropulos, Kevin M. Zurick, Matthew T. Bernards, and Heather K. Hunt, "Tailoring the Protein Adsorption Properties of Whispering Gallery Mode Optical Biosensors," Langmuir 28 (44), pp. 15743–15750, 2012

[26] Carlos Moreno-Hernández, D. Monzón-Hernández, Joel Villatoro, "Contactless optical fiber refractive index sensor for liquid and solid samples," Sixth European Workshop on Optical Fibre Sensors, paper 99161A, 2016.

[27] L. Pavesi and G. Guillot, "Optical Interconnects - the silicon approach," Springer-Verlag, Heidelberg, 2006.

[28] D.G. Rabus, "Integrated Ring Resonators: The Compendium," Springer Series in Optical Sciences, 2007.

[29] John Heebner, Rohit Grover, and Tarek Ibrahim, "OpticalMicroresonators: Theory, Fabrication, and Applications," Springer Series in Optical Sciences, 2008.

[30] Ioannis Chremmos, Otto Schwelb, and Nikolaos Uzunoglu, "Photonic Microresonator Research and Applications, Springer Series in Optical Sciences, 2010.

[31] Matthew R. Foreman, Jon D. Swaim, and Frank Vollmer, "Whispering gallery mode sensors," Adv. Opt. Photon. 7, pp. 168-240, 2015.

[32] Limin Xiao and T. A. Birks, "High finesse microfiber knot resonators made from double-ended tapered fibers," Opt. Lett. 36, pp. 1098-1100, 2011.

[33] M. Sumetsky, Y. Dulashko, J. M. Fini, A. Hale, and D. J. DiGiovanni, "The Microfiber Loop Resonator: Theory, Experiment, and Application," J. Lightwave Technol. 24, pp. 242-250, 2006.

[34] Kyriaki Kosma, Gianluigi Zito, Kay Schuster, and Stavros Pissadakis, "Whispering gallery mode microsphere resonator integrated inside a microstructured optical fiber," Opt. Lett. 38, pp. 1301-1303, 2013.

[35] Vanessa Zamora, Antonio Díez, Miguel V. Andrés, and Benito Gimeno, "Refractometric sensor based on whispering-gallery modes of thin capillaries," Opt. Express **15**, pp. 12011-12016, 2007.

[36] Ming Ding, Ganapathy Senthil Murugan, Gilberto Brambilla, and Michalis N. Zervas, "Whispering gallery mode selection in optical bottle microresonators," Appl. Phys. Lett. 100, 081108, 2012.

[37] J. D. Suter, I. M. White, H. Zhu, H. Shi, C. W. Caldwell, and X. Fan, "Label-free quantitative DNA detection using the liquid core optical ringresonator," Biosens. Bioelectron. 23, pp.1003–1009, 2008.

[38] Anna Boleininger, Thomas Lake, Sophia Hami and Claire Vallance, "Whispering Gallery Modes in Standard Optical Fibres for Fibre Profiling Measurements and Sensing of Unlabelled Chemical Species," Sensors 2010, 10(3), 2010.

[39] Kevin D. Heylman, Kassandra A. Knapper, and Randall H. Goldsmith, "Photothermal Microscopy of Nonluminescent Single Particles Enabled by Optical Microresonators," J. Phys. Chem. Lett., 5 (11), pp. 1917–1923, 2014.

[40] Jonathan M. Ward, Yong Yang & Síle Nic Chormaic, "Glass-on-Glass Fabrication of Bottle-Shaped Tunable Microlasers and their Applications," *Scientific Reports* **6**, 25152, 2016.

[41] John A. Buck, "Fundamentals of optical fibers," Wiley series in pure and applied optics, 1995.

[42] Frank Träger, "Handbook of Lasers and Optics," Springer, 2nd Edition, 2012.

[43] C. Vassallo, "Optical Waveguide Concepts", Elsevier Science Publishers B.V., 1991.

[44] R. Olshansky, "Propagation in Glass Optical Waveguides," Rev. Modern Phys., 51:2, pp. 341–367, 1979.

[45] J. Gowar, "Optical Communication Systems," Prentice Hall International, Inc., 1984.

[46] S. Kawakami and H. Tanji, "Evolution of power distribution in graded-index fibres," Electr. lett., 19(3), pp. 100–102, 1983.

[47] Ming-Jun Li and Daniel A. Nolan, "Optical Transmission Fiber Design Evolution," J. Lightwave Technol. 26, pp. 1079-1092, 2008.

[48] Hirokazu Kubota, Toshio Morioka, "Few-mode optical fiber for mode-division multiplexing," Optical Fiber Technology 17, pp. 490–494, 2011.

[49] Pierre Sillard, Marianne Bigot-Astruc, and Denis Molin, "Few-Mode Fibers for Mode-Division-Multiplexed Systems," J. Lightwave Technol. 32, pp. 2824-2829, 2014.

[50] John van Weerdenburg, Amado Velazquez-Benitez, Roy van Uden, Pierre Sillard, Denis Molin, Adrian Amezcua-Correa, Enrique Antonio-Lopez, Maxim Kuschnerov, Frans Huijskens, Hugo de Waardt, Ton Koonen, Rodrigo Amezcua-Correa, and Chigo Okonkwo, "10 Spatial mode transmission using low differential mode delay 6-LP fiber using all-fiber photonic lanterns," Opt. Express 23, pp. 24759-24769, 2015.

[51] L. Grüner-Nielsen, Y. Sun, R. V. S. Jensen, J. W. Nicholson, and R. Lingle, "Recent Advances in Low DGD Few-mode Fibre Design, Fabrication, Characterization and Experiments," in Optical Fiber Communication Conference, OSA Technical Digest (online) (Optical Society of America), paper M2C.3, 2015.

[52] P. Sillard, D. Molin, M. Bigot-Astruc, H. Maerten, D. van Ras, and F. Achten, "Low-DMGD 6-LP-Mode Fiber," in Optical Fiber Communication Conference, OSA Technical Digest (online) (Optical Society of America), paper M3F.2, 2014.

[53] Pierre Sillard, Denis Molin, Marianne Bigot-Astruc, Koen De Jongh, Frank Achten, Amado M. Velázquez-Benítez, Rodrigo Amezcua-Correa, and Chigo M. Okonkwo, "Low-Differential-Mode-Group-Delay 9-LP-Mode Fiber," J. Lightwave Technol. 34, pp. 425-430, 2016.

[54] Timothy A. Birks and Youwei W. Li," The Shape of Fiber Tapers," J. Lightwave Technol. 10. No. 4, 1992.

[55] J.D. Love, W.M. Henry, W.J. Stewart, R.J. Black, S. Lacroix, and F. Gonthier, "Tapered single-mode fibres and devices Part 1: Adiabaticity criteria," IEE PROCEEDINGS-J, Vol. 138, No. 5, 1991.

[56] Suzanne Lacroix, François Gonthier, and Jacques Bures, "Modeling of symmetric 2 × 2 fused-fiber couplers," Appl. Opt. 33, pp. 8361-8369, 1994.

[57] Bishnu P. Pal, Partha Roy Chaudhuri, M. R. Shenoy, "Fabrication and Modeling of Fused Biconical Tapered Fiber Couplers," Fiber and Integrated Optics, 22, pp. 97–117, 2003.

[58] Chams Baker and Martin Rochette, "Highly nonlinear hybrid AsSe-PMMA microtapers," Opt. Express 18, pp. 12391-12398, 2010.

[59] Suzanne Lacroix, François Gonthier, and Jacques Bures, "All-fiber wavelength filter from successive biconical tapers," Opt. Lett. 11, pp. 671-673, 1986.

[60] Jingyi Lou, Yipei Wang, and Limin, "Microfiber Optical Sensors: A Review," Sensors, 14, pp. 5823-5844, 2014.

[61] Gilberto Brambilla, Fei Xu, Peter Horak, Yongmin Jung, Fumihito Koizumi, Neil P. Sessions, Elena Koukharenko, Xian Feng, Ganapathy S. Murugan, James S. Wilkinson, and David J. Richardson, "Optical fiber nanowires and microwires: fabrication and applications," Adv. Opt. Photon. 1, pp. 107-161, 2009.

[62] Tong Rand Ismaeel, Timothy Lee, Bernard Oduro, Yongmin Jung, and Gilberto Brambilla, "All-fiber fused directional coupler for highly efficient spatial mode conversion," Opt. Express 22, pp. 11610-11619, 2014.

[63] Chams Baker and Martin Rochette, "A generalized heat-brush approach for precise control of the waist profile in fiber tapers," Opt. Mater. Express 1, pp. 1065-1076, 2011.

[64] S. Pricking and H. Giessen, "Tapering fibers with complex shape," Opt. Express 18, pp. 3426-3437, 2010.

[65] K.A. Stasiewicz, R. Krajewski, L.R. Jaroszewicz, M. Kujawińska, R. Świłło, "Influence of tapering process on changes of optical fiber refractive index distribution along a structure," Opto-Electronics Review 18:102, 2010.

[66] Cheng-Ling Lee, Kuo-Hsiang Lin, Nan-Kuang Chen, "Analysis of optical properties of fundamental-mode in waveguide tapered fibers," Microelectronics Reliability 50, pp. 726–729, 2010.

[67] S. W. Haruna, K. S. Lim, C. K. Tio, K. Dimyati, H. Ahmad, "Theoretical analysis and fabrication of tapered fiber," Optik 124, pp. 538–543, 2013.

[68] R. J. Black, R. Bourbonnais, "Core-mode cutoff for finite-cladding lightguides," IEE Proceedings J – Optoelectronics, Vol. 133, Issue 6, pp. 377 – 384, 1986.

[69] Alexandre Felipe, Guilherme Espíndola, Hypolito J. Kalinowski, José A. S. Lima, and Aleksander S. Paterno, "Stepwise fabrication of arbitrary fiber optic tapers," Opt. Express 20, pp. 19893-19904, 2012.

[70] Jacques Bures and René Ghosh, "Power density of the evanescent field in the vicinity of a tapered fiber," J. Opt. Soc. Am. A 16, pp. 1992-1996, 1999.

[71] L. C. Ozcan, V. Treanton, F. Guay, and R. Kashyap, "Highly symmetric optical fiber tapers fabricated with a CO2 laser," Photon. Technol. Lett. 19, pp. 656–658, 2007.

[72] Oh, S. T., Han, W. T., Paek, U. C. and Chung, Y., Azimuthally symmetric long-period fiber gratings fabricated with CO2 laser. Microw. Opt. Technol. Lett., 41, pp. 188–190, 2004.

[73] Jonathan M. Ward, Danny G. O'Shea, Brian J. Shortt, Michael J. Morrissey, Kieran Deasy, and Síle G. Nic Chormaic, "Heat-and-pull rig for fiber taper fabrication," Rev. Sci. Instrum. 77, 083105, 2006.

[74] James N. McMullin, "The ABCD matrix in graded index tapers used for beam expansion and compression," Appl. Opt. 28, pp. 1298-1304, 1989.

[75] Cen Xia, Neng Bai, Ibrahim Ozdur, Xiang Zhou, and Guifang Li, "Supermodes for optical transmission," Opt. Express 19, pp. 16653-16664, 2011.

[76] Haoshuo Chen, Nicolas K. Fontaine, Roland Ryf, Binbin Guan, S. J. Ben Yoo, and Ton (A. M. J.) Koonen, "Design Constraints of Photonic-Lantern Spatial Multiplexer Based on Laser-Inscribed 3-D Waveguide Technology," J. Lightwave Technol. 33, pp. 1147-1154, 2015.

[77] P. N. Moar, S. T. Huntington, J. Katsifolis, L. W. Cahill, A. Roberts and K. A. Nugent, "Fabrication, modeling, and direct evanescent field measurement of tapered optical fiber sensors," J. Appl. Phys. 85, 3395, 1999.

[78] Sergio G. Leon-Saval, Alexander Argyros, and Joss Bland-Hawthorn, "Photonic lanterns: a study of light propagation in multimode to single-mode converters," Opt. Express 18, pp. 8430-8439, 2010.

[79] S. G. Leon-Saval, T. A. Birks, J. Bland-Hawthorn, and M. Englund, "Multimode fiber devices with single-mode performance," Opt. Lett. 30, pp. 2545-2547, 2005.

[80] Sergio G. Leon-Saval, Christopher H. Betters, and Joss Bland-Hawthorn, "The Photonic TIGER: a multicore fiber-fed spectrograph," Proc. SPIE 8450, Modern Technologies in Space- and Ground-based Telescopes and Instrumentation II, 84501K, 2012.

[81] Danny Noordegraaf, Peter M. W. Skovgaard, Martin D. Nielsen, and Joss Bland-Hawthorn, "Efficient multi-mode to single-mode coupling in a photonic lantern," Opt. Express 17, pp. 1988-1994, 2009.

[82] Hai-Jiao Yu, Qi Yan, Zong-Jun Huang, He Tian, Yu Jiang, Yong-Jun Liu, Jian-Zhong Zhang and Wei-Min Sun, "Photonic lantern with multimode fibers embedded," Research in Astronomy and Astrophysics, Vol. 14 No. 8, pp. 1046–1054, 2014.

[83] S. Yerolatsitis, I. Gris-Sánchez, and T. A. Birks, "Adiabatically-tapered fiber mode multiplexers," Opt. Express 22, pp. 608-617, 2014.

[84] R. Ryf, N. K. Fontaine, and R.-J. Essiambre, "Spot-Based Mode Couplers for Mode-Multiplexed Transmission in Few-Mode Fiber," IEEE Photon. Technol. Lett. 24(21), pp. 1973–1976, 2012.

[85] Nicolas K. Fontaine, Roland Ryf, Joss Bland-Hawthorn, and Sergio G. Leon-Saval, "Geometric requirements for photonic lanterns in space division multiplexing," Opt. Express 20, pp. 27123-27132, 2012.

[86] Sergio G. Leon-Saval, Nicolas K. Fontaine, Joel R. Salazar-Gil, Burcu Ercan, Roland Ryf, and Joss Bland-Hawthorn, "Mode-selective photonic lanterns for space-division multiplexing," Opt. Express 22, pp. 1036-1044, 2014.

[87] N. K. Fontaine, S. G. Leon-Saval, R. Ryf, J. R. Salazar-Gil, B. Ercan, and J. Bland-Hawthorn, "Mode-Selective Dissimilar Fiber Photonic-Lantern Spatial Multiplexers for Few-Mode Fiber," in 39th European Conference and Exposition on Optical Communications, OSA Technical Digest (CD) (Optical Society of America), paper PD1.C.3, 2013.

[88] A. M. Velazquez-Benitez, J. C. Alvarado, G. Lopez-Galmiche, J. E. Antonio-Lopez, J. Hernández-Cordero, J. Sanchez-Mondragon, P. Sillard, C. M. Okonkwo, and R. Amezcua-Correa, "Six mode selective fiber optic spatial multiplexer," Opt. Lett. 40, pp. 1663-1666, 2015.

[89] Bin Huang, Nicolas K. Fontaine, Roland Ryf, Binbin Guan, Sergio G. Leon-Saval, R. Shubochkin, Y. Sun, R. Lingle, and Guifang Li, "All-fibre mode-group-selective photonic lantern using graded-index multimode fibres," Opt. Express 23, pp. 224-234, 2015.

[90] (Oct., 2016). LZM-100 LAZERMaster™ Laser Splicing System [Online]. https://www.aflglobal.com/Products/Fusion-Splicing/Specialty-Fusion-Splicing-Equipment/Splicers/LAZERMaster-LZM-100-Laser-Splicing-System.aspx

[91] William Klimowych, "Annular Heating of Optical Fiber with a CO2 Laser Using Reflective Axicon Elements," White Paper, AFL, 2014.

[92] A. Velázquez-Benítez, J. Antonio-López, J. Alvarado-Zacarías, G. Lopez-Galmiche, P. Sillard, D. van Ras, et al., "Scaling the Fabrication of Higher Order Photonic Lanterns Using Microstructured Preforms," European Conference on Optical Communication (ECOC), Valencia, Spain, paper Tu.3.3.2, 2015.

[93] J. Bland-Hawthorn, S.C. Ellis, S.G. Leon-Saval, R. Haynes, M.M. Roth, H.-G. Löhmannsröben, A.J. Horton, J.-G. Cuby, T.A. Birks, J.S. Lawrence, P. Gillingham, S.D. Ryder & C. Trinh, "A complex multi-notch astronomical filter to suppress the bright infrared sky," Nature Communications 2, Article number:581, 2011.

[94] Robert Olshansky, "Mode Coupling Effects in Graded-Index Optical Fibres," Appl. Opt. 14, pp. 935-945, 1975.

[95] P. Sillard, M. Astruc, D. Boivin, H. Maerten, and L. Provost, "Few-Mode Fiber for Uncoupled Mode-Division Multiplexing Transmissions," in 37th European Conference and Exposition on Optical Communications, OSA Technical Digest (CD) (Optical Society of America), paper Tu.5.LeCervin.7, 2011.

[96] P. Sillard, "Few-Mode Fibers for Space Division Multiplexing," in Optical Fiber Communication Conference, OSA Technical Digest (online) (Optical Society of America), paper Th1J.1, 2016.

[97] Amy Van Newkirk, J. E. Antonio-Lopez, Amado Velazquez-Benitez, Jacques Albert, Rodrigo Amezcua-Correa, and Axel Schülzgen, "Bending sensor combining multicore fiber with a mode-selective photonic lantern," Opt. Lett. 40, pp. 5188-5191, 2015.

[98] Yi Weng, Ezra Ip, Zhongqi Pan, and Ting Wang, "Advanced Spatial-Division Multiplexed Measurement Systems Propositions—From Telecommunication to Sensing Applications: A Review," Sensors, Vol. 16, Iss. 9, p. 1387, 2016.

[99] Keang-Po Ho and Joseph M. Kahn, "Mode-dependent loss and gain: statistics and effect on mode-division multiplexing," Opt. Express 19, pp. 16612-16635, 2011.

[100] N. K. Fontaine, R. Ryf, M. A. Mestre, B. Guan, X. Palou, S. Randel, Y. Sun, L. Gruner-Nielsen, R. V. Jensen, and R. Lingle, "Characterization of Space-Division Multiplexing Systems using a Swept-Wavelength Interferometer," in Optical Fiber Communication Conference/National Fiber Optic Engineers Conference 2013, OSA Technical Digest (online) (Optical Society of America), paper OW1K.2, 2013.

[101] Joel Carpenter, Benjamin J. Eggleton, and Jochen Schröder, "110x110 optical mode transfer matrix inversion," Opt. Express 22, pp. 96-101, 2014.

[102] Raphael Dahan, Leopoldo L. Martin, and Tal Carmon, "Droplet optomechanics," Optica 3, pp. 175-178, 2016.

[103] Bruce A. Block, Todd R. Younkin, Paul S. Davids, Miriam R. Reshotko, Peter Chang, Brent M. Polishak, Su Huang, Jingdong Luo, and Alex K. Y. Jen, "Electro-optic polymer cladding ring resonator modulators," Opt. Express 16, pp. 18326-18333, 2008.

[104] Andrea L. Martin, Deniz K. Armani, Lan Yang, and Kerry J. Vahala, "Replica-molded high-Q polymer microresonators," Opt. Lett. **29**, pp. 533-535, 2004.

[105] Ahmed Akelah and A. Moet, "Functionalized Polymers and their Applications," Springer Netherlands, 1990.

[106] Kim, H., Kim, Y. and Chang, J. Y., "Polymers for Luminescent Sensing Applications," Macromol. Chem. Phys., pp. 215, 1274–1285, 2014.

[107] Reinher Pimentel-Domínguez, Amado M. Velázquez-Benítez, J. Rodrigo Vélez-Cordero, Mathieu Hautefeuille, Francisco Sánchez-Arévalo, and Juan Hernández-Cordero, "Photothermal Effects and Applications of Polydimethylsiloxane Membranes with Carbon Nanoparticles," Polymers 8(4), 2016.

[108] Priimagi, A. and Shevchenko, A., "Azopolymer-based micro- and nanopatterning for photonic applications," Journal of Polymer Science Part B: Polymer Physics, 52, pp. 163–182, 2014.

[109] M. Smietana, M. L. Korwin-Pawlowski, W. J. Bock, G. R. Pickrell, and J. Szmidt, "Refractive index sensing of fiber optic long-period grating structures coated with a plasma deposited diamond-like carbon thin film," Meas. Sci. Technol., Vol. 19, No. 8, p. 085301, 2008.

[110] L. Cheng-Ling, “Spectral analysis of waveguide tapered microfiber with an ultrathin metal coating,” Opt. Exp., Vol. 18, No. 14, pp. 14768–14777, 2010.

[111] M. A. Butler and D. S. Ginley, “Hydrogen sensing with palladium coated optical fibers,” J. Appl. Phys., Vol. 64, No. 7, pp. 3706–3712, 1988.

[112] L. E. Scriven, “Physics and applications of dip coating and spin coating,” Mater. Res. Soc. Symp. Proc., Vol. 121, pp. 717–729, 1988.

[113] C. R. Zamarreño, P. Sanchez, M. Hernaez, I. Del Villar, C. Fernandez-Valdivielso, I. R. Matias, and F. J. Arregui, “Sensing properties of indium oxide coated optical fiber devices based on lossy mode resonances,” IEEE Sensors J., Vol. 12, No. 1, pp. 151–155, 2012.

[114] V. A. Márquez-Cruz and J. A. Hernández-Cordero, “Fiber optic Fabry–Perot sensor for surface tension analysis,” Opt. Exp., Vol. 22, No. 3, pp. 3028–3038, 2014.

[115] S.-M. Chuo and L. A. Wang, “Propagation loss, degradation and protective coating of long drawn microfibers,” Opt. Commun., vol. 284, no. 12, pp. 2825–2828, 2011.

[116] S. R. Schmid and A. F. Toussaint, “Optical fiber coatings,” Specialty Optic Fibers Handbook, A. Mendez and T. F. Morse, Eds. Amsterdam, The Netherlands: Elsevier, pp. 95–122, 2007.

[117] Amado M. Velázquez-Benítez, Moisés Reyes-Medrano, J. Rodrigo Vélez-Cordero, and Juan Hernández-Cordero, "Controlled Deposition of Polymer Coatings on Cylindrical Photonic Devices," J. Lightwave Technol. 33, pp. 176-182, 2015.

[118] G. Kakarantzas, S. G. Leon-Saval, T. A. Birks, and P. St. J. Russell, “Low-loss deposition of sol gel-derived silica films on tapered fibers,” Opt. Lett., Vol. 29, No. 7, pp. 694–696, 2004.

[119] Z. Y. Xu, Y. H. Li, and L. J. Wang, “A versatile technique to functionalize optical microfibers via modified sol-gel dip-coating method,” Opt. Lett., Vol. 39, No. 1, pp. 34–36, 2014.

[120] Bogaerts, W., De Heyn, P., Van Vaerenbergh, T., De Vos, K., Kumar Selvaraja, S., Claes, T., Dumon, P., Bienstman, P., Van Thourhout, D. and Baets, R, “Silicon microring resonators,” Laser & Photon. Rev., 6, pp. 47–73,2012.

[121] Kristopher J. Rowland, Alexandre François, Peter Hoffmann, and Tanya M. Monro, "Fluorescent polymer coated capillaries as optofluidic refractometric sensors," Opt. Express 21, pp. 11492-11505, 2013.

[122] A. D. Ryck and D. Quéré, “Inertial coating of a fibre,” J. Fluid Mech., Vol. 311, pp. 219–237, 1996.

[123] D. Quéré, “Fluid coating on a fiber,” Annu. Rev. Fluid Mech., Vol. 31, pp. 347–384, 1999.

[124] D. A. White and J. A. Tallmadge, “A theory of withdrawal of cylinders from liquid baths,” AIChE J., Vol. 12, no. 2, pp. 333–339, 1966.

[125] H. Ma, A. K.-Y. Jen, and L. R. Dalton, “Polymer-based optical waveguides: Materials, processing, and devices,” Adv. Mater., vol. 14, pp. 1339–1365, 2002.

[126] L. Rayleigh, “On the instability of jets,” Proc. London Math. Soc., vol. 10, pp. 4–13, 1878.

[127] B. Magny, S. Pelletier, G. Albrighton, and G. Eisele, “Importance of monomer interfacial tension for UV curable Litho Inks performance,” presented at the Rad Tech Conf., Indianapolis, IN, USA, 2002.

[128] (Oct., 2016). Sylgard184 Silicone Elastomer: Product Information-Electronics, Dow Corning Co., USA. [Online]. Available: http://www.dowcorning.com/DataFiles/090276fe80190b08.pdf

[129] S.Wu, “Calculation of interfacial tension in polymer systems,” J. Polymer. Sci. C, vol. 34, no. 1, pp. 19–30, 1971.

[130] Daniel T. Cassidy, Derwyn C. Johnson, and Kenneth O. Hill, "Wavelength-dependent transmission of monomode optical fiber tapers," Appl. Opt. 24, pp. 945-950, 1985.

[131] R. J. Black, S. Lacroix, F. Gonthier and J. D. Love, "Tapered single-mode fibres and devices—Part 2: Experimental and theoretical quantification," IEE Proc. J. Optelectron., vol. 138, no. 5, pp. 355–364, 1991.

[132] R. Zhao and C. W. Macosko, "Slip at polymer–polymer interfaces: Rheological measurements on coextruded multilayers," J. Rheol., Vol. 46, pp. 145–167, 2002.

[133] L. Ying-Chih, L. Yen-Ching, and W. Hsien-Hung, "Drastic changes in interfacial hydrodynamics due to wall slippage: Slip-intensified film thinning, drop spreading, and capillary instability," Phys. Rev. Lett., Vol. 111, No. 13, p. 136001, 2013.

[134] J. R. Vélez-Cordero, A. M. Velázquez-Benítez, and J. Hernández-Cordero, "Thermocapillary flow in glass tubes coated with photoresponsive layers," Langmuir, Vol. 30, No. 18, pp. 5326–5336, 2014.

[135] Holger Schmidt and Aaron R. Hawkins, "The photonic integration of non-solid media using optofluidics," Nature Photonics 5, pp. 598–604, 2011.

[136] Chantal Paquet, Eugenia Kumacheva, "Nanostructured polymers for photonics," Materials today, Volume 11, Issue 4, pp 48–56, 2008.

[137] Sebastian Valouch, Heinrich Sieber, Siegfried Kettlitz, Carsten Eschenbaum, Uwe Hollenbach, and Uli Lemmer, "Direct fabrication of PDMS waveguides via low-cost DUV irradiation for optical sensing," Opt. Express 20, pp. 28855-28861, 2012.

[138] Amado M. Velázquez-Benítez and Juan Hernández-Cordero, "Optically Driven All-Fiber Polarization Rotator," J. Lightwave Technol. 29, pp. 1671-1676, 2011.

[139] C. R. Mendonça, L. Misoguti, A. A. Andrade, S. B. Yamaki, V.D. Dias, T. D. Z. Atvars, O. N. Oliveira Jr, "Photoinduced birefringence in di-azo compounds in polystyrene and poly(methyl methacrylate) guest–host systems," Optical Materials, Vol. 30, No. 2, , pp. 216–221, 2007.

[140] Govind P. Agrawal, "Nonlinear Fiber Optics," Academic Press, 3rd Ed., 2001.

[141] Huang, M. and Meng, F., "Synthesis of Yb3+/Er3+ co-dopants sodium yttrium fluoride up-conversion fluorescence materials," Luminescence, 20, pp. 276–278, 2005.

[142] Anna Boleininger, Thomas Lake, Sophia Hami and Claire Vallance, "Whispering Gallery Modes in Standard Optical Fibres for Fibre Profiling Measurements and Sensing of Unlabelled Chemical Species," Sensors 9, pp. 1765-1781, 2009.

[143] D. Jandura, D. Pudis, S. Berezina, "Photonic devices prepared by embossing in PDMS," Applied Surface Science, 2016.

APPENDIX A: PDMS COMPOSITES

The method listed here presents the fabrication of functional polymers using polydimethylsiloxane (PDMS) as the host matrix for different materials. PDMS is a thermally curable elastomer comprised by two materials: a base polymer which is silicone oil, and a curing agent that generates a cross-linking effect. Functional polymer composites preparation was fabricated using Dow Corning Sylgard 184 PDMS. Incorporation of additional compounds into PDMS involves the use of chloroform ($CHCl_3$), aiming only at reducing the viscosity of the silicone oil of the PDMS. This approach generates a uniform distribution of the compound inside the silicone oil, yielding a material with homogeneous properties and avoiding further modification of the materials. The fabrication process includes the following steps:

- The required base material (silicone oil) is weighted inside of a glass beaker.
- The desired compound to be incorporated is added in a given concentration in weight compared to the total PDMS amount, and simply poured into the beaker.
- Chloroform is added into the beaker in a proportion of 0.75 mL per gram of PDMS in order to lower the viscosity and resulting in a liquid solution which allows the mixture of the PDMS and the compound.
- The materials are mixed to by means of using a magnetic bar activated by a hot plate with magnetic stirrer, while heated at 150 °C until full evaporation of the $CHCl_3$. After $CHCl_3$ complete evaporation, the resulting composite is left to cold down at room temperature.
- The curing agent is added with a given ratio compared to the base material and both parts are mixed by hand during two minutes.
- Air captured during the mixing process is removed thru a degassing process.
- The PDMS+compound mixture is deposited into the containers of the coating system and the coating process is executed.
- Solidification of the composites is achieved upon heating at 80 °C during 2 hours.

APPENDIX B: PUBLICATIONS

REFEREED JOURNALS

G. Lopez-Galmiche, Z. Sanjabi Eznaveh, J. E. Antonio-Lopez, *A. M. Velazquez Benitez*, J. Rodriguez Asomoza, J. J. Sanchez Mondragon, C. Gonnet, P. Sillard, G. Li, A. Schülzgen, C. M. Okonkwo, and R. Amezcua Correa, **Few-mode erbium-doped fiber amplifier with photonic lantern for pump spatial mode control**, Opt. Lett. 41, pp. 2588-2591, 2016. https://doi.org/10.1364/OL.41.002588

Reinher Pimentel-Domínguez, *Amado M. Velázquez-Benítez*, J. Rodrigo Vélez-Cordero, Mathieu Hautefeuille, Francisco Sánchez-Arévalo, and Juan Hernández-Cordero, **Photothermal Effects and Applications of Polydimethylsiloxane Membranes with Carbon Nanoparticles**, Polymers, 8(4), 84, 2016. DOI:10.3390/polym8040084

He Wen, Cen Xia, *Amado M. Velázquez-Benítez*, Naresh Chand, Jose Enrique Antonio-Lopez, Bin Huang, Huiyuan Liu, Hongjun Zheng, Pierre Sillard, Xiang Liu, Frank Effenberger, Rodrigo Amezcua-Correa, and Guifang Li, **First Demonstration of Six-Mode PON Achieving a Record Gain of 4 dB in Upstream Transmission Loss Budget**, J. Lightwave Technol. 34, pp. 1990-1996, 2016. http://dx.doi.org/10.1109/JLT.2015.2503121

Pierre Sillard, Denis Molin, Marianne Bigot-Astruc, Koen De Jongh, Frank Achten, *Amado M. Velázquez-Benítez*, Rodrigo Amezcua-Correa, and Chigo M. Okonkwo, **Low-Differential-Mode-Group-Delay 9-LP-Mode Fiber**, J. Lightwave Technol. 34, pp. 425-430, 2016. http://dx.doi.org/10.1109/JLT.2015.2463715

Juan Montoya, Chris Aleshire, Christopher Hwang, Nicolas K. Fontaine, *Amado Velázquez-Benítez*, Dale H. Martz, T.Y. Fan, and Dan Ripin, **Photonic lantern adaptive spatial mode control in LMA fiber amplifiers**, Opt. Express 24, pp. 3405-3413, 2016. https://doi.org/10.1364/OE.24.003405

Amy Van Newkirk, J. E. Antonio-Lopez, *Amado Velazquez-Benitez*, Jacques Albert, Rodrigo Amezcua-Correa, and Axel Schülzgen, **Bending sensor combining multicore fiber with a mode-selective photonic lantern**, Opt. Lett. 40, pp. 5188-5191, 2015. https://doi.org/10.1364/OL.40.005188

A. M. Velazquez-Benitez, J. C. Alvarado, G. Lopez-Galmiche, J. E. Antonio-Lopez, J. Hernández-Cordero, J. Sanchez-Mondragon, P. Sillard, C. M. Okonkwo, and R. Amezcua-Correa, **Six mode selective fiber optic spatial multiplexer**, Opt. Lett. 40, pp. 1663-1666, 2015. https://doi.org/10.1364/OL.40.001663

John van Weerdenburg, *Amado Velázquez-Benitez*, Roy van Uden, Pierre Sillard, Denis Molin, Adrian Amezcua-Correa, Enrique Antonio-Lopez, Maxim Kuschnerov, Frans Huijskens, Hugo de Waardt, Ton Koonen, Rodrigo Amezcua-Correa, and Chigo Okonkwo, **10 Spatial mode transmission using low**

differential mode delay 6-LP fiber using all-fiber photonic lanterns, Opt. Express 23, pp. 24759-24769, 2015. https://doi.org/10.1364/OE.23.024759

Amado M. Velázquez Benítez, Moisés Reyes-Medrano, J. Rodrigo Velez-Cordero, Juan Hernandez-Cordero, **Controlled Deposition of Polymer Coatings on Cylindrical Photonic Devices**, IEEE Journal of Lightwave Technology, 33, pp. 176-182, 2015. http://dx.doi.org/10.1109/JLT.2014.2377173

Cen Xia, Naresh Chand, *A. M. Velázquez-Benítez*, Zhiqun Yang, Xiang Liu,1 Jose Enrique Antonio-Lopez, He Wen, Benyuan Zhu, Ningbo Zhao, Frank Effenberger, Rodrigo Amezcua-Correa, and Guifang Li, **Time-division-multiplexed few-mode passive optical network**, Opt. Express 23, pp. 1151-1158, 2015. https://doi.org/10.1364/OE.23.001151

CONFERENCE ARTICLES

A. M. Velazquez-Benitez, M. S. Cano-Velazquez, and J. Hernandez-Cordero, **Fiber Coupled Optically Tunable Polymer/Glass Microring Resonators**, in Latin America Optics and Photonics Conference, (Optical Society of America, 2016), paper LTu5C.5. https://doi.org/10.1364/LAOP.2016.LTu5C.5

N. K. Fontaine, B. Huang, Z. Sanjabi Eznaveh, H. Chen, C. Jin, B. Ercan, *A. Velázquez-Benítez*, S. H. Chang, R. Ryf, A. Schülzgen, J. Carlos Alvarado, P. Sillard, C. Gonnet, E. Antonio-Lopez, and R. Amezcua Correa, **Multi-mode Optical Fiber Amplifier supporting over 10 Spatial Modes**, in Optical Fiber Communication Conference Postdeadline Papers, OSA Technical Digest (online) (Optical Society of America, 2016), paper Th5A.4. https://doi.org/10.1364/OFC.2016.Th5A.4

H. Chen, R. Ryf, N. K. Fontaine, *A. M. Velázquez-Benítez*, J. Antonio-López, C. Jin, B. Huang, M. Bigot, dmolin, F. Achten, P. Sillard, and R. Amezcua Correa, **High Spectral Efficiency Mode-Multiplexed Transmission over 87-km 10-Mode Fiber**, in Optical Fiber Communication Conference, OSA Technical Digest (online) (Optical Society of America, 2016), paper Th4C.2. https://doi.org/10.1364/OFC.2016.Th4C.2

J. van Weerdenburg, *A. M. Velázquez-Benítez*, R. G. H. v. Uden, E. Antonio-Lopez, P. Sillard, D. Molin, M. Bigot, A. Amezcua-Correa, F. Huijskens, F. Achten, H. de Waardt, T. Koonen, R. Amezcua Correa, and C. M. Okonkwo, **10 Spatial Mode Transmission over 40km 50µm Core Diameter Multimode Fiber**, in Optical Fiber Communication Conference, OSA Technical Digest (online) (Optical Society of America, 2016), paper Th4C.3. https://doi.org/10.1364/OFC.2016.Th4C.3

D. Yu, J. v. Weerdenburg, E. Silekens, R. G. H. v. Uden, M. Tang, D. Liu, *A. M. Velazquez-Benitez*, P. Sillard, D. Molin, M. Bigot, R. Amezcua Correa, H. de Waardt, T. Koonen, S. Fu, and C. M. Okonkwo, **Trellis Coded Modulation Transmission over 40km 6-LP Mode Fiber**, in Optical Fiber Communication Conference, OSA Technical Digest (online) (Optical Society of America, 2016), paper Th4C.5. https://doi.org/10.1364/OFC.2016.Th4C.5

R. Ryf, H. Chen, N. K. Fontaine, *A. M. Velázquez-Benítez*, José Antonio-López, C. Jin, B. Huang, M. Bigot-Astruc, D. Molin, F. Achten, P. Sillard, and R. Amezcua-Correa, **10-Mode mode-multiplexed transmission over 125-km single-span multimode fiber**, in European Conference on Optical Communication (ECOC), 2015, 2015, paper PDP.3.3. http://dx.doi.org/10.1109/ECOC.2015.7341687

He Wen, Hongjun Zheng ; Qi Mo, *A. M. Velázquez-Benítez*, Cen Xia, Bing Huang, Huiyuan Liu, Huang Yu, Jose Enrique Antonio Lopez, Rodrigo Amezcua Correa, and Guifang Li, **Analog fiber-optic links using high-order fiber modes**, in European Conference on Optical Communication (ECOC), 2015, paper ID: 0269. http://dx.doi.org/10.1109/ECOC.2015.7341821

J. J. A van Weerdenburg, *A. M. Velazquez-Benitez*, R. G. H. van Uden, P. Sillard, D. Molin, A. Amezcua-Correa, J. E. Antonio-Lopez, M. Kuschnerov, F. M. Huijskens, H. de Waardt, A. M. J. Koonen, R. Amezcua-Correa, and C. M. Okonkwo, **10 Spatial mode transmission over low differential mode group delay fibre employing all-fibre photonic lanterns**, in European Conference on Optical Communication (ECOC), 2015, paper Th.1.2.5. http://dx.doi.org/10.1109/ECOC.2015.7341841

A. M. Velázquez-Benítez, J. E. Antonio-López, J. C. Alvarado-Zacarías, G. Lopez-Galmiche, P. Sillard, D. Van Ras, C. Okonkwo, H. Chen, R. Ryf, N. K. Fontaine, and R. Amezcua-Correa, **Scaling the fabrication of higher order photonic lanterns using microstructured preforms**, in European Conference on Optical Communication (ECOC), 2015, paper Tu.1.5.2. http://dx.doi.org/10.1109/ECOC.2015.7341939

G. López-Galmiche, Z. Sanjabi Eznaveh, L. A. Herrera Piad, *A. M. Velazquez-Benitez*, J. Rodriguez-Asomoza, E. Antonio-Lopez, J. J. Sanchez-Mondragon, C. Gonnet, P. Sillard, G. Li, A. Schülzgen, C. Okonkwo, and R. Amezcua-Correa, **Six Mode Erbium-doped Fiber Amplifier Using Mode Selective Photonic Lantern**, in Asia Communications and Photonics Conference 2015, C. Lu, J. Luo, Y. Ji, K. Kitayama, H. Tam, K. Xu, P. Ghiggino, and N. Wada, eds., OSA Technical Digest (online) (Optical Society of America, 2015), paper AM2B.5. https://doi.org/10.1364/ACPC.2015.AM2B.5

A. Van Newkirk, *A. M. Velázquez-Benítez*, J. E. Antonio-Lopez, J. Albert, R. Amezcua Correa, and A. Schulzgen, **3D Bending Sensor Combining Multicore Fiber with a Mode-Selective Photonic Lantern**, in Workshop on Specialty Optical Fibers and Their Applications, OSA Technical Digest (online) (Optical Society of America, 2015), paper WT4A.6. https://doi.org/10.1364/WSOF.2015.WT4A.6

Nicolas K. Fontaine, Roland Ryf ; Haoshuo Chen, *Amado Velazquez Benitez*, J. E. Antonio Lopez, R. Amezcua Correa, Binbin Guan, Burcu Ercan, Ryan P. Scott, S. J. Ben Yoo, Lars Grüner-Nielsen, Yi Sun, Robert J. Lingle, **30×30 MIMO transmission over 15 spatial modes**, in Optical Fiber Communication Conference Postdeadline Papers, OSA Technical Digest (online) (Optical Society of America, 2015), paper Th5C.1. https://doi.org/10.1364/OFC.2015.Th5C.1

A. M. Velazquez-Benitez, J. C. Alvarado-Zacarias, G. Lopez-Galmiche, E. Antonio-Lopez, A. Schülzgen, D. Van Ras, P. Sillard, C. M. Okonkwo, and R. Amezcua-Correa, **Six Spatial Modes Photonic Lanterns**,

in Optical Fiber Communication Conference, OSA Technical Digest (online) (Optical Society of America, 2015), paper W3B.3. https://doi.org/10.1364/OFC.2015.W3B.3

Mildred Cano-Velázquez, *Amado Velázquez-Benítez*, Rodrigo Vélez-Cordero, and Juan Hernandez-Cordero, **Functional Polymer Coatings for Photonic Devices**, Latin America Optics and Photonics Conference (LAOP), Cancun Mexico, LTu3D, 2014. https://doi.org/10.1364/LAOP.2014.LTu3D.3

Cen Xia, Naresh Chand, *A. M. Velázquez-Benítez*, Xiang Liu, Jose Enrique Antonio Lopez, He Wen, Benyuan Zhu, Frank Effenberger, Rodrigo Amezcua-Correa, and Guifang Li, **Demonstration of World's First Few-Mode GPON,** European Conference on Optical Communication (ECOC), Cannes, France, PD.1.5, 2014. http://dx.doi.org/10.1109/ECOC.2014.6964260